C.P. No. 1106

C.P. No. 1106

MINISTRY OF TECHNOLOGY

AERONAUTICAL RESEARCH COUNCIL

CURRENT PAPERS

Low Speed Flight Tests on a Tailless Delta Wing Aircraft (Avro 707B)

Part 3 - Lateral Stability and Control

by

D. H. Perry, J. C. Morrall

and

W. G. A. Port

Aerodynamics Dept, R.A.E., Bedford

LONDON: HER MAJESTY'S STATIONERY OFFICE

1970

PRICE *17s 0d* [*85p*] NET

U.D.C. 533.65 : 533.693.3 : 533.6.013.413

C.P. No.1106*
April 1960

ROYAL AIRCRAFT ESTABLISHMENT

LOW SPEED FLIGHT TESTS ON A TAILLESS DELTA WING AIRCRAFT (AVRO 707B)
PART 3 - LATERAL STABILITY AND CONTROL

by

D. H. Perry, M.A.
J. C. Morrall, B.Sc.Tech.
W. G. A. Port
Aerodynamics Department, R.A.E., Bedford

SUMMARY

This report describes some measurements of lateral stability and control which were made as part of a series of low speed flight tests on the Avro 707B.

Measurements of the aileron and rudder powers, by flying the aircraft with asymmetric wing weights and with a small parachute attached to one wing tip, enabled the sideslip derivatives ℓ_v, n_v, y_v and the damping derivative ℓ_p to be measured. These derivatives were used to estimate the period, damping and roll-yaw ratio of the lateral oscillation for comparison with actual flight measurements.

The measurements of the control powers and sideslip derivatives were in reasonable agreement with the wind tunnel measurements, and the changes which occurred at high lift coefficient were consistent with the changes in wing flow shown by smoke and tuft studies, reported in Part 4 of this series of reports. The derived period and roll-yaw ratio of the lateral oscillation were in fair agreement with the flight measurements but analysis of the damping of the motion emphasised the need for more accurate methods of estimating the rotary derivatives, n_r and n_p, and the lateral inertia of the aircraft.

Pilot opinion of the lateral handling of the aircraft at low speed is also reported.

---

*Replaces R.A.E. Report Aero 2638 - A.R.C. 22242.

CONTENTS

1 INTRODUCTION

The lateral behaviour of aircraft at approach airspeeds has become increasingly important during the past few years, for the introduction of instrument approach aids has demanded much greater precision in maintaining the approach flight path whilst the changes in aerodynamic configuration required for high performance have led to a general deterioration in aircraft lateral characteristics. The lateral oscillation, which may be initiated by gusts during turbulent weather or by sideslip induced when making small corrections to course, is a complex motion which may be both tiring and difficult to control. At the lower speeds used during the landing flare, poor lateral behaviour may also prove to be a more realistic limit to touch down speed than a speed margin over the conventional stall.

The importance of the lateral oscillation in aiming flight at high speed has been recognized for some time and the theory of the motion is well advanced. The behaviour of the aircraft may therefore be accurately predicted, either by numerical analysis or by an analogue computer, provided that the aerodynamic derivatives and the moments of inertia of the aircraft are known. In the early stages of design this information is necessarily supplied by wind tunnel tests or estimation, but it is very desirable that it should later be checked by flight measurement, so that confidence can be placed in these early design procedures.

The lateral stability derivatives may be most easily measured in flight if some means exists for measuring the rolling and yawing moments produced by the controls. In most aircraft this is not possible and initial assumptions of values for the control powers, based on wind tunnel measurement or estimates, have to be made before the derivatives can be deduced from the flight tests. In the Avro 707B special provision had been made for carrying asymmetric ballast weight in the wings and for streaming a parachute from either wing tip. Once the control powers had been measured against these applied moments, several of the derivatives could be found by measuring the control deflections during steady lateral manoeuvres.

Wherever possible the flight measurements have been compared with the results of wind tunnel tests and with estimates. Flight measurement of the characteristics of the lateral oscillation have also been compared with estimates of these characteristics based on the exact solution of the equations of motion. These exact solutions have then been compared with the results from approximate relationships which are often used for rapid calculation.

A brief summary of pilot opinion of the lateral characteristics of the aircraft has been included so that the significance of the numerical results in terms of pilot handling may be assessed.

The tests described in this report form part of a comprehensive low speed investigation of the Avro 707B. The general handling characteristics of the aircraft, together with measurements of the lift and drag, are presented in Part 1[1]; measurements of the longitudinal stability and control are described in Part 2[2] and the results of flow visualization and some miscellaneous tests will be presented in Part 4[8].

2 DESCRIPTION OF THE AIRCRAFT

The Avro 707B was one of a series of 1/3rd scale research aircraft built to give aerodynamic and handling experience of the tailless delta configuration in support of the design of the Avro Vulcan bomber. It was a single seat aircraft powered by one Rolls Royce Derwent VIII turbo jet engine mounted in the fuselage and having the intake in the dorsal position ahead of the fin. This was not the intake arrangement which was to be used on the bomber aircraft, but it was chosen for simplicity on the Avro 707B which was primarily intended for low speed investigations.

A fuller description of the aircraft is given in Part 1[1] of this series of reports; the principal dimensions are provided in Table 1 and a general arrangement drawing and photographs are reproduced in Figs.1 and 2.

The delta shape of the wing planform had been slightly modified by sweeping back the trailing edge of the ailerons to provide increased aileron chord. The sweepback on the wing quarter chord line was 44.5°, the thickness chord ratio 10% and the wing taper ratio 0.04. Control was provided by separate ailerons and elevators mounted along the wing trailing edge, and by a conventional fin and rudder. Landing flaps were not fitted. Air brakes could be extended above and below the wing and the tests in the landing configuration were made with these brakes out; their position on the wing upper surface may be seen in Fig.2, in which the starboard brake is slightly raised.

3 INSTRUMENTATION

General details of the comprehensive instrumentation carried in this aircraft are given in Ref.1. The special apparatus - wing weights and wing tip parachutes - which were used when measuring the rolling and yawing moments due to the ailerons and rudder, are described in Appendix A.

The control surface angles and the measurements of the remote reading instruments were transmitted by Desynn position indicators to an auto-observer panel which was photographed six times per second. The rates of roll and yaw about the datum axes of the aircraft were measured by spring constrained rate gyros. The angle of sideslip was measured by an R.A.E. Mk.2 wind vane, mounted on the boom ahead of the fuselage which also carried the pitot static head; position error corrections for the readings of this head were taken from Ref.1.

4 RANGE OF THE INVESTIGATION

Most of the flight tests were carried out over the speed range 250 knots to 105 knots in the cruising configuration and 160 knots to 110 knots in the landing configuration; the higher speed was determined by the structural limitations of the aircraft when flying with wing weights and wing tip parachutes and the lower speed by the handling of the aircraft. These speeds correspond to a range of trimmed lift coefficient from $C_L = 0.12$ to $C_L = 0.65$ and to a range of Reynolds number, based on the wing aerodynamic mean chord, from 13.8×10^6 to 35×10^6.

The tests in the landing configuration, with the undercarriage down and the airbrakes extended, could not be carried to such high lift coefficients as those reached in the cruising configuration owing to the inferior handling of the aircraft in this condition at low speeds.

In some of the dynamic tests the lateral inertia of the aircraft was artificially increased by loading ballast weights in both wings. The changes in the inertia coefficients produced by this loading are shown in Fig.49; the rolling moment of inertia was increased by 60% and the yawing moment of inertia by 17%.

The weight of the aircraft and the cg position varied slightly with the consumption of fuel and with changes in the ballasting, but the results have been converted to a mean weight of 8700 lb (9500 lb for the tests with the increased inertia) and to a cg position of 0.320 $\bar{c}$.

All the tests were made at 10000 feet and at the power setting required for trimmed level flight.

In forming the aerodynamic derivatives, the wing area based on the apex definition has been used and the results are presented with reference to 'wind-body' axes - axes which move with the body but which are orientated in it along the wind direction in steady trimmed flight.

The wind tunnel measurements with which the flight results have been compared were made by Messrs. A. V. Roe & Co. on a 1/8th scale model and are reported in Refs.3 and 4. The condition of the model corresponded to the cruising configuration of the flight tests and the Reynolds number, based on the wing aerodynamic mean chord was, 1.88×10^6. The results of the tunnel tests have been converted to the apex wing area definition and to the flight cg position (0.320 $\bar{c}$).

5 RESULTS

Measurements of the rolling and yawing moments due to the controls are given in section 5.1, measurements of the sideslip derivatives ℓ_v, n_v and y_v in section 5.2 and of the rolling derivative ℓ_p in section 5.3. Measurements of the characteristics of the lateral oscillation and pilot opinion of the lateral behaviour of the aircraft are given in sections 5.4 and 5.5. A comparison with the appropriate wind tunnel and theoretical work is given in each section.

Flight measurements of the variation of lift and drag with incidence for the aircraft in the cruising configuration, taken from Ref.1, are reproduced in Fig.3. Extension of undercarriage and airbrakes led to a reduction of about 10% in the trimmed lift curve slope.

5.1 The control powers

5.1.1 The aileron rolling power

The aileron rolling power has been measured by finding the control angles needed to trim the aircraft when flying with an asymmetric ballast weight mounted in one wing. Details of the flight test technique and methods of analysis are described in Appendix A. The tests were made over the speed range from 250 knots to 95 knots (160 knots to 100 knots in the landing configuration), corresponding to a range of trimmed lift coefficient from $C_L = 0.12$ to $C_L = 0.76$. At all but the lowest speed the aileron power was measured over the available range of sideslip, and the tests were repeated with different asymmetric loadings to examine the variation of control power with control angle.

Typical measurements of the aileron and rudder angles to trim for various asymmetric ballast loadings are plotted against sideslip in Figs.4 and 5. Examination of the results at different angles of sideslip and for different applied rolling moments showed that the rolling power was independent of

sideslip over the range tested ($\beta = \pm 7.5^{\circ}$) and increased linearly with control angle ($\xi = \pm 12.5^{\circ}$). Similar sets of results were obtained for each of the speeds tested.

The variation of the aileron rolling moment coefficient, ℓ_{ξ}, with lift coefficient is shown in Fig.6.

The slight reduction in the aileron power which was measured at the lower lift coefficient was found to be consistent with the predicted effects of aeroelasticity at the higher test airspeeds.

The changes in aileron power which occurred at high lift coefficient were associated with the onset of flow separation over the outer parts of the wing. Flow visualization studies, which will be fully described in a later report[8], have shown that the flow separation developed in a way which is typical of this type of delta planform of moderate thickness-chord ratio. An area of detached flow over the outboard wing sections was divided from the attached region inboard by a clearly defined boundary which lay roughly chordwise across the wing. This boundary moved progressively inboard as the incidence was increased, as shown in Fig.7, where the position at which the boundary crossed the trailing edge is plotted against lift coefficient. The lift coefficients at which the separation boundary reached the outboard end of the aileron and that at which half of the aileron span was covered by separated flow are also shown on the curve of aileron rolling coefficient, Fig.6. The aileron power was progressively reduced as the separation boundary moved over the outer half of the ailerons and it had fallen by about 25% when the boundary reached the aileron mid span position, but further inboard movement caused little reduction in rolling power.

The measurements in the landing configuration showed a slight, but consistent, reduction over those in the cruising configuration. This is thought to be due to changes in the spanwise lift loading when the undercarriage and airbrakes were extended; at high lift coefficients, Fig.7 shows that the separation boundary was further inboard at a given lift coefficient in the landing configuration and this was associated with a greater incidence[1].

The accuracy of the measurements is thought to be within ±5%, except for the tests at the lowest lift coefficient, $C_L = 0.125$, where the aileron deflections needed to balance the applied rolling moment were small, and at the highest lift coefficient, $C_L = 0.76$, where the snatching of the controls due to flow separation made accurate trimming difficult.

Estimates of the aileron rolling moment coefficient have been made using the Data Sheets issued by the Royal Aeronautical Society and these are compared in Fig.8 with the results of the wind tunnel tests[3] and with the flight measurements. Initially it was found that large discrepancies existed between the tunnel and flight results, but these may be explained by differences between the model and the aircraft and by different flow conditions. The geared balance tabs which were fitted to the full scale ailerons and which may be seen in Figs.1 and 2, were not represented on the model. It is also known from smoke flow tests that the aileron gaps in part of the flight range were effectively unsealed. Estimates based on the R.Ae.Soc. Data Sheets showed that the geared tabs would lead to a reduction in aileron power of about 10%, and that unsealing the aileron gaps would reduce the aileron power by 5%. Simple estimates of the effects of aeroelastic distortion, based on the factor $1 - \left[\frac{V}{V_R}\right]^2$, and using design estimates of the aileron reversal speed, V_R, showed that a further reduction in aileron power of the order of 10% at 140 knots was to be expected and these estimates also predicted the measured reduction in rolling power at the higher test airspeeds with reasonable accuracy.

The tunnel measurements, when modified for the effects of the geared tabs and aeroelasticity, are in satisfactory agreement with the flight results, whilst the estimates, which included the same allowances for the tabs and aeroelasticity but were made for the ailerons with unsealed gaps, agree well with the flight results. The reduction in the aileron power due to wing flow separation is seen to occur at a lower lift coefficient in the tunnel than in flight; the earlier separation at the lower Reynolds number of the tunnel test was also shown in a comparison (Fig.7), of the results of tunnel flow visualization tests with flight results.

5.1.2 The aileron yawing moments

Some measurements of aileron yawing moments were made during the same series of tests, the test method being described in Appendix A. The variation of the aileron yawing moment coefficient, n_ξ, with lift coefficient is shown in Fig.9.

At the higher speeds the changes in rudder angle to trim with various applied rolling moments were too small to be detected and no reliable results were obtained. At the lower speeds, where the changes in rudder angle became appreciable, the flight and tunnel measurements were in good agreement, Fig.10.

It might have been expected however, that the earlier flow separation in the tunnel tests would have led to larger adverse yawing moments.

5.1.3 The rudder yawing power

The rudder yawing power has been measured by finding the control angles needed to trim the aircraft when flying with a small parachute attached to one wing tip. Details of the equipment used in these yawing tests, the flight test techniques and the methods of analysis are given in Appendix A.

The tests were made over the speed range 250 knots to 105 knots (160 knots to 110 knots in the landing configuration) corresponding to a range of trimmed lift coefficient from $C_L = 0.12$ to $C_L = 0.65$. The rudder power was measured over the available range of sideslip and the tests were repeated with different sizes of parachute to examine the change in control power with control angle.

Typical measurements of rudder and aileron angles to trim, plotted against sideslip for various applied yawing moments, are shown in Figs.11, 12 and 13. Examination of the results at different angles of sideslip and for different applied yawing moments showed that the yawing power was independent of sideslip over the range tested ($\beta = \pm 7.5^{\circ}$), and that the yawing moment produced by the rudder increased linearly with control angle ($\zeta = \pm 15^{\circ}$). Similar sets of results were obtained at each of the speeds tested.

The non-linearity of the curve of rudder angle against sideslip at the higher lift coefficient shown in Figs.12 and 13 was found to be due to a variation in the yawing moment derivative n_v with sideslip (see section 5.2.2).

The variation of the rudder yawing moment coefficient, n_ζ, with lift coefficient is shown in Fig.14. The yawing power remained constant over the range of speed and lift coefficient tested, and it was not affected by extension of the airbrakes or undercarriage.

The accuracy of the measurements is thought to be within ±5% - the major sources of inaccuracy lay in assessing the magnitude and direction of the loading applied by the parachute when it was spinning in the wing tip vortex or in a region of separated wing flow.

The agreement between the flight results and the tunnel measurements, shown in Fig.15, is good over the whole test range. The tunnel tests, which were extended to higher incidences than were possible in flight, showed that the rudder power was maintained up to very high incidence.

5.1.4 The rudder rolling moment

It was not possible to measure the rolling moment exerted by the rudder during these tests, (for instance by measuring the aileron angles to trim), since unknown extraneous rolling moments were caused by the wing tip parachute. Estimates of the rudder rolling moment coefficient, ℓ_ζ, derived from the measured yawing coefficients by assuming a centre of pressure for the fin and rudder, are shown in Fig.16. The estimates are in poor agreement with the wind tunnel measurements but this is probably due to errors in estimating the position of the centre of pressure; wind tunnel tests on the isolated fin and fuselage have shown that the wing interference effect on the fin centre of pressure position was large but this was not allowed for in the estimates.

5.2 The stability derivatives due to sideslip

The rolling and yawing moments due to sideslip have been found from measurements of the control angles needed to hold the aircraft in steady non-turning sideslips, since the rolling and yawing moments applied by these control angles could be calculated from the results given in section 5.1. The sideforce due to sideslip was calculated from measurements of the angle of bank developed during the sideslips by considering the equilibrium of the lateral forces acting on the aircraft. These measurements and calculations are described in greater detail in Appendix A. The measured aileron, rudder and bank angles are plotted against sideslip in Figs.17-22.

5.2.1 The rolling moment due to sideslip

The linear increase of aileron angle with sideslip showed that the rolling derivative, ℓ_v, was independent of sideslip over the range tested ($\beta = \pm 10^\circ$), since ℓ_ξ did not vary with aileron angle. The variation of ℓ_v with lift coefficient is shown for the cruising and landing configurations in Fig.23; extension of airbrakes and undercarriage led to a slight increase in $-\ell_v$. The reduction in $-\ell_v$ which occurred at high lift coefficient was presumably due to the onset of flow separation at the wing tips.

The accuracy of the measurements is thought to be within ±5% except at the highest lift coefficient, where the effects of flow separation made trimming the aircraft difficult, and at low lift coefficient where the measurements of aileron power were not sufficiently accurate.

The flight measurements are compared with the wind tunnel results[4] and with estimates based on the R.Ae.Soc. Data Sheets in Fig.24. The numerical

agreement between flight and tunnel measurements is good at the lower lift coefficients, but the earlier flow separation at the tunnel Reynolds number leads to an earlier divergence from the linear relationship between ℓ_v and C_L. Comparison of the slopes of the curves of ℓ_v against C_L in the attached flow regime show rather poor agreement. The slope predicted by the estimates, also shown in Fig.24, is in general agreement with that of the tunnel results, but there is a discrepancy in the values at zero lift. Wind tunnel tests on the isolated body[5] have shown that the effects of wing-body interference may be large.

5.2.2 The yawing moment due to sideslip

The linear relationship between rudder angle and sideslip at low lift coefficient showed that the yawing derivative, n_v, was independent of sideslip over the range tested ($\beta = \pm 10^\circ$), since n_ζ was also constant with rudder angle. At high lift coefficient however, the relationship between rudder angle and sideslip was no longer linear, Figs.19 and 20. Since n_ζ remained constant with rudder angle, these non-linearities indicated a reduction in n_v at small angles of sideslip. Local values of n_v at angles of sideslip $\beta = 0$, $\beta = 5^\circ$ and $\beta = 7.5^\circ$ have therefore been calculated. The changes of n_v with sideslip at high lift coefficient are not fully understood; they are confirmed however by pilots' reports of the handling of the aircraft (see section 5.6).

The variation of n_v with lift coefficient for the cruising and landing configurations is shown in Fig.25; extension of the airbrakes and undercarriage led to a 10% reduction in the value of the derivative.

The accuracy of the measurements is thought to be within ±5% except at the highest lift coefficients.

For comparison with the measurements made in steady sideslips, values of n_v have also been calculated from flight measurements of the period of the lateral oscillation. The dependence of the period on the value of the derivative is given by the approximate relationship.

$$T = \frac{2\pi s}{V}\sqrt{\frac{\mu_2}{\left(\frac{n_v}{i_C} + \frac{i_E}{i_C}\frac{\ell_v}{i_A}\right)}}$$ of Ref.6.

It is shown in section 5.5 that this relationship gives results in very close agreement with those obtained by exact solution of the equations of motion.

The values of n_v given by the two flight test techniques are compared in Fig.26. The discrepancy between them is rather large but it is thought to be due, in part at least, to errors in the estimation of the lateral inertia coefficients - the difference would be accounted for, for example, by a 20% error in the estimation of the yawing inertia.

The flight measurements are compared, in Fig.26, with the results of wind tunnel tests[4] and estimates based on the R.Ae.Soc. Data Sheets. Both tunnel tests and estimates are in good agreement with the results of the sideslipping tests, but in the case of the estimates this is felt to be largely fortuitous, since the estimate is formed from several conflicting contributions, each having large interference terms. The tunnel measurements failed however, to show the variation in n_v with sideslip at high lift coefficients which was found in flight.

5.2.3 Sideforce due to sideslip

The calculations of the sideforce derivative y_v, which depends largely on measurements of the angle of bank, are of limited accuracy (±10%) owing to difficulty in measuring the small angles involved with sufficient precision. The variation of y_v with lift coefficient is shown for the two configurations in Fig.27; extension of the undercarriage and airbrakes led to an increase in y_v of 20%.

The flight measurements are compared with the results of wind tunnel tests[4] in Fig.28. The agreement is not particularly good, probably because of the limited accuracy of both flight and tunnel measurements.

5.3 The rolling moment due to rate of roll, ℓ_p

The damping derivative in roll, ℓ_p, was found by considering the equilibrium of the rolling moments which acted on the aircraft when the ailerons were rapidly applied and then held fixed in the displaced position. The tests were made over a speed range from 250 knots to 120 knots and at the higher speeds the motion rapidly subsided into an almost steady rate of roll. Under these conditions the rolling power of the ailerons, which had already been measured by the tests with asymmetric wing weights (section 5.1), formed the major term in the equations of equilibrium. At the lower airspeeds the aircraft's rolling motion became more complicated, since the increased adverse yawing power of the ailerons (section 5.1.2), combined with lateral accelerations produced by the aircraft's weight, led to large angles of sideslip which, at the

lowest speeds, dominated the motion. Under these conditions a steady rate of roll was not achieved and it was necessary to take account of the moments produced by sideslip and rate of yaw in the analysis (see Appendix A, section 6). A time history of a roll at the lowest airspeed tested, showing the fluctuation in rate of roll as the sideslip varied, is reproduced in Fig.29.

The measurements of ℓ_p were made over the speed range 250 knots to 120 knots (160 knots to 125 knots in the landing configuration) corresponding to a range of lift coefficient from 0.125 to 0.50. The results of tests which were made using half the available aileron travel were consistent with those using full aileron. The measurements were repeated when the lateral inertia of the aircraft had been increased by mounting ballast weights in the wings and the results of the tests at both normal and increased inertia were used in calculating the damping derivative ℓ_p. It will be seen from Fig.36 that consistent results were achieved from both sets of tests, except at high lift coefficients where rapid changes in the angle of sideslip made the rolling motion unsteady. In this analysis it has been assumed that the rolling moment applied by the ailerons during the roll was the same as that measured statically. In practice the rolling effectiveness would be affected at high incidence by the changes in incidence produced by the rolling motion and this assumption is not strictly valid.

For comparison with the results obtained from the aileron rolling tests, calculations of ℓ_p were made from flight measurements of the roll-yaw amplitude ratio of the lateral oscillation. Values of ℓ_p were found, by trial and error, which satisfied the relationship for roll-yaw ratio obtained in Ref.6 by approximate factorization of the stability quartic. The two sets of results, which are compared in Fig.36, are in good agreement at low lift coefficient, but show opposite trends at high lift coefficient where the oscillatory value for ℓ_p tends to fall and that derived from the steady rolls to rise. Since the results from the rolling tests are suspect at the high lift coefficients and the reduction in ℓ_p at high lift coefficient shown by the oscillatory tests is consistent with the effect of wing tip flow separation, the latter results have been used in performing the stability calculations described in section 5.6.

Wind tunnel measurements of ℓ_p were not available for comparison with the flight results, but estimates based on the charts issued by the Royal Aeronautical Society are shown in Fig.36.

Measurements of the rolling helix angle, pb/2V, per unit aileron angle, have been plotted against trimmed lift coefficient in Fig.31. This is a parameter which has been much used in the past as a measure of aircraft rolling performance, but its practical significance diminishes where sideslip can build up and affect the rate of roll. (The rates of roll used in forming the helix angles shown in Figs.31 and 32 were the initial peak rates.) The helix angles measured on the aircraft with increased lateral inertia are shown in Fig.32; the reduction in the rate of roll in the latter case was due to the larger angles of sideslip attained because of the higher response time of the high inertia aircraft.

The time taken for the aircraft to bank through ten degrees after the sudden application of aileron, a parameter recently advocated as being of greater value than the rolling helix angle in assessing aircraft rolling performance at low speeds, is shown in Figs.33 and 34. Pilot opinions of the aircraft's rolling performance are discussed in section 5.6.

The rolling acceleration produced by the ailerons has been measured by the criterion of the effective time lag proposed in Ref.9. This lag is defined as the difference in time between the actual initial movement of the control and the time at which the measured steady rolling motion would have started if the rate of roll had been developed instantaneously. It depends therefore both on the speed with which the ailerons are applied and on the inertia and damping of the aircraft. For the test results shown in Fig.35 the mean time to apply the ailerons was 0.4 seconds. The increase in time lag when the rolling moment of inertia was increased by 60% may be clearly seen in Fig.35.

5.4 The lateral oscillation - flight measurements

Measurements of the characteristics of the lateral oscillation over the speed range 250 knots to 110 knots (175 knots to 110 knots in the landing configuration) were made at 10000 feet. The motion was initiated from trimmed level flight by a rapid displacement and recentralization of the rudder; in most of the tests the controls were then held fixed in their neutral positions, but a few measurements were made to examine the effect of freeing the controls.

The features of the oscillation which are most apparent to the pilot - period, damping and roll to yaw amplitude ratio - are shown in Fig.37. The phase angle between the rolling and yawing motion, which is a parameter of

importance in the analysis of the oscillation, is also shown in Fig.37. Pilot opinion of the effect of the oscillation on aircraft handling is reported in section 5.6.

The period of the oscillation became longer as the airspeed decreased, being about 2.5 seconds at 250 knots and 3.5 seconds at the normal approach speed of 120-125 knots. The damping remained fairly constant between 250 knots and 140 knots, (log dec = 0.45), but at slower speeds the damping increased reaching a log dec of 0.60 at the approach speed. These values of damping would be increased by about 15% for the aircraft operating at sea level. The rolling to yawing amplitude ratio increased with reducing airspeed from $|p/r|$ = 2.1 at 250 knots to $|p/r|$ = 3.4 at 115 knots.

Extension of the undercarriage and airbrakes had no effect on the oscillation within the accuracy of the measurements.

The effect of freeing the controls was not examined in detail but a few results are shown in Fig.39. Freeing the rudder alone appeared to increase the damping of the oscillation but the damping with all the controls free was similar to that with the controls fixed.

The lateral inertia of the aircraft could be increased by mounting 450 lb ballast weights internally in both wings at 77% of the semispan. In this way the rolling moment of inertia was increased by 60% and the yawing moment of inertia by 17%. Measurements of the characteristics of the lateral oscillation with this loading are shown in Fig.38. Comparison with the measurements made with the normal inertia show that the damping was roughly halved throughout the speed range, the period slightly increased and the roll-yaw ratio was unaltered. These effects are discussed in section 5.5.

5.5 The lateral oscillation - comparison with theory

The flight measurements of the characteristics of the lateral oscillation have been compared with those obtained by exact solution of the equations of motion using an electrical analogue computer. The equations of motion were those for the rigid aircraft and were based on the conventional assumptions of linear derivatives and small disturbances. The work was hampered by an inadequate knowledge of the rotary derivatives, ℓ_r, n_r and n_p, and by the reliance which had to be placed on estimates for the inertia coefficients of the aircraft. Flight data, derived from the tests described in sections 5.2 and 5.3, were used for the sideslip derivatives ℓ_v, n_v and y_v, and for the

rolling derivative ℓ_p. The validity of the use of static measurements of the sideslip derivatives in calculations of the oscillatory motion has been examined in several wind tunnel tests; these have shown that the static values may only be used with confidence when the wing flow is completely attached. As explained in section 5.3, the value used for ℓ_p at high lift coefficient was itself derived from flight measurements of the roll-yaw ratio of the lateral oscillation. Its use in making estimates of the characteristics of the oscillation which are to be compared with the flight measurements is therefore open to criticism. However it is justified on the grounds that this derivative has only a second order effect on the period and damping of the oscillation. For the remaining derivatives ℓ_r, n_r and n_p, and for the inertia coefficients i_A, i_C and i_E reliance has had to be placed on estimates. The assumed variation of these with lift coefficient is shown in Fig.49.

The same data as that used in the stability calculations has been substituted in several of the approximate relationships which are sometimes used for rapid calculation, so that their validity may be verified. Vector diagrams representing the motion have also been drawn so that relative importance of the contributions made by various terms in the equations may be examined. Finally the effects of the increase in lateral inertia tested in flight have been calculated for comparison with the flight measurements.

The measurements of the period of the oscillation are compared with the estimates in Fig.40. The values given by exact solution of the equations of motion are in reasonable agreement with the measurements over the range of lift coefficient. The agreement between the exact solution and the approximate relationship 'A' which was derived in Ref.6:-

$$T = \frac{2\pi s}{V}\sqrt{\frac{\mu_2}{\frac{n_v}{i_C} + \frac{i_E}{i_C}\frac{\ell_v}{A}}} \quad \text{sec}$$

is seen to be very good. Since flight data was used for the aerodynamic derivatives n_v and ℓ_v it seems probable that the slightly longer period given by the estimates was due to errors in calculating the inertia coefficients. The discrepancy would be accounted for by an overestimate of 20% in the yawing moment of inertia.

Approximation 'B':-

$$T = 2\pi\hat{t}\sqrt{\frac{i_C}{\mu_2 n_v}}$$

in which the rolling motion of the oscillation is neglected, is in fair agreement with the exact solution at low lift coefficients, but diverges rapidly at the higher lift coefficients when the rolling and product of inertia terms become important.

The flight measurements of the damping of the oscillation are compared with the estimates in Fig.41. Except at the lowest lift coefficients the agreement between the measured results and those predicted by exact solution of the equations of motion is poor. Analysis of the motion by the time vector method, which is described below, showed, however, that the damping, which depended primarily on the derivative n_r at the low lift coefficient, became increasingly dependent on terms containing the derivative n_p and the product of inertia as the lift coefficient was increased. Since reliance has had to be placed on estimation for each of the parameters n_r, n_p and i_E, the lack of agreement is perhaps not surprising.

Despite the lack of numerical agreement between the estimates and the measurements, the analysis of the motion by the time vector method will be described in some detail, since it gives a valuable insight into the relative importance of the various contributions. The principles of the time vector method have been described in Ref.7.

Vector diagrams of the oscillation for the normal and for the increased inertia conditions at lift coefficients, $C_L = 0.2$ and $C_L = 0.4$ are given in Figs.45 to 48. The damping of the oscillation is proportional to the tangent of the damping angle, ϵ_D, which is shown in the yawing moments diagram of each set of figures. It will be seen that this damping angle consists of the apex angle of the yawing moments polygon, modified by the small phase angle ϵ_ψ. ϵ_ψ is determined by the sideforce polygon which is, in turn, dependent upon the rolling moment diagram.

For $C_L = 0.20$ and normal inertia, Fig.45, the apex angle of the yawing moments diagram is determined primarily by the $\frac{n_r}{i_C}\dot{\psi}$ vector; the small

contributions due to $\frac{n_p}{i_C}\dot{\phi}$ and $\frac{i_E}{i_C}\ddot{\phi}$ being of similar magnitude and opposite sense. The phase angle, ε_ψ, also contributes to the damping.

In the diagrams for the same lift coefficient ($C_L = 0.20$) but increased inertia, Fig.46, the apex angle of the yawing moments diagram is almost identical, but the favourable damping contribution of the phase angle, ε_ψ, has been lost. This may be traced to the sideforces diagram where clockwise rotation of the C_L ϕ vector has eliminated the angle ε_ψ. The rotation of the ϕ vector may in turn be traced to the rolling moments diagram where the increased magnitude of the inertia ($\ddot{\phi}$) vector, due to the increased lateral inertia, can only be accomplished by clockwise rotation of the $\dot{\phi}$, $\ddot{\phi}$ (and thus ϕ) vectors.

Fig.47 shows the vector diagrams for the normal inertia aircraft at a lift coefficient, $C_L = 0.4$. The non-dimensional circular frequency, ω, of the motion has increased and the phasing diagram shows the increased importance of the acceleration and rate vectors compared with the displacement vectors. In the yawing moments diagram the contribution of the $\frac{n_r}{i_C}\psi$ vector to the size of the apex angle is similar to that at the lower lift coefficient, but it is now overshadowed by the much increased damping contribution of the product of inertia term, $\frac{i_E}{i_C}\ddot{\phi}$. This stems from the increased inclination of the aircraft principal axes to the wind axes due to the larger wing incidence. The contribution of the phase angle ε_ψ has now become unfavourable and this may be traced in the sideforce diagram to the increase in the length of the C_L ϕ vector at the higher lift coefficient.

The diagrams for the increased inertia condition at lift coefficient, $C_L = 0.40$ are shown in Fig.48. As with the case at the lower lift coefficient, the damping is affected by the clockwise rotation of the ϕ, $\dot{\phi}$ and $\ddot{\phi}$ vectors which is dictated by the rolling moments diagram. This both increases the phase angle ε_ψ in the undamping sense and also rotates the important $\frac{i_E}{i_C}\ddot{\phi}$ vector in the yawing moments diagram so as to reduce the apex angle.

The vector diagrams underline the complexity of the damping at high lift coefficient and show the difficulty of producing a simplified relationship. The results obtained by substitution in the approximate relationship 'C':

$$\delta = -\pi\sqrt{\frac{i_C}{\mu_2\, n_v}}\left(\frac{n_r}{i_C} + y_v\right)$$

are compared with the flight measurements and solution of the exact equations of motion in Fig.41. Comparison with the vector diagrams shows the approximations which are involved in the relationship 'C'. The term n_r/i_C corresponds to the apex angle of the yawing moments diagram, so that the effects of the $\frac{i_E}{i_C}\ddot{\phi}$ and $\frac{n_p}{i_C}\dot{\phi}$ terms are ignored. The second term, y_v, represents the phase angle ε_ψ, and it will be seen from the sideforces diagram that the important term, $C_L\,\phi$, has been omitted. Lastly, the circular frequency has been approximated by a simplified relationship corresponding to Case B in Fig.40.

Fig.41 shows that the simplified relationship 'C' gives values of the damping which are too high at low lift coefficient and this is due primarily to the omission of the term $C_L\,\phi$ in the side forces equation, so that the favourable damping contribution of the phase angle ε_ψ is overestimated. At high lift coefficient the damping given by 'C' is too low and this is due to the omission of the $\frac{i_E}{i_C}\dot{\phi}$ term in the yawing moments equation, offset to some extent by the overestimation of the damping due to ε_ψ and the circular frequency of the oscillation.

The exact solution of the equations of motion have already been used to calculate the rolling derivative ℓ_p from flight measurements of the roll-yaw amplitude ratio of the oscillation (see section 5.3). Estimates of the roll-yaw ratio based on the approximate relationship 'D':

$$\left|\frac{p}{r}\right| = \frac{\ell_v}{\ell_p}\sqrt{\frac{\mu_2\, i_C}{n_v}}$$

are shown in Fig.42 and are good agreement with the flight measurements (and therefore with the exact theory) at low lift coefficients, but diverge rather rapidly at high lift coefficient. This is partly due to use of the approximate relationship for the circular frequency corresponding to Case B in Fig.40.

The estimates of the phase lag between the rolling and yawing motions are compared with the flight measurements in Fig.43. The discrepancies would again be resolved by a 20% error in the estimation of the yawing moment of inertia. At the time these tests were completed suitable equipment was not available for measuring the rolling and yawing inertia of the aircraft on the ground, but it is felt that these measurements should be considered an essential part of lateral stability testing.

5.6 Lateral manoeuvrability and handling characteristics

A general description of the handling characteristics of the aircraft has been given in Part 1 of this series of reports, but those topics which relate to the lateral handling of the aircraft, especially at and below the approach airspeed, are dealt with in more detail below.

The approach speed which was used in the normal flying of the aircraft - 120-125 knots on the approach, falling to 110 knots at touchdown - was dictated both by longitudinal and lateral handling. Below 115 knots problems of speed and flight path control due to the drag characteristics of the aircraft became apparent, whilst slight lateral snatching of the manually controlled ailerons, associated with the onset of flow separation at the wing tips, began at about 118 knots.

The various aspects of lateral handling are dealt with below.

The Ailerons. Pilots considered the ailerons to be both effective and responsive throughout the speed range used in normal flight. Lateral stick forces measured in aileron rolls are shown in Fig.30; they varied from light at low speeds to heavy at the higher speeds, so that full aileron travel could not be applied with one hand above about 250 knots.

The value of the rolling helix angle, $pb/2V = 0.045$, available on the approach using full aileron travel, was rather low by current standards and this was primarily due to the adverse effects of sideslip which are mentioned in section 5.3. Calculations based on the measured derivatives ℓ_p and ℓ_ξ showed that a helix angle $pb/2V = 0.075$, might have been expected in the absence of yawing effects. The unsteadiness of the rate of roll when rolling to large angles of bank is shown in the time history, Fig.29, and was most noticeable to the pilot when performing complete rolls at low speed.

The time to bank to 10^o (shown in Figs.33 and 34), which may be a better criterion of the rolling manoeuvrability when correcting disturbances due to gusts or when making small alterations to course, compares favourably with current standards. This is because this time depends more closely on the initial rolling acceleration of the aircraft and the adverse effects of sideslip do not have time to build up.

It is perhaps valuable to compare the rolling performance of the Avro 707B on the approach with that of the Meteor, a contemporary straight wing jet fighter aircraft, since the approach speed and rolling inertia coefficient of

the two aircraft were very similar. The performance of each aircraft is summarized in the table below.

Aircraft	Avro 707B	Meteor N.F.11
Approach speed	120 knots	120 knots
Wing span, b	33 feet	43 feet
Rate of roll due to full aileron. Sea level	32°/sec	28°/sec
$\frac{pb}{2V}$ for full aileron	0.045	0.051
Time to bank to 10° (measured at 10000 feet)	0.65 sec	0.75 sec

The response and effectiveness of the Meteor were considered to be only moderate in its night fighter role, and neither aircraft compared well with the performance of more recent swept wing aircraft (for instance, the F-86E with a rate of roll of 43°/sec, $pb/2V \approx 0.075$; and the Hunter, 65°/sec, $pb/2V = 0.084$).

Tests in which the rolling inertia of the aircraft was increased by 77% have been described in sections 5.3 and 5.4. Pilots noticed the slower response of the aircraft, shown in Fig.35 by the increase 'effective time lag', but found that this was offset to some extent by the reduced response of the aircraft to random disturbances.

The adverse yawing moments produced by the ailerons at the approach lift coefficient were too small to be appreciated. At the higher lift coefficient, where they were increasing rapidly with the wing tip flow separation, they did not excite comment, but this may have been due to the erratic yawing of the aircraft in this condition.

The behaviour of the ailerons at speeds below the normal approach speed is described below.

The Rudder. Pilots found that the rudder was effective and responsive over the normal range of flight speeds. At very low speeds however they found that the rudder control was poor. Since the flight measurements described in section 5.1 have shown that the rudder yawing moment derivative was constant over the whole speed range, this must be attributed to the natural reduction in control response with reduced airspeed.

Crosswind Landing. The aircraft was landed without difficulty in crosswind components of up to 18 knots at the normal approach speed. During test approaches at lower speeds it was found that with crosswind components of 12-14 knots speed could not be reduced below 100-105 knots, since almost full aileron control was needed to balance the rolling moment produced when the crosswind correction was made just before touchdown.

The Lateral Oscillation. Whilst commenting on the magnitude of the roll-yaw ratio of the lateral oscillation, which was considerably larger than that of contemporary straight wing aircraft, pilots found that the characteristics of the oscillation were acceptable when making normal airfield landings by day. The damping of the oscillation just attained the current A.P.970 standard (log dec = 0.69) at approach speeds, but fell below it at higher speeds. Pilots found it easy, however, to aid the damping by the use of ailerons.

No tests were made with the aircraft in bad weather so that the acceptability of the lateral oscillation under instrument approach conditions has not been assessed.

Flight at low airspeeds. The handling characteristics of the aircraft at speeds below the normal approached speed were dominated by the effects of the wing tip flow separation on the manually operated ailerons. The onset of flow separation was marked by slight snatching of the ailerons which began at about 118 knots (C_L = 0.5) and which became progressively more intense as the speed was reduced. At the lower speeds the ailerons became overbalanced. This behaviour was accompanied by erratic and intermittent wing dropping which could however be held by rapid, firm, aileron movements. The aileron response and effectiveness, although reduced, were still surprisingly good. Initially it was felt that the intermittent wing dropping might have been produced by the aileron snatching and overbalance, but later tests on the Avro 707A, which was fitted with irreversible power controls, showed similar characteristics.

At about 98 knots (C_L = 0.73) random yawing of the aircraft began, but this could be controlled by firm use of the rudder. As the speed was further reduced to 90 knots (C_L = 0.87) directional control became very poor and large movements of the rudder and ailerons were needed to keep the aircraft level. At the lowest speeds it was found to be impossible to hold the aircraft in the neutral sideslip position as it would rapidly yaw until it became stabilised at about 5° of sideslip in either direction. At these speeds however the aircraft could be held steadily at larger angles of sideslip where the directional 'wandering' and aileron snatching would largely disappear.

Comparison with the flight measurements of section 5.1.1 (Figs.6 and 7) shows that the initial snatching of the ailerons coincided with the movement of the separation boundary onto the outer end of the aileron. Fig.6 also shows that, even when the flow over most of the wing ahead of the ailerons was separated, the aileron power had fallen by only 25%, so that the pilots reports of the satisfactory aileron effectiveness at low speeds were supported by the measurements.

The variation of the yawing moment derivative, n_v, with angle of sideslip at high lift coefficient has been mentioned in section 5.2.2. It will be seen from Fig.25 that, although no test measurements are available at the highest lift coefficients, the 'wandering' motion of the aircraft above $C_L = 0.73$ would be explained by the reduced, or negative, directional stability at small angles of sideslip, whilst the ability to stabilise the aircraft at larger sideslip angles is also indicated.

6 CONCLUSIONS

Lateral control powers and stability derivatives have been measured over a range of lift coefficient from $C_L = 0.12$ to $C_L = 0.65$. Measurements of the aileron power were extended up to $C_L = 0.76$.

At the higher lift coefficients the aileron rolling power was progressively reduced as the wing tip flow separation covered the outer half of the aileron and this was accompanied by an increase in the adverse aileron yawing moments. The yawing moment coefficient continued to increase as the flow separation moved further inboard but the rolling power remained fairly constant. The yawing power of the rudder remained constant over the range tested. Wind tunnel measurements of the control powers were in reasonable agreement with the flight results when account was taken of the effects of aeroelasticity and of small discrepancies between the model and the aircraft.

At low lift coefficients the tunnel and flight measurements of ℓ_v and n_v were in reasonable numerical agreement, but the slopes of the curves of ℓ_v against C_L did not agree well. At high lift coefficients the lower Reynolds number of the tunnel tests led to an earlier reduction in $-\ell_v$ due to the earlier wing tip flow separation. The flight measurements at high lift coefficient also showed that n_v varied with the angle of sideslip, but this was not apparent in the tunnel tests.

The damping of the lateral oscillation was equal to the requirement of A.P.970 at the normal approach speed but fell below it at higher speeds. Pilots found that the characteristics of the lateral oscillation were satisfactory for the normal type of airfield landing by day and they were able to increase the natural damping by the use of the ailerons.

Estimates of n_v from the period the lateral oscillation were in poor agreement with the static measurements and this is thought to be due to errors in the estimation of the aircraft's moment of inertia. Estimates of the rolling derivative ℓ_p from the roll-yaw ratio of the lateral oscillation agreed well, at low lift coefficient, with the results from aileron rolls, but showed large differences at high lift coefficient where the rolling results were suspect.

Estimates of the period of the oscillation using flight measurements, where possible, for the lateral derivatives, were in reasonable agreement with the flight results. Estimates of the damping were in poor agreement with the flight measurements and this is thought to be due to the lack of accurate estimated values of the aircraft moments of inertia and of the rotary derivatives n_r and n_p.

Appendix A

FLIGHT TEST TECHNIQUES AND METHODS OF ANALYSIS

A.1 The aileron rolling power

In this aircraft special provision had been made for carrying lead ballast weights internally on either wing spar so that known rolling moments could be applied to the aircraft without altering its external shape. The rolling moment which may be applied by fixed out of balance weights is limited by the need to leave adequate aileron control for take-off and landing, and on this aircraft it was found that the pilot wished to have at least half the control travel remaining after he had trimmed the applied moment at the approach airspeed. This requirement limits the accuracy of the technique at high airspeeds where the aileron angles needed to trim the weight are small. The maximum asymmetric weight which could be carried was 430 lb on an arm of 12.6 ft. The weight was increased in several stages during the tests to examine the variation of the control power with control angle and also to familiarize the pilot progressively with the handling of the aircraft.

Each series of tests was made at the same indicated airspeed so that changes in the weight of the aircraft due to different ballasting and fuel loads led to variations in the operating lift coefficient. Since the important derivatives in the equation for rolling equilibrium varied with lift coefficient it was necessary to correct the measured aileron angles to a mean lift coefficient.

The largest corrections were of the order of 5% so that approximate values for the gradients $d\ell_v/dC_L$ and $d\ell_\xi/dC_L$ and for the aileron power could be used with sufficient accuracy in the relationship

$$\Delta\xi = -\frac{\Delta C_L}{\ell_\xi}\left[\beta\frac{d\ell_v}{dC_L} + \xi\frac{d\ell_\xi}{dC_L}\right].$$

Typical sets of curves for angles which have been corrected in this way are shown in Figs.4 and 5.

The equation for rolling equilibrium in a steady straight sideslip with an applied rolling moment M_1 may be written:

$$\ell_\xi\,\xi_1 + \ell_\zeta\,\zeta_1 + \ell_v\,\beta + \frac{M_1}{\rho V^2\,Ss} = 0$$

and for the same angle of sideslip without the applied rolling moment

$$\ell_\xi\,\xi_o + \ell_\zeta\,\zeta_o + \ell_v\,\beta = 0$$

so that for a given angle of sideslip and assuming that the rolling moment due to sideslip derivative, ℓ_v, is independent of aileron angle, the aileron rolling moment coefficient may be expressed by:

$$\ell_\xi = -\left[\frac{\ell_\zeta (\zeta_1 - \zeta_o)}{(\xi_1 - \xi_o)} + \frac{M_1}{\rho V^2 S s (\xi_1 - \xi_o)}\right]$$

where the gradients $\frac{\zeta_1 - \zeta_o}{\xi_1 - \xi_o}$ and $\frac{M_1}{\xi_1 - \xi_o}$ are most conveniently found by cross-plotting from the sets of results such as Figs.4 and 5. The rolling moment coefficient of the rudder, ℓ_ζ, was estimated from measurements made during the yawing tests (Appendix A, section A.4).

A.2 The aileron yawing moments

Measurements of the aileron yawing moment may be made from the same series of tests by observing the change in the rudder angle needed to trim as the ailerons were deflected to balance the applied rolling moment. The tests were made in level flight so that the asymmetric wing weights applied a pure rolling moment about the wind-body axis.

The equation of yawing equilibrium in a steady straight sideslip with the ailerons deflected to balance an applied rolling moment M_1 may be written:

$$n_\zeta \zeta_1 + n_\xi \xi_1 + n_v \beta = 0$$

and for the same angle of sideslip without the applied rolling moment

$$n_\zeta \zeta_o + n_\xi \xi_o + n_v \beta = 0$$

so that a given angle of sideslip and assuming the yawing moment derivative due to sideslip, n_v, is independent of the control positions

$$n_\xi = -\frac{n_\zeta (\zeta_1 - \zeta_o)}{\xi_1 - \xi_o}$$

where the gradient $\frac{\zeta_1 - \zeta_o}{\xi_1 - \xi_o}$ is most conveniently found by cross-plotting from the sets of results such as Fig.5. The yawing power of the rudder, n_ξ, was found from tests with a parachute streamed from one wing tip which are described in the next section.

A.3 The rudder yawing power

The measurements of the rudder power were similar in character to those of the aileron power, but the external yawing moment was applied by a small parachute attached to one wing tip. The parachute load was measured by the deflection of a spring and the direction in which it streamed by a wire 'finger' attached to the parachute chord; these measurements were displayed on the auto-observer by desynn position transmitters. The parachute could be streamed in flight by releasing a covering cap, but after the initial tests it was found more convenient to take off with the parachute already streamed. In most cases the parachute was jettisoned before landing, but on several occasions, under calm conditions, the aircraft was landed with the parachute in position. Four parachute sizes, 30 in, 25 in, 21 in and 17 in were used to provide a range of loading of 400 lb to 100 lb for test speeds between 250 knots and 105 knots. The attachment point of the parachute was 15.2 feet from the aircraft centre line, but the moment arm varied with the direction in which the parachute streamed.

Typical sets of measurements of the control angles needed to trim with various sizes of parachute are shown in Figs.11-13.

The equation of yawing equilibrium in a steady straight sideslip with an applied yawing moment M_2 may be written:

$$n_\zeta \zeta_2 + n_\xi \xi_2 + n_v \beta + \frac{M_2}{\rho V^2 Ss} = 0$$

and for the same angle of sideslip without the applied yawing moment

$$n_\zeta \zeta_o + n_\xi \xi_o + n_v \beta = 0$$

so that for a given angle of sideslip and assuming that the yawing moment due to sideslip derivative, n_v, is independent of the control positions.

$$n_\zeta = -\left[\frac{n_\xi (\xi_2 - \xi_o)}{(\zeta_2 - \zeta_o)} + \frac{M_2}{(\zeta_2 - \zeta_o)\, \rho V^2 Ss}\right]$$

where the gradients $\frac{\xi_2 - \xi_o}{\zeta_2 - \zeta_o}$ and $\frac{M_2}{\zeta_2 - \zeta_o}$ may be found by cross-plotting from the sets of results, Figs.11-13.

A.4 The rudder rolling moment

It was not possible to measure the rudder rolling moment directly by observing the changing aileron angles needed to trim with different applied yawing moments (and thus different rudder angles) because the parachute itself produced a rolling moment as it streamed in the downwash field behind the wing and the apparatus for measuring this stream angle could not readily be fitted. The rudder rolling moments have therefore been derived by estimating the fin and rudder loading from the measurements of the rudder yawing power and assuming a centre of pressure for this loading.

A.5 The stability derivatives due to sideslip

The stability derivatives due to sideslip have been measured by considering the equilibrium of the yawing moments, rolling moments and sideforces acting on the aircraft when it is flown in steady straight sideslips.

Rolling moments

$$\ell_v \beta + \ell_\xi \xi + \ell_\zeta \zeta = 0$$

Yawing moments

$$n_v \beta + n_\xi \xi + n_\zeta \zeta = 0$$

Sideforces

$$Y_v \beta + Y_\xi \xi + Y_\zeta \zeta + \tfrac{1}{2} C_L \phi = 0.$$

The rolling and yawing moments due to the controls ℓ_ξ, n_ξ, n_ζ have been measured from the tests with wing weights and parachutes. The gradients ξ/β, ζ/β and ϕ/β were measured from the sideslipping test results shown in Figs.17-22. The derivatives ℓ_ζ and Y_ζ were calculated from the flight measurements of the rudder yawing power, n_ζ, whilst the sideforce term due to aileron deflection $Y_\xi \xi$ was neglected.

Over most of the test range the control deflections increased linearly with sideslip but at high lift coefficients the rudder angle curves became non-linear. Local values for the gradient ζ/β were then used to calculate several local values for n_v at various angles of sideslip.

6 The damping in roll derivative ℓ_p

The equation for the rolling equilibrium of an aircraft in a steady roll due to constant aileron displacement may be written

$$\ell_\xi \xi + \ell_\zeta \zeta + \ell_v \beta + \ell_r \frac{rb}{2V} + \ell_p \frac{pb}{2V} = 0.$$

In practice the angle of sideslip and rate of yaw vary continuously during the manoeuvre so that the rate of roll is exactly constant only at specific instants during the motion. At high speeds, and in the absence of inertia cross-coupling effects, the angles of sideslip and the rate of yaw are small and a nearly constant rate of roll is achieved. At low speeds the slow rate of roll allows large amounts of sideslip to be built up by the lateral acceleration due to the aircraft's weight, whilst the effects of aileron adverse yaw are generally more severe. The former effect may be reduced by starting the roll from a banked turn and rolling towards the horizontal so that the aircraft is only slightly banked during its acceleration to a steady rate of roll. It has also been found possible for the pilot to reduce the angle of sideslip by moving the rudder during the roll, but this leads to larger rates of yaw and the measurements made in this way have been found to be less consistent than those made with the rudder fixed.

The measurement of ℓ_p given in Fig.36 were calculated from the gradients of the curves of

$$\left[\ell_\xi \xi + \ell_\zeta \zeta + \ell_v \beta + \ell_r \frac{rb}{2V}\right]$$

plotted against $\frac{pb}{2V}$, for a given lift coefficient, where the functions were evaluated from points during the roll when the rate of roll was constant.

Table 1

AVRO 707B, VX.790

PRINCIPAL DATA RELATING TO THE AIRCRAFT

Item		Value	Unit
WING			
Span		33	ft
Area (apex definition)		366.5	sq ft
Standard mean chord (apex definition)		11.11	ft
Aerodynamic mean chord		14.35	ft
Chord at aircraft centre line		21.67	ft
Tip chord		0.87	ft
Aspect ratio		2.97	-
Taper ratio		0.04	-
Sweepback of the leading edge		52.43	degrees
Sweepback of the $\frac{1}{4}$ chord line (inboard)		44.30	degrees
Sweepback of the $\frac{1}{4}$ chord line (outboard)		44.80	degrees
Sweepback of the trailing edge (inboard)		0	degrees
Sweepback of the trailing edge (outboard)		4.5	degrees
Dihedral		-0.85	degrees
Washout		0	
Wing-body setting		2.5	degrees
Thickness-chord ratio		10	per cent
Wing section		NACA 0010 (modified)	
AILERONS			
Total area (per aileron)		11.55	sq ft
Area aft of the hinge line (per aileron)		8.38	sq ft
Mean chord aft of the hinge line		1.26	ft
Span perpendicular to aircraft centre line		6.64	ft
Control chord ratio, inboard end		0.15	
Control chord ratio, mid		0.18	
Control chord ratio, outboard end		0.30	
Spanwise limits on aircraft		0.496 to 0.898	semispan
Type of balance		Set back hinge and geared tab	
Percentage balance		0.38	
Control gap (constant across span)		0.192	inches
Neutral setting		3° up to wing chord	
Range of aileron movement		±15	degrees
Stick gearing		0.555	rad/ft
Trailing edge angle (mean)		9.9	degrees
AILERON GEARED TAB			
Area of geared tab aft of hinge,	port	1.15	sq ft
	stbd.	0.97	sq ft
Geared tab span/aileron span	port	0.505	
	stbd.	0.391	
Tab chord/local aileron chord (constant)		0.25	
Tab gearing	port	0.91 : 1	
	stbd.	1.00 : 1	

Table 1 (Contd)

Item	Value	Unit
AILERON TRIM TAB		
Trim tab area aft of hinge	0.246	sq ft
Trim tab span/aileron span	0.092	
Trim tab chord/local control chord	0.25	
Angular movement	±9.5°	degrees
FIN		
Gross area (including fuselage below fin)	43.62	sq ft
Net area	27.76	sq ft
Dorsal fin area	6.41	sq ft
Height above aircraft datum line	7.71	ft
Mean body depth	3.3	ft
Mean chord	4.55	ft
Root chord (on aircraft datum)	7.5	ft
Tip chord	2.5	ft
Taper ratio	0.33	
Geometric aspect ratio	1.34	
Sweepback of the leading edge	49.4	degrees
Sweepback of the ¼ chord line	44.0	degrees
Sweepback of the trailing edge	27.4	degrees
Thickness chord ratio at fuselage size	9.1	per cent
Thickness chord ratio at tip (theoretical)	8.0	per cent
Airfoil section	NACA 0010 (modified)	
RUDDER		
Total area	9.26	sq ft
Area aft of the hinge	6.80	sq ft
Mean chord aft of the hinge	1.49	ft
Control chord ratio (mid)	0.32	
Span	4.57	ft
Spanwise limits (above aircraft datum)	2.14 to 6.71	ft
Percentage balance	0.362	
Control gap (constant across span)	0.25	inches
Trailing edge angle (mean)	8.0	degrees
Range of rudder movement	±15°	degrees
Rudder pedal gearing	0.871	rad/ft
RUDDER ANTI-BALANCE TAB		
Area aft of hinge	0.67	sq ft
Tab chord/local control chord	0.19	
Span	1.79	ft
Tab gearing (anti-balance)	0.71 : 1	
ELEVATORS		
For details of the elevators see Ref.1.		

Table 1 (Contd)

Item		Value	Unit
AIR BRAKES			
Gross area (including hinge arms)	upper	1.51	sq ft
	lower	2.21	sq ft
Net area	upper	1.13	sq ft
	lower	1.42	sq ft
Chord	upper	4	in
	lower	5	in
Angular deflection		60	degrees
MISCELLANEOUS			
Normal all up weight at take off		9600	lb
Mean all up weight for tests (normal inertia)		8700	lb
Mean all up weight (increased inertia)		9500	lb
Fuel capacity		225	gallons
Engine thrust line (to aircraft datum)		4^{o}	degrees

LIST OF SYMBOLS

Symbol	Definition	Units
A	moment of inertia about the 'wind-body' axis of x	slug-feet^2
A_o	moment of inertia about the 'principal' axis of x	slug-feet^2
b	wing span	feet
C	moment of inertia about the 'wind-body' axis of Z	slug-feet^2
C_o	moment of inertia about the 'principal' axis of Z	slug-feet^2
$\bar{c}$	wing aerodynamic mean chord	feet
E	product of inertia with reference to the 'wind-body' axes of x and Z	slug-feet^2
$i_{A_o} = \frac{A_o}{m s^2}$ $i_{C_o} = \frac{C_o}{m s^2}$	inertia coefficients w.r.t. 'principal' axes	-
$i_A = i_{A_o} \cos^2\varepsilon + i_{C_o} \sin^2\varepsilon$	inertia coefficient w.r.t. 'wind-body' axis of x	-
$i_C = i_{A_o} \sin^2\varepsilon + i_{C_o} \cos^2\varepsilon$	inertia coefficient w.r.t. 'wind-body' axis of Z	-
$i_E = i_{C_o} - i_{A_o} \sin\varepsilon \cos\varepsilon$	product of inertia coefficient	-
L_β	rate of change of rolling moment with angle of sideslip	lb-feet per radian
L_ξ	rate of change of rolling moment with aileron angle	lb-feet per radian
L_ζ	rate of change of rolling moment with rudder angle	lb-feet per radian
L_p	rate of change of rolling moment with rate of roll	lb-feet per radian per second
L_r	rate of change of rolling moment with rate of yaw	lb-feet per radian per second
$\ell_\xi = \frac{L_\xi}{\rho V^2 Ss}$	rolling moment coefficient due to aileron angle ('aileron power')	-
$\ell_\zeta = \frac{L_\zeta}{\rho V^2 Ss}$	rolling moment coefficient due to rudder angle	-

LIST OF SYMBOLS (Contd)

Symbol	Definition	Units
$\ell_p = \frac{L_p}{\rho V^2 Ss^2}$	rolling moment coefficient due to rate of roll	-
$\ell_r = \frac{L_r}{\rho V^2 Ss^2}$	rolling moment coefficient due to rate of yaw	-
$\ell_v = \frac{L_\beta}{\rho V^2 Ss} \equiv \frac{L_v}{\rho V Ss}$	rolling moment coefficient due to sideslip	-
M_1	rolling moment due to asymmetric wing weights	lb-feet
M_2	yawing moment due to a wing tip parachute	lb-feet
m	mass of aircraft	slugs
N_β	rate of change of yawing moment with angle of sideslip	lb-feet per radian
N_ξ	rate of change of yawing moment with aileron angle	lb-feet per radian
N_ζ	rate of change of yawing moment with rudder angle	lb-feet per radian
N_p	rate of change of yawing moment with rate of roll	lb-feet per radian per second
N_r	rate of change of yawing moment with rate of yaw	lb-feet per radian per second
$n_\xi = \frac{N_\xi}{\rho V^2 Ss}$	yawing moment coefficient due to aileron angle	-
$n_\zeta = \frac{N_\zeta}{\rho V^2 Ss}$	yawing moment coefficient due to rudder angle ('rudder power')	-
$n_p = \frac{N_p}{\rho V^2 Ss^2}$	yawing moment coefficient due to rate of roll	-
$n_r = \frac{N_r}{\rho V^2 Ss^2}$	yawing moment coefficient due to rate of yaw	-
$n_v = \frac{N_\beta}{\rho V^2 Ss}$	yawing moment coefficient due to sideslip	-
p	rate of roll about the 'wind-body' axis of x	radians/sec
r	rate of yaw about the 'wind-body' axis of Z	radians/sec

LIST OF SYMBOLS (Contd)

Symbol	Definition	Units
S	wing area	feet^2
s	$= \frac{b}{2}$ wing semi-span (the standard lateral unit of length)	feet
T	period of the short period lateral oscillation	seconds
$\hat{t}$	$= \frac{m}{\rho S V}$ the unit of aerodynamic time	-
V	true air speed	feet/sec
v	component of velocity along the y-axis	feet/sec
W	weight of aircraft	lb
Y_β	rate of change of sideforce with angle of sideslip	lb per radian
y_v	$= \frac{Y_\beta}{\rho V^2 S} \equiv \frac{Y_v}{\rho V S}$ sideforce coefficient due to sideslip	-
α	wing incidence	radians
β	angle of sideslip	radians
δ	logarithmic decrement of the short period lateral oscillation	-
ε	angle between the principal x-axis of the aircraft and the 'wind-body' axis of x	-
ε_D	damping angle of the short period lateral oscillation (see section 6)	-
ε_ψ	phase angle between rolling and sideslipping motions of the short period lateral oscillation	-
ε_p	phase angle between the rolling and yawing moments of the short period lateral oscillation	-
ζ	rudder angle (measured parallel to line of flight)	radians
η	elevator angle	radians
μ_2	$= \frac{m}{\rho S s}$ lateral relative density	-
ξ	aileron angle	radians
ϕ	angle of bank	radians
$\dot{\psi}$	rate of turn	radians/sec

REFERENCES

No.	Author	Title, etc.
1	J. C. Morrall W. G. A. Port	Low speed flight tests on a tailless delta wing aircraft (Avro 707B). Part 1 - General Tests. To be published as A.R.C. C.P.1104
2	W. G. A. Port J. C. Morrall	Low speed flight tests on a tailless delta wing aircraft (Avro 707B). Part 2 - Longitudinal Stability and Control. R.A.E. Technical Report 67198 (1967) To be published as A.R.C. C.P.1105
3	A. V. Roe & Co. Ltd.	Avro 707B aircraft. The measurement of aileron and rudder powers on a 1/8th scale model. WT Report 707/52
4	A. V. Roe & Co. Ltd.	Avro 707B aircraft. Tests to determine the lateral stability derivatives ℓ_v, n_v, y_v. WT Report 707/50
5	A. V. Roe & Co. Ltd.	1/8th scale model tests in the Avro 9 ft x 7 ft wind tunnel. Six component tests on the 707A fuselage with and without fin and rudder. WT Report 707/31
6	H. H. B. M. Thomas S. Neumark	Interim note on stability and response characteristics of supersonic aircraft (linear theory). R.A.E. Technical Note Aero 2412 (1955) A.R.C. 18263
7	K. H. Doetsch	The time vector method for stability investigations. R.A.E. Technical Report Aero 2495 A.R.C. R & M 2945 (1953)
8	D. H. Perry J. C. Morrall W. G. A. Port	Low speed flight tests on a tailless delta aircraft (Avro 707B). Part 4 - Wing Flow. R.A.E. Technical Report Aero 2639 (1960) To be published as A.R.C. C.P.1107
9	D. Adamson	Note on the effect of size of aircraft upon the difficulties involved in landing. A.R.C. R & M 2567 (1947)

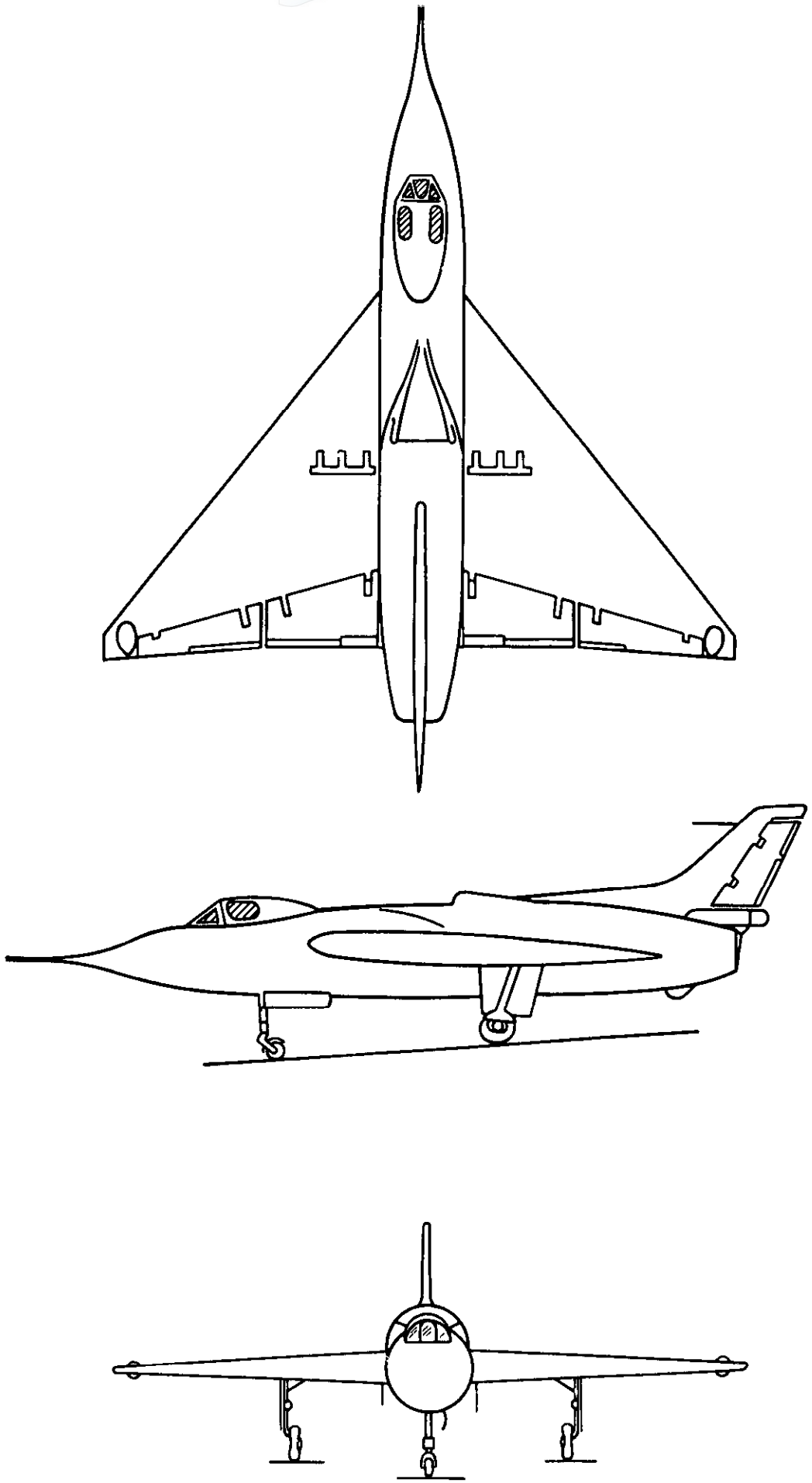

Fig.1 General arrangement of Avro 707B VX790

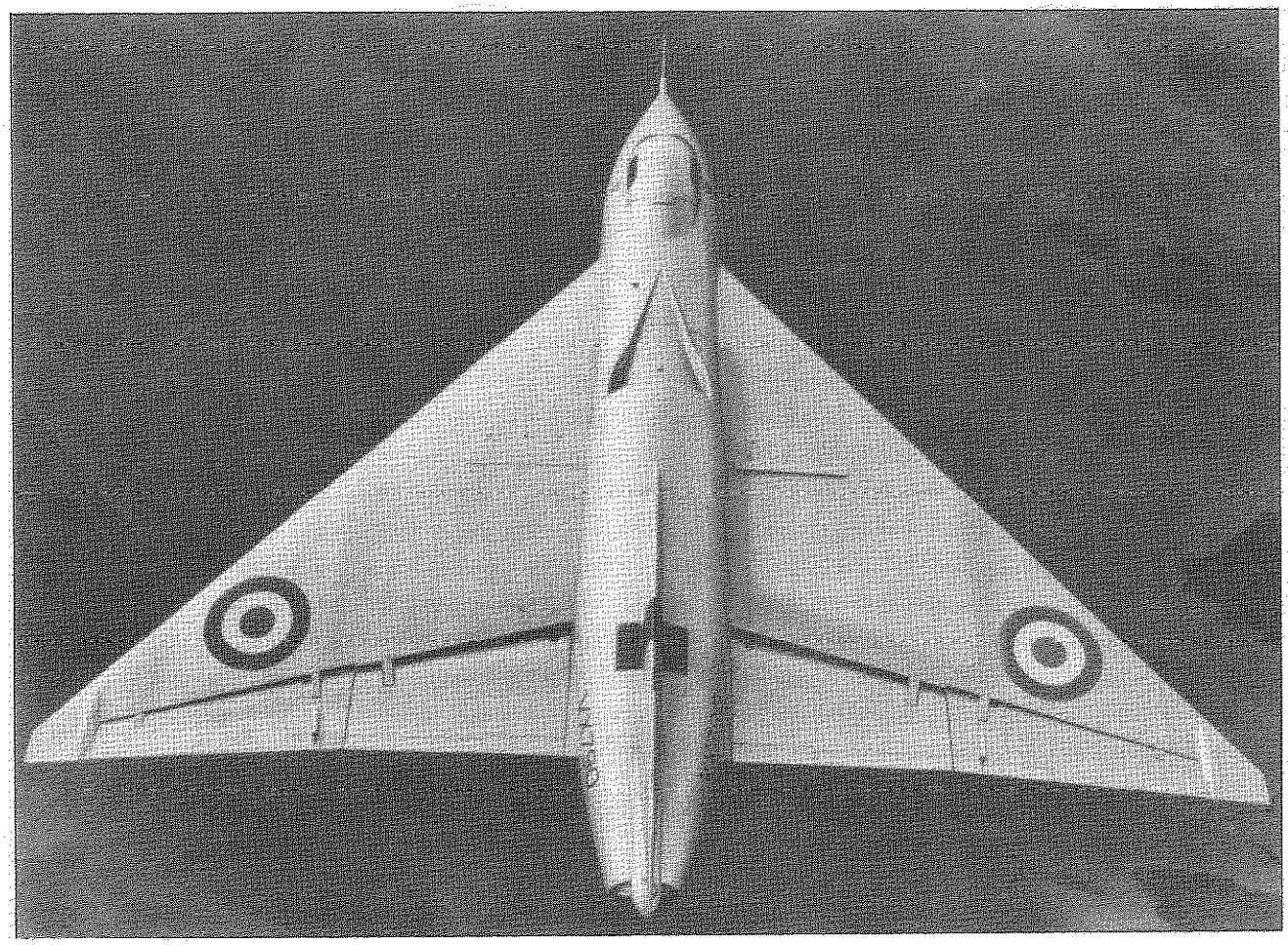

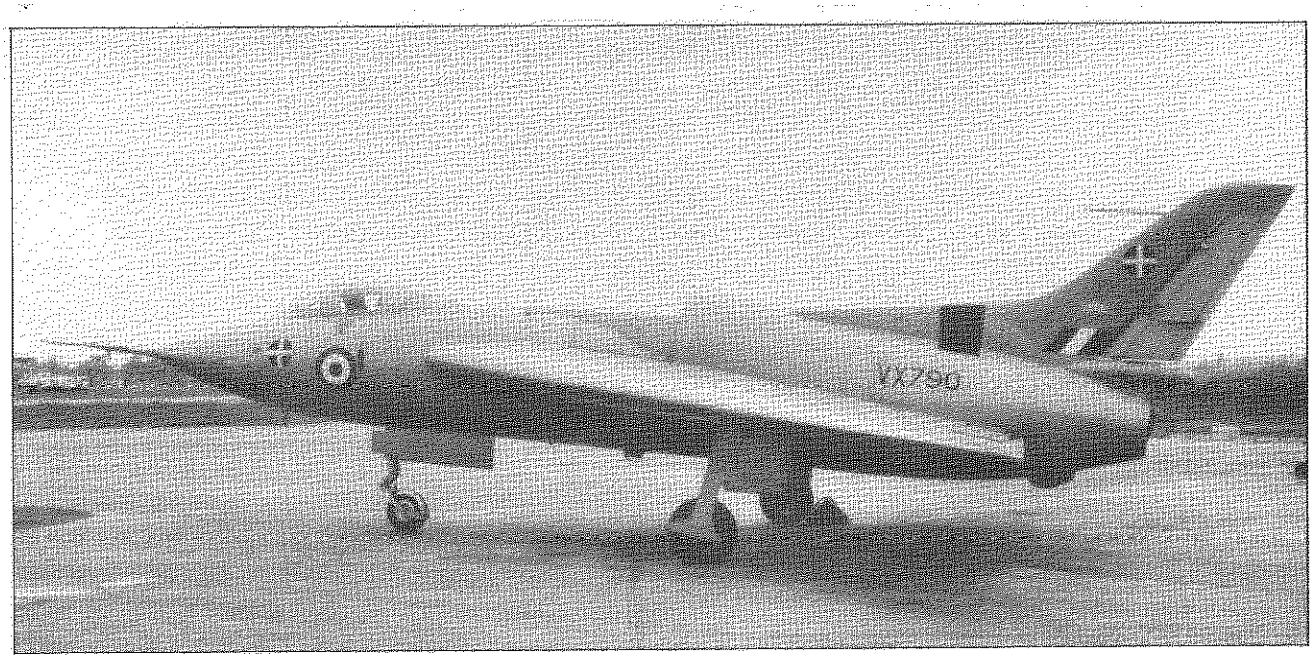

FIG.2. AVRO. 707B

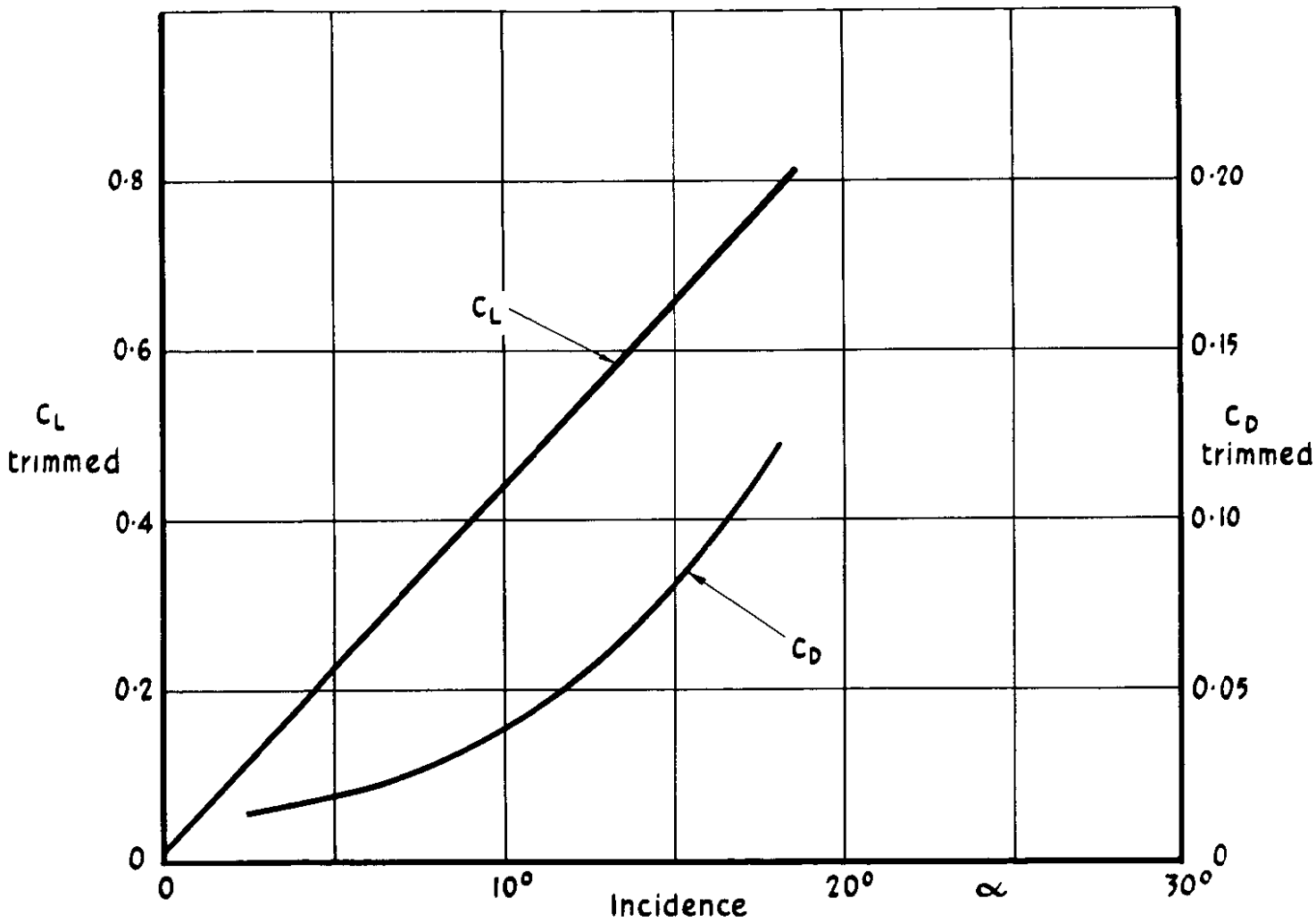

Fig.3 Variation of the lift and drag coefficients with incidence Cruising configuration (from Ref 1)

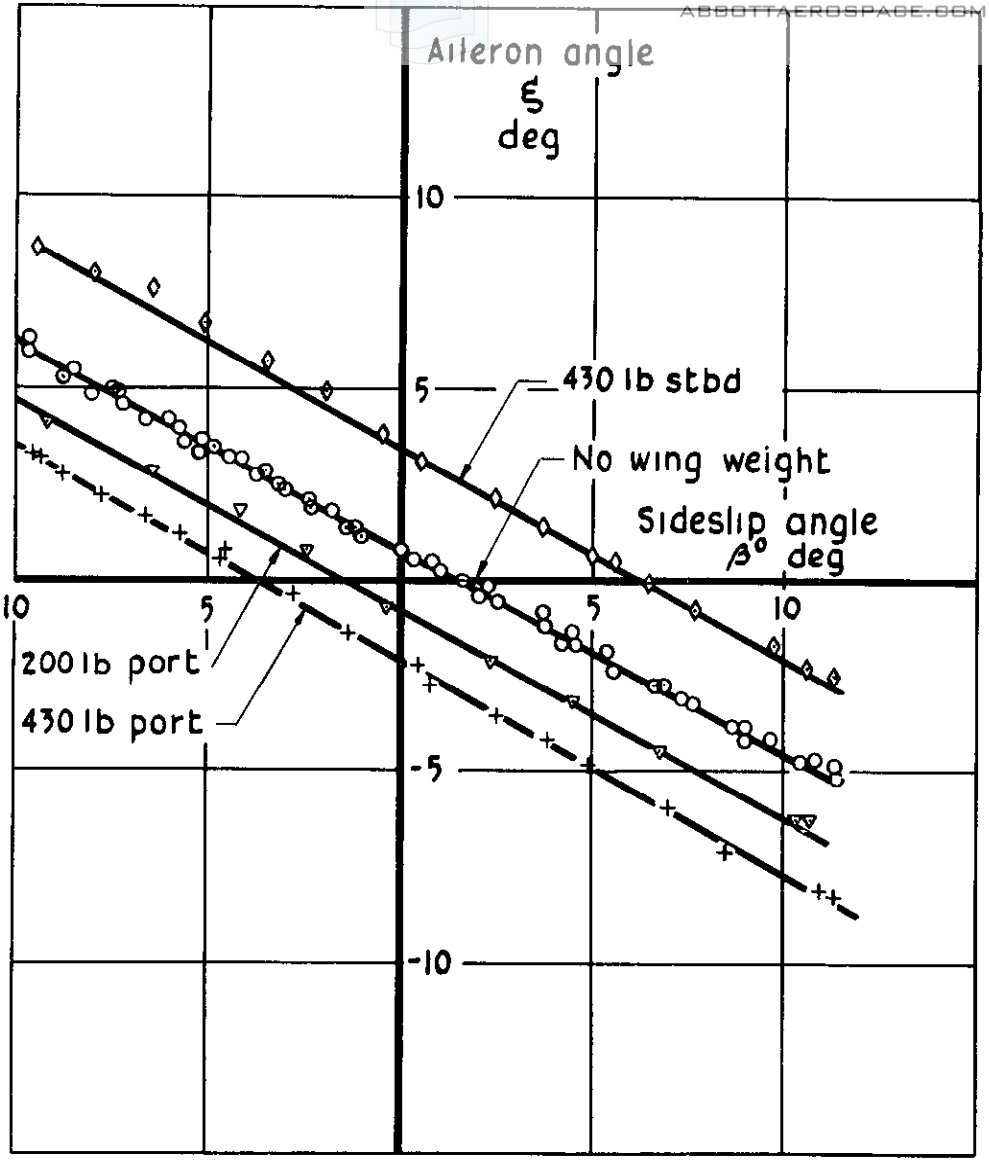

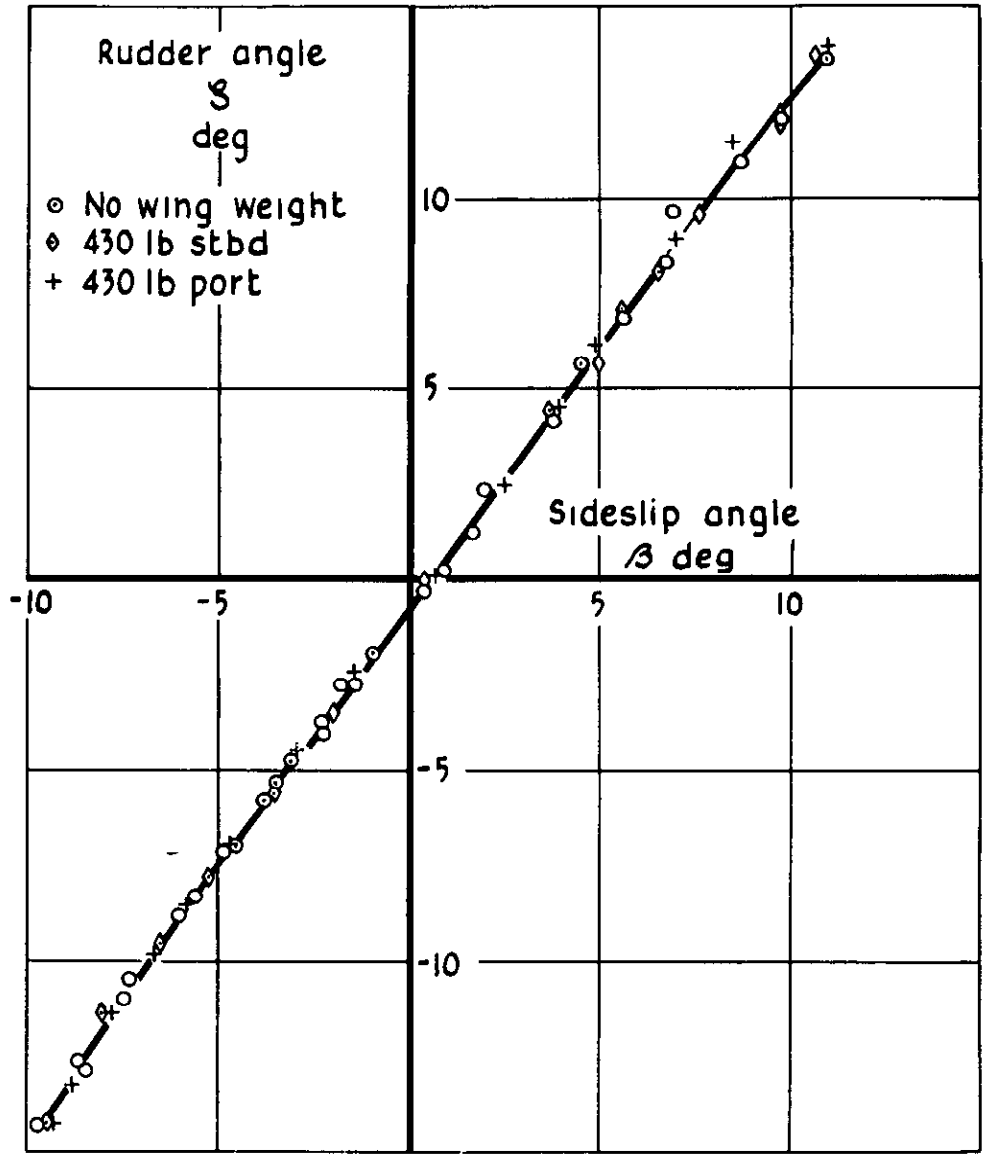

Fig.4 Aileron and rudder angles to trim straight sideslips with wing tip weights.
Cruising configuration $C_L = 0{\cdot}22$ (179 kt)

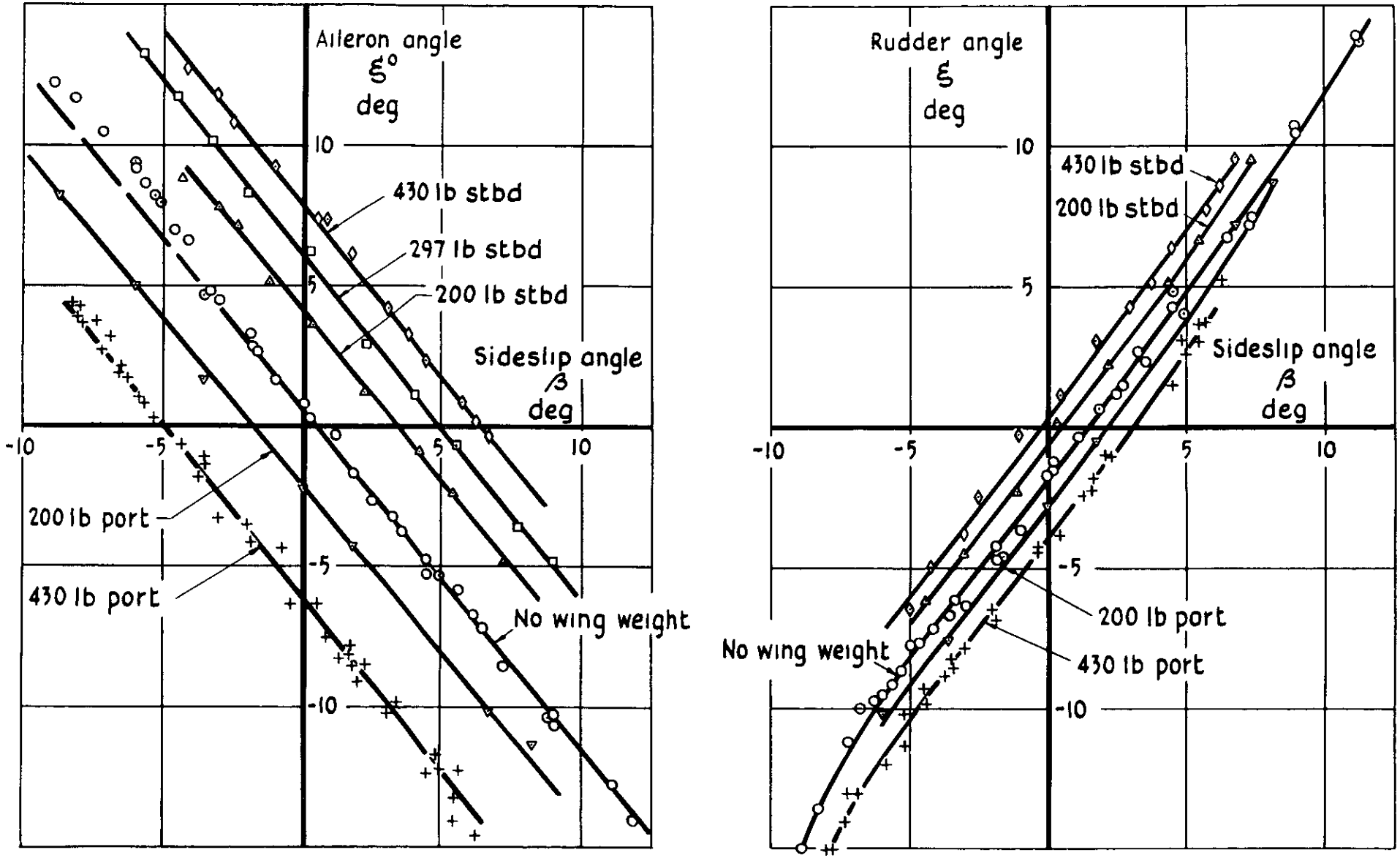

Fig 5 Aileron and rudder angles to trim straight sideslips with wing tip weights.
Landing configuration $C_L = 0{\cdot}485$ (119 kt)

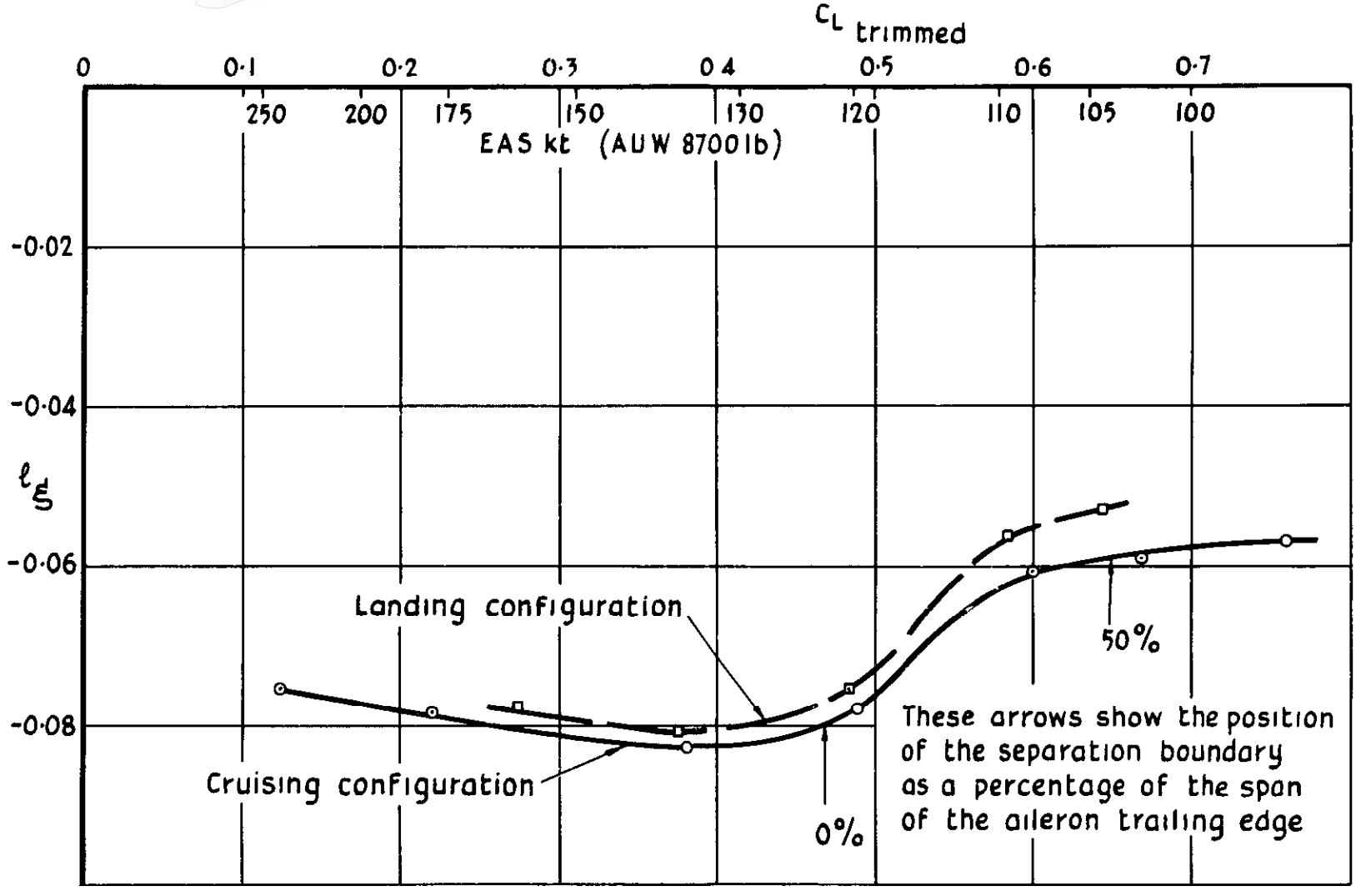

Fig.6 Variation of the aileron rolling power with lift coefficient

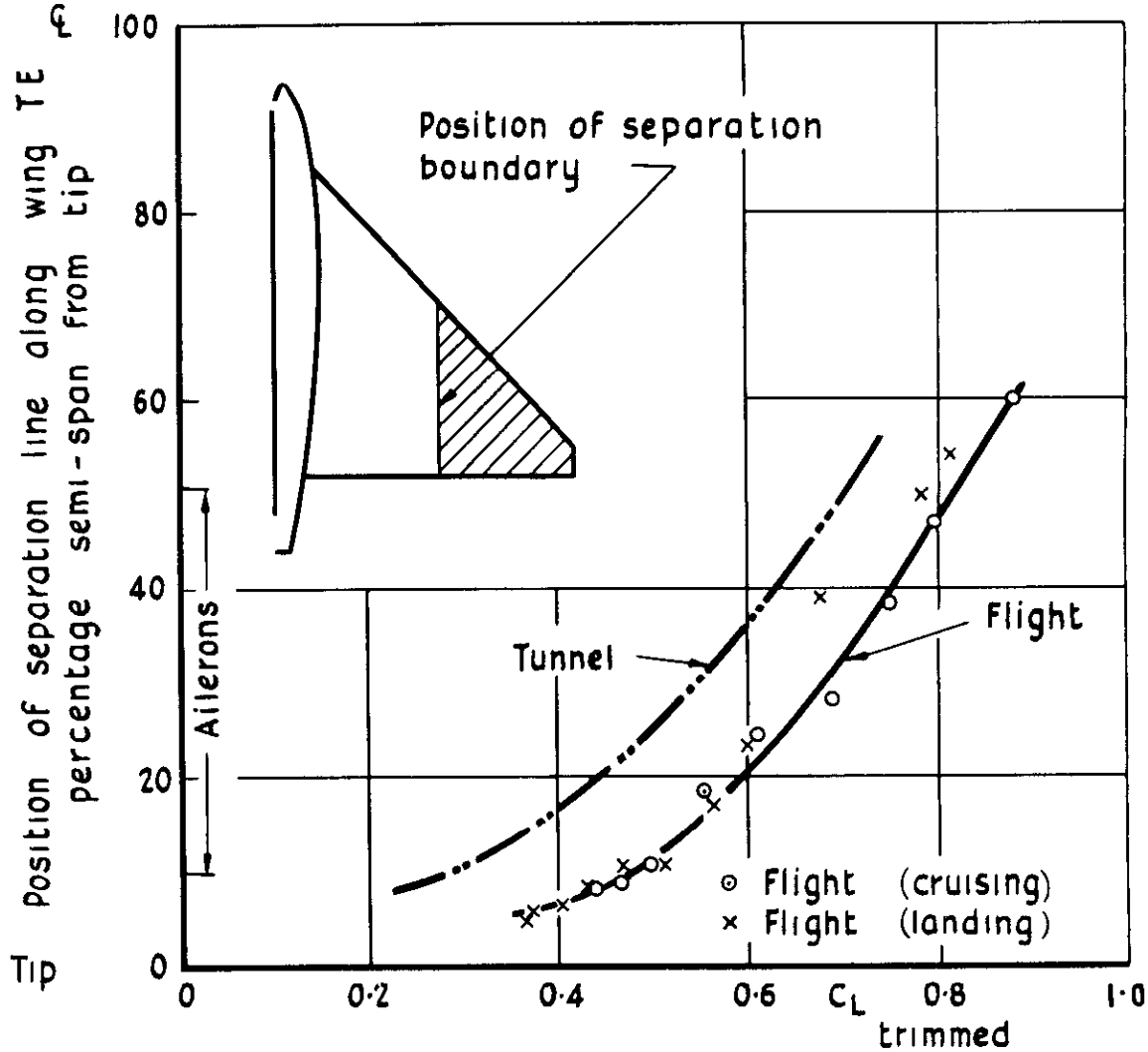

Fig.7 Variation of the spanwise position of the separation boundary with lift coefficient

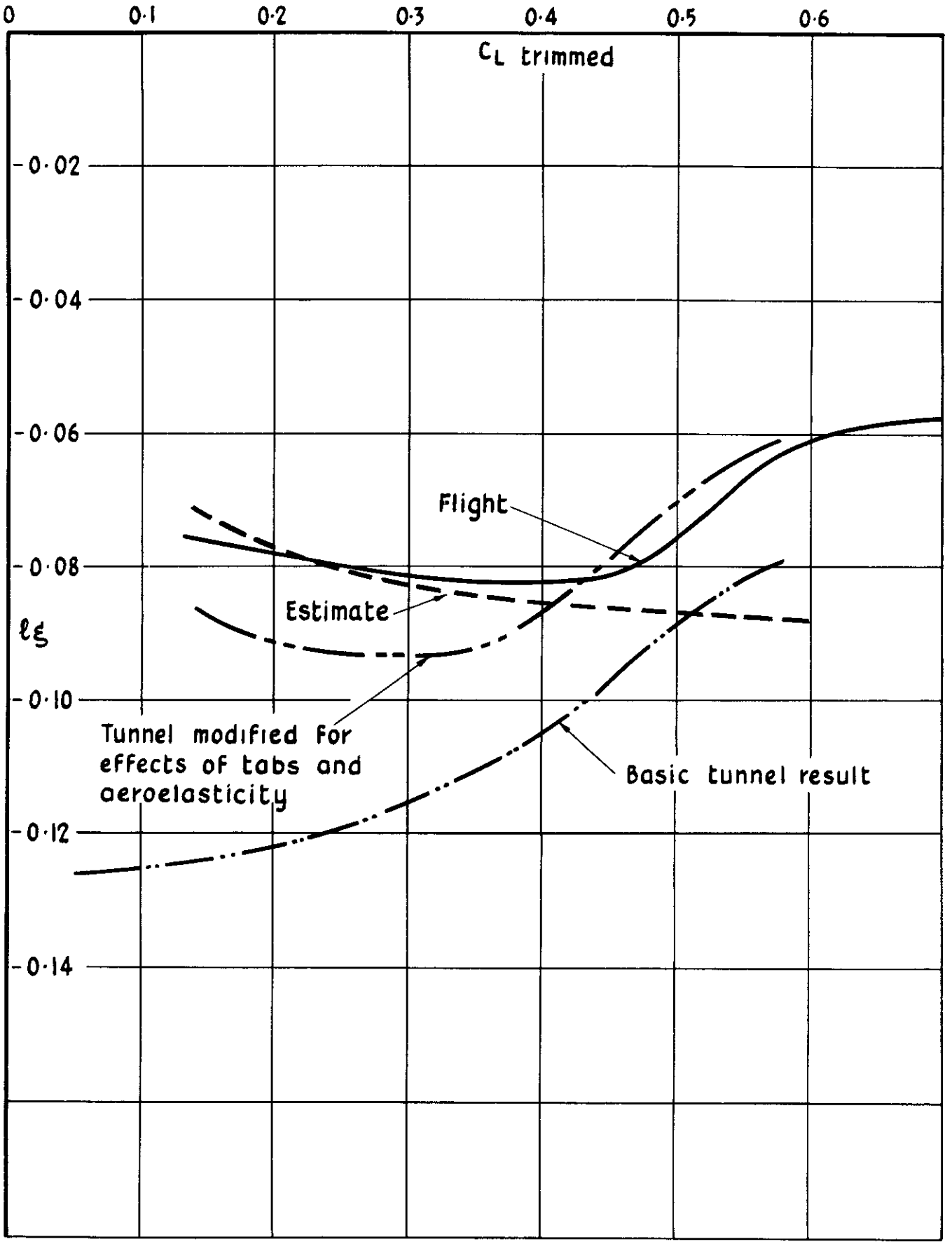

Fig 8 Comparison of flight, tunnel and estimated values of the aileron rolling power (ℓ_ξ)

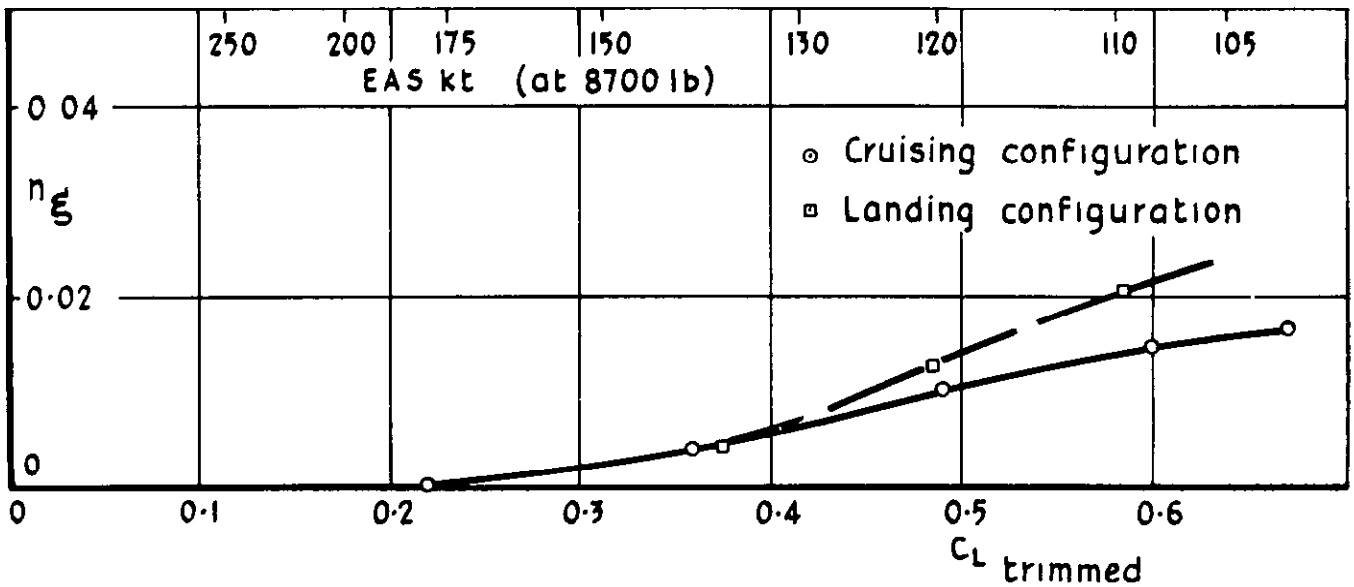

Fig.9 Variation of the aileron yawing moment coefficient with lift coefficient

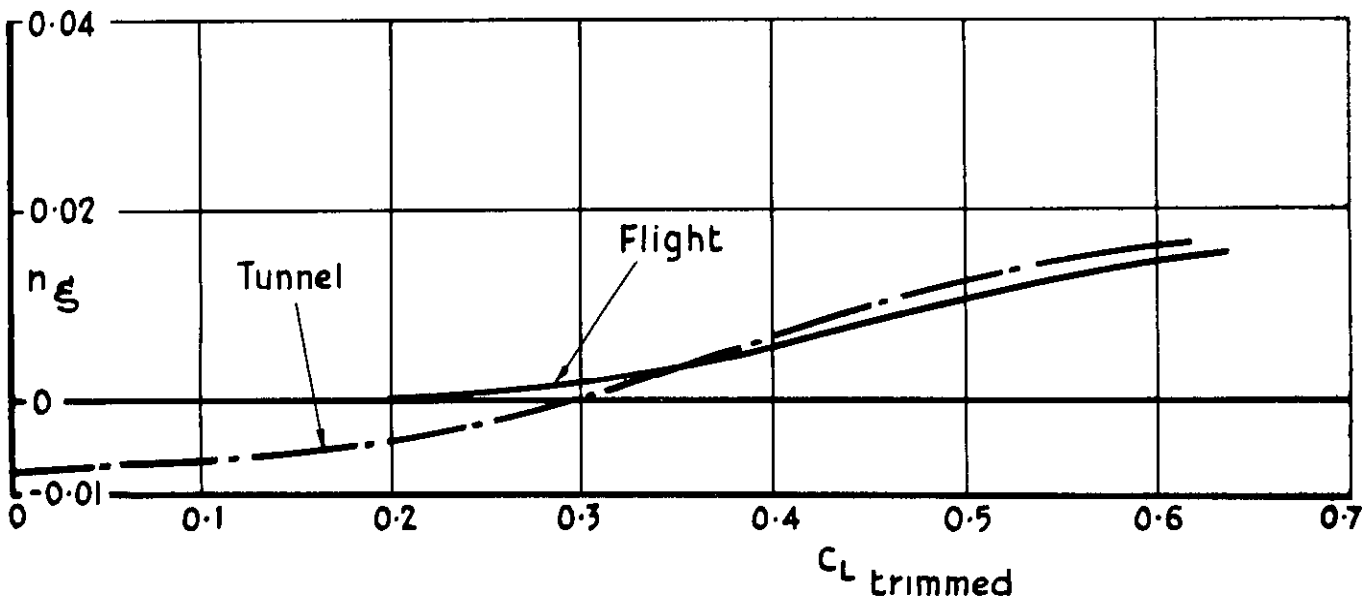

Fig.10 Comparison of flight and tunnel values of the aileron yawing moment coefficient

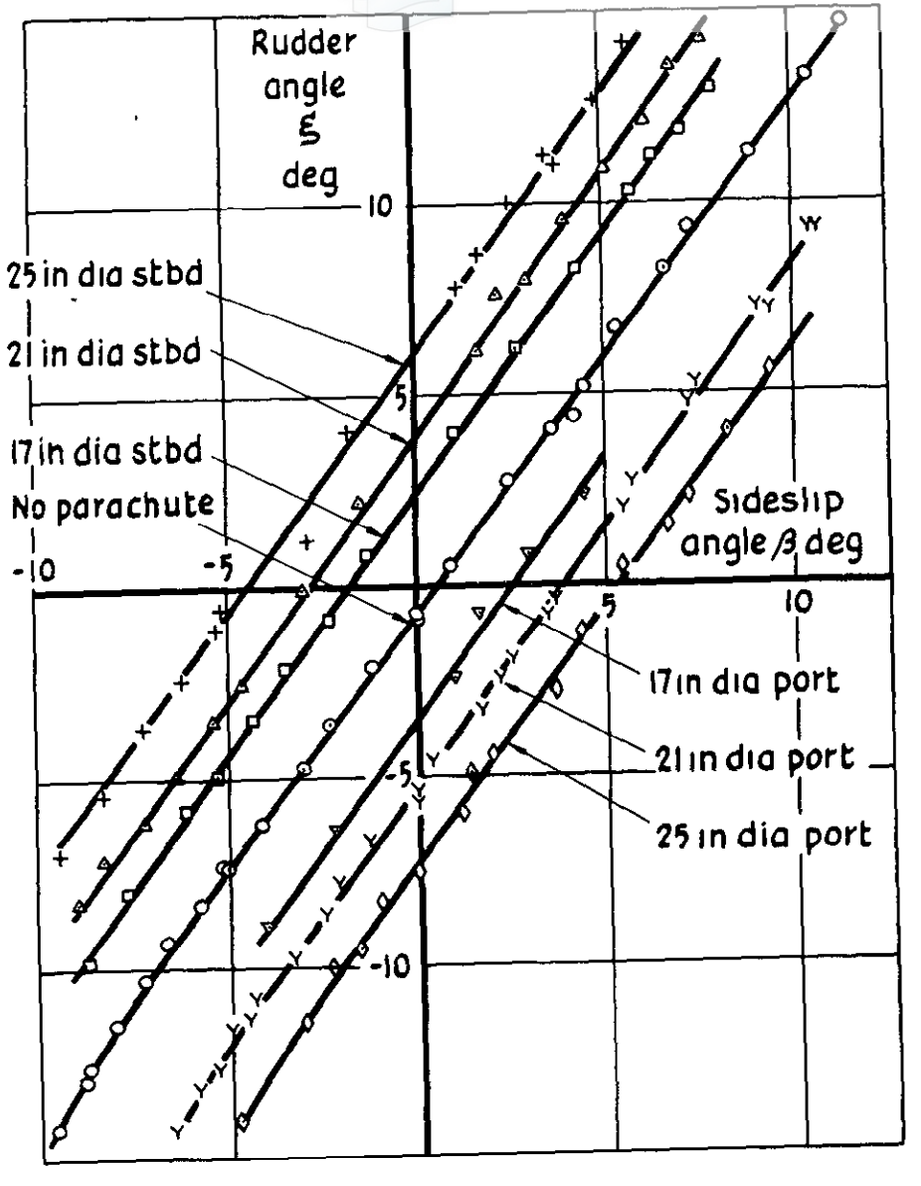

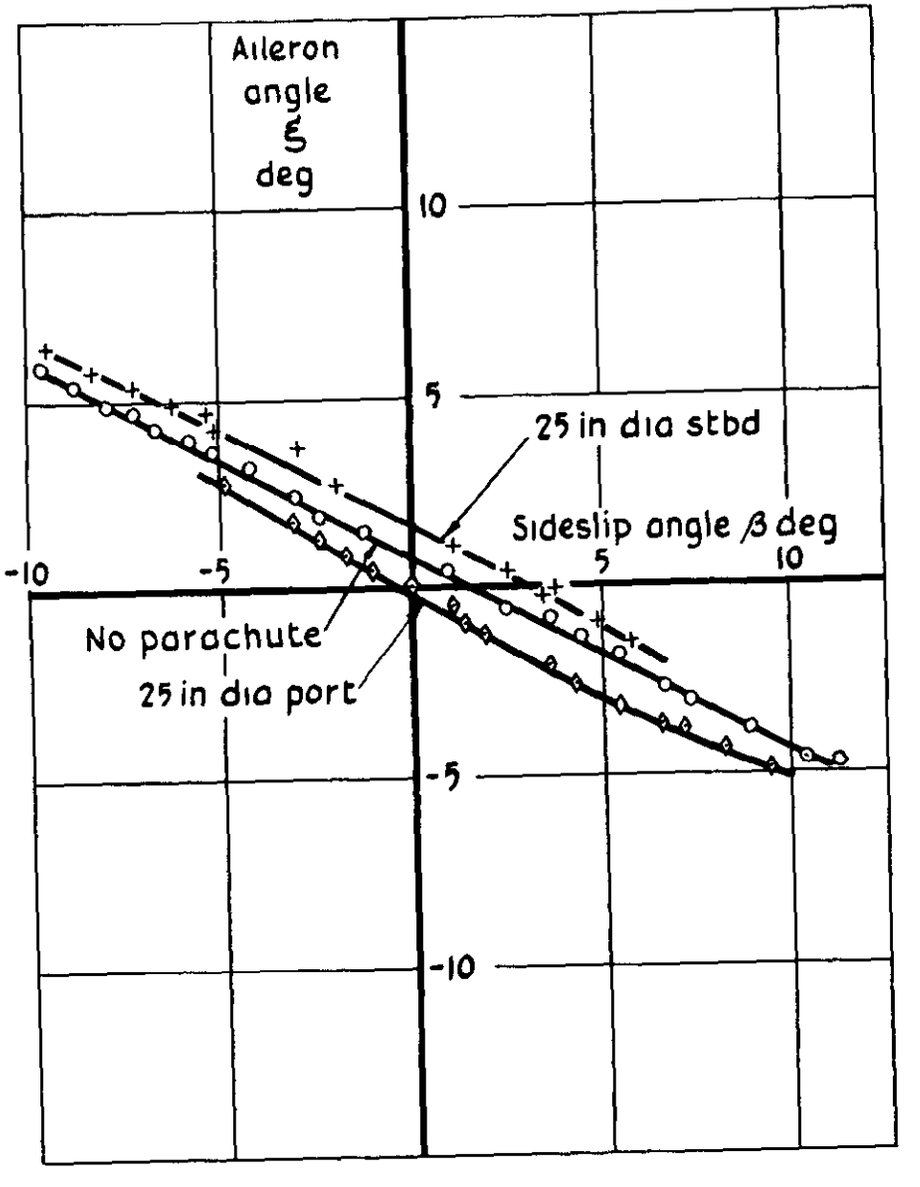

Fig.11 Rudder and aileron angles to trim straight sideslips with wing tip parachutes.
Cruising configuration $C_L = 0{\cdot}22$ (179 kt)

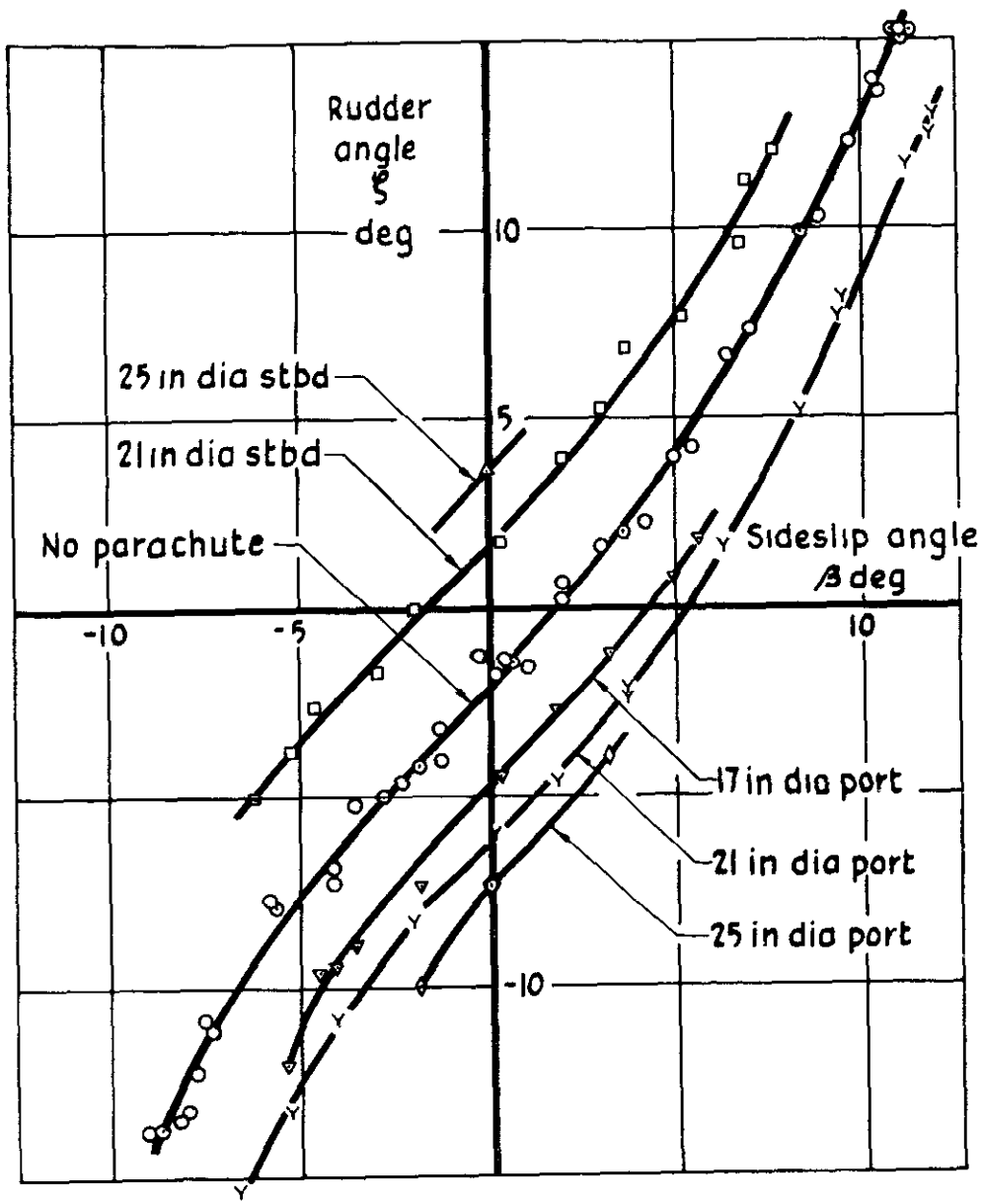

Fig.12 Cruising configuration $C_L = 0{\cdot}65$ (105 kt)

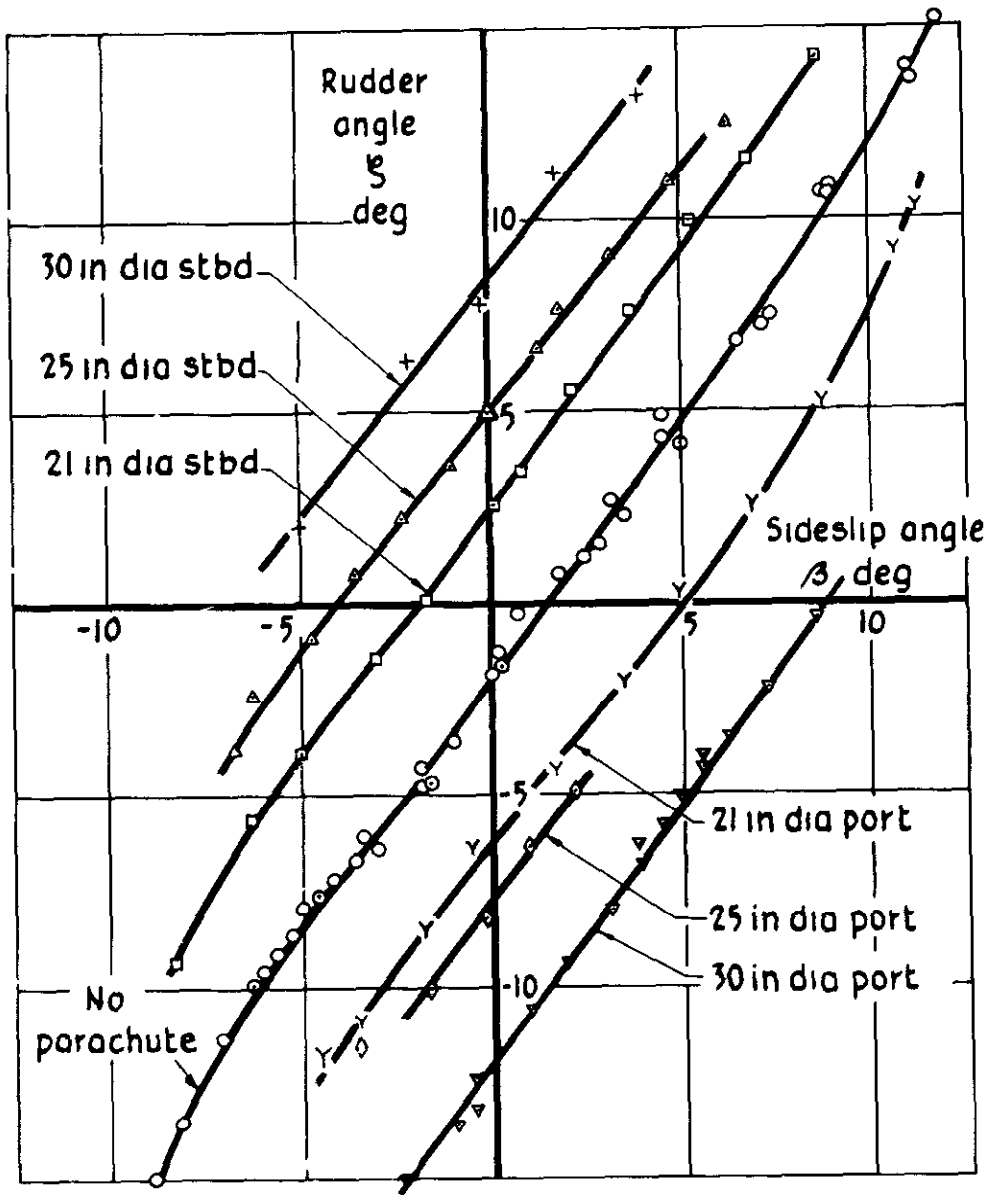

Fig.13 Landing configuration $C_L = 0{\cdot}485$ (119 kt)

Rudder angles to trim straight sideslips with wing tip parachutes

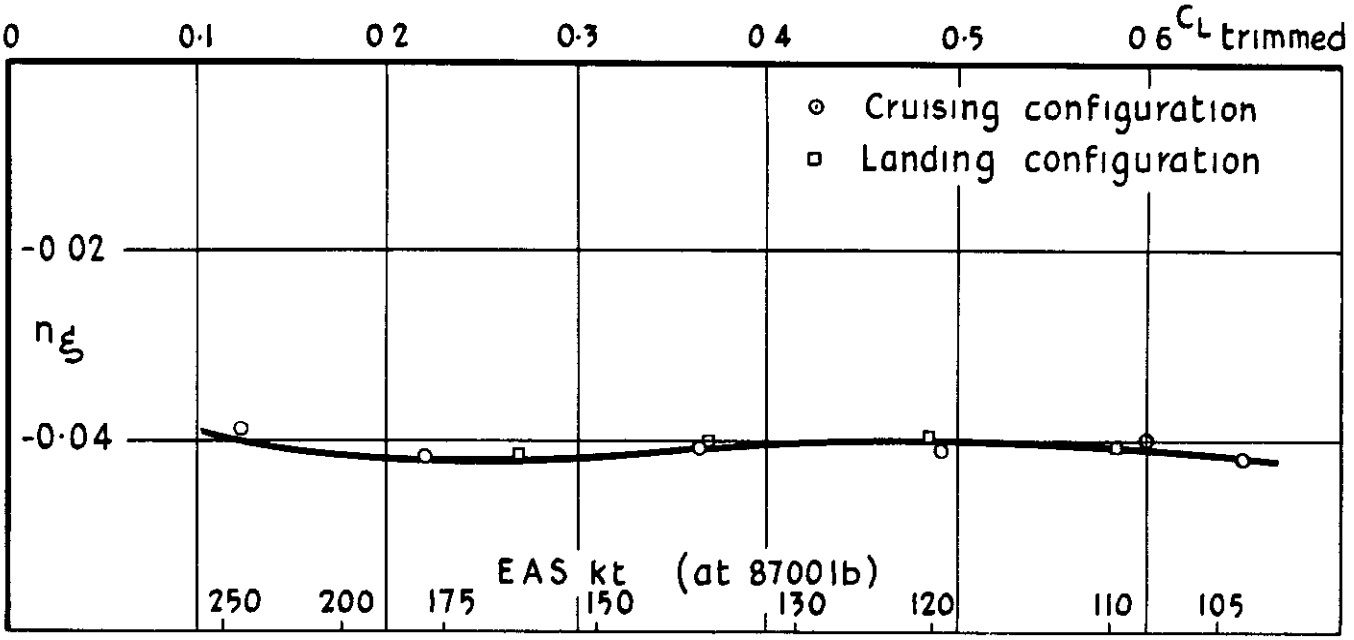

Fig. 14 Variation of the rudder yawing power with lift coefficient

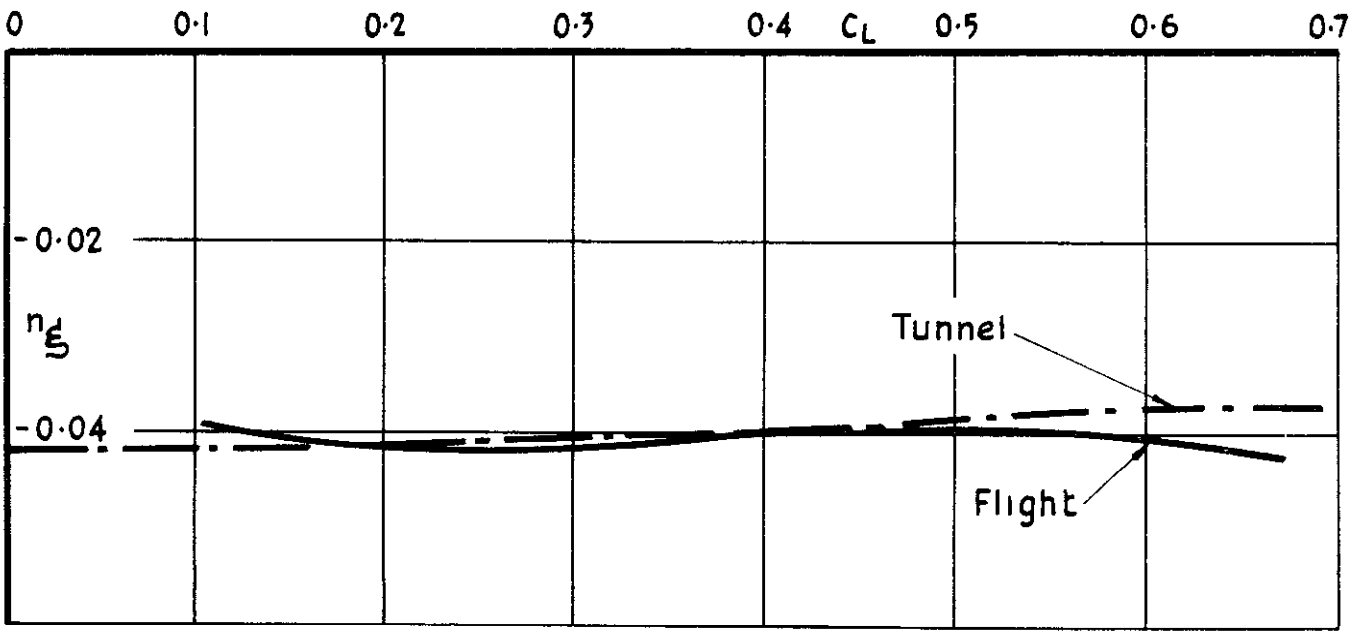

Fig. 15 Comparison of flight and tunnel values of the rudder yawing power

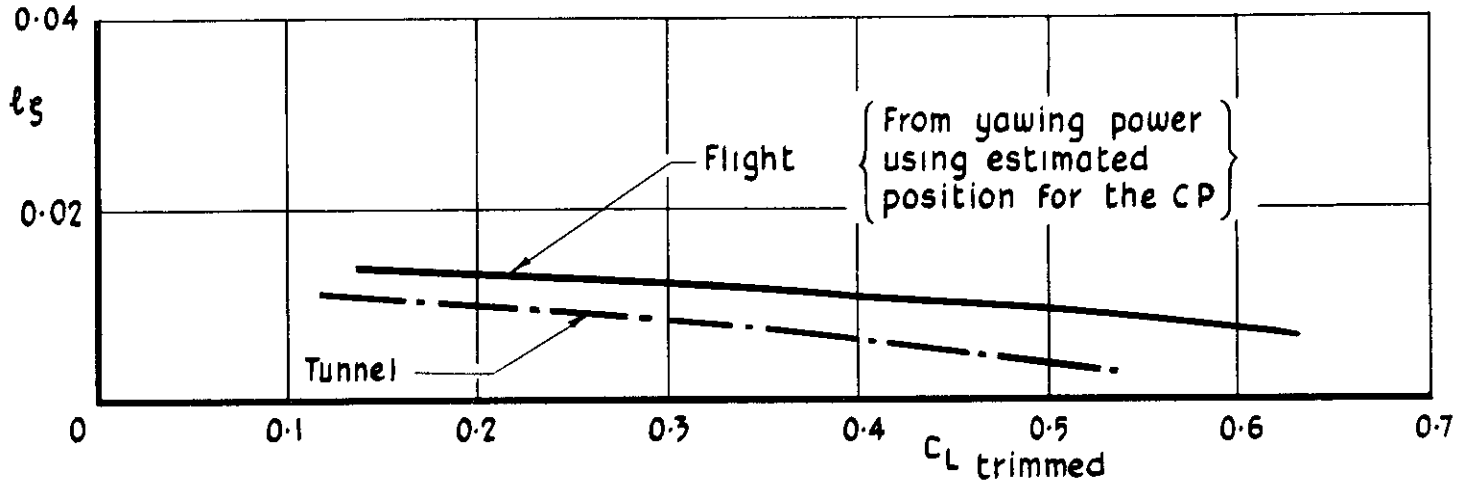

Fig 16 Comparison of flight and tunnel values of the rudder rolling moment coefficient

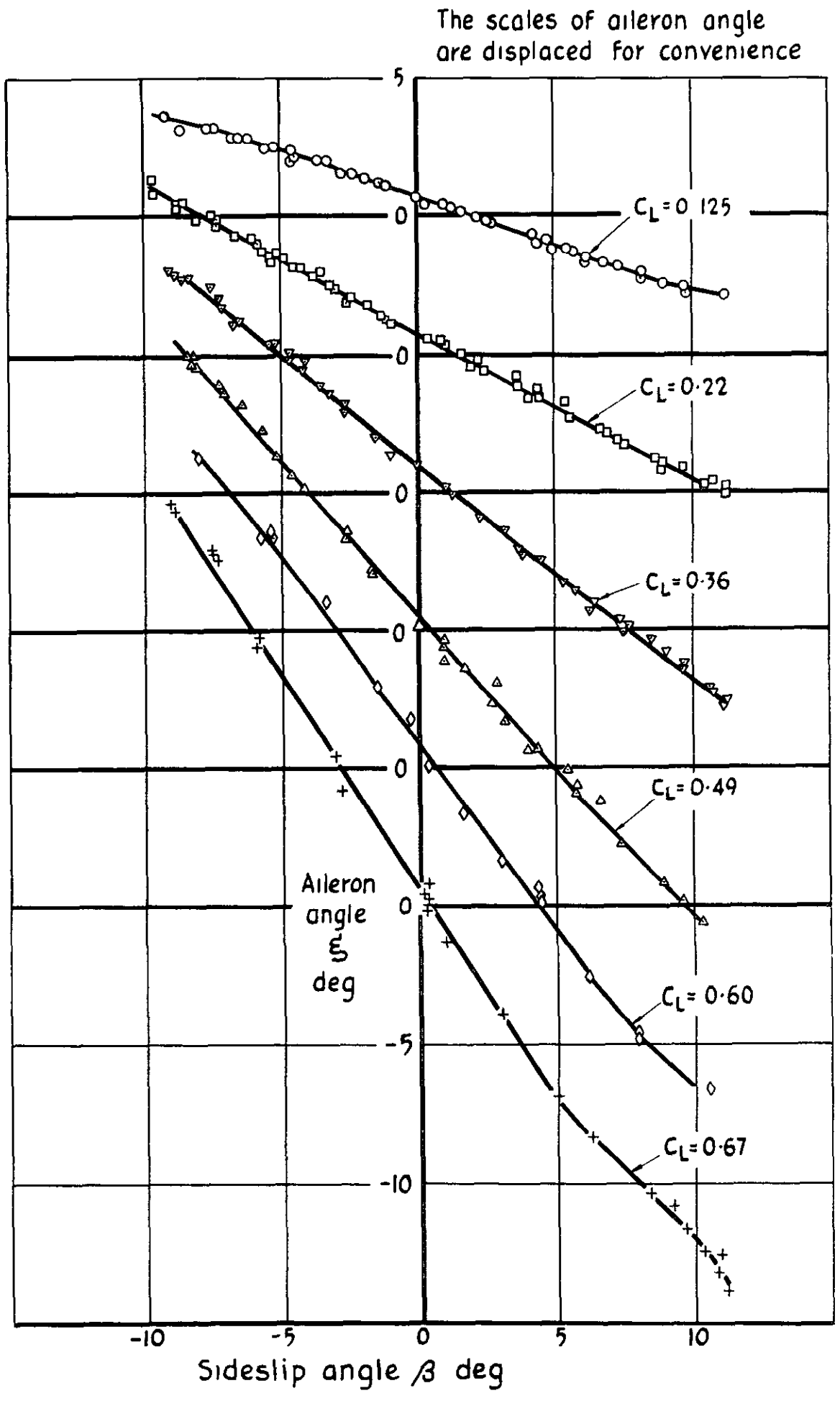

Fig 17 Aileron angles to trim straight sideslips Cruising configuration

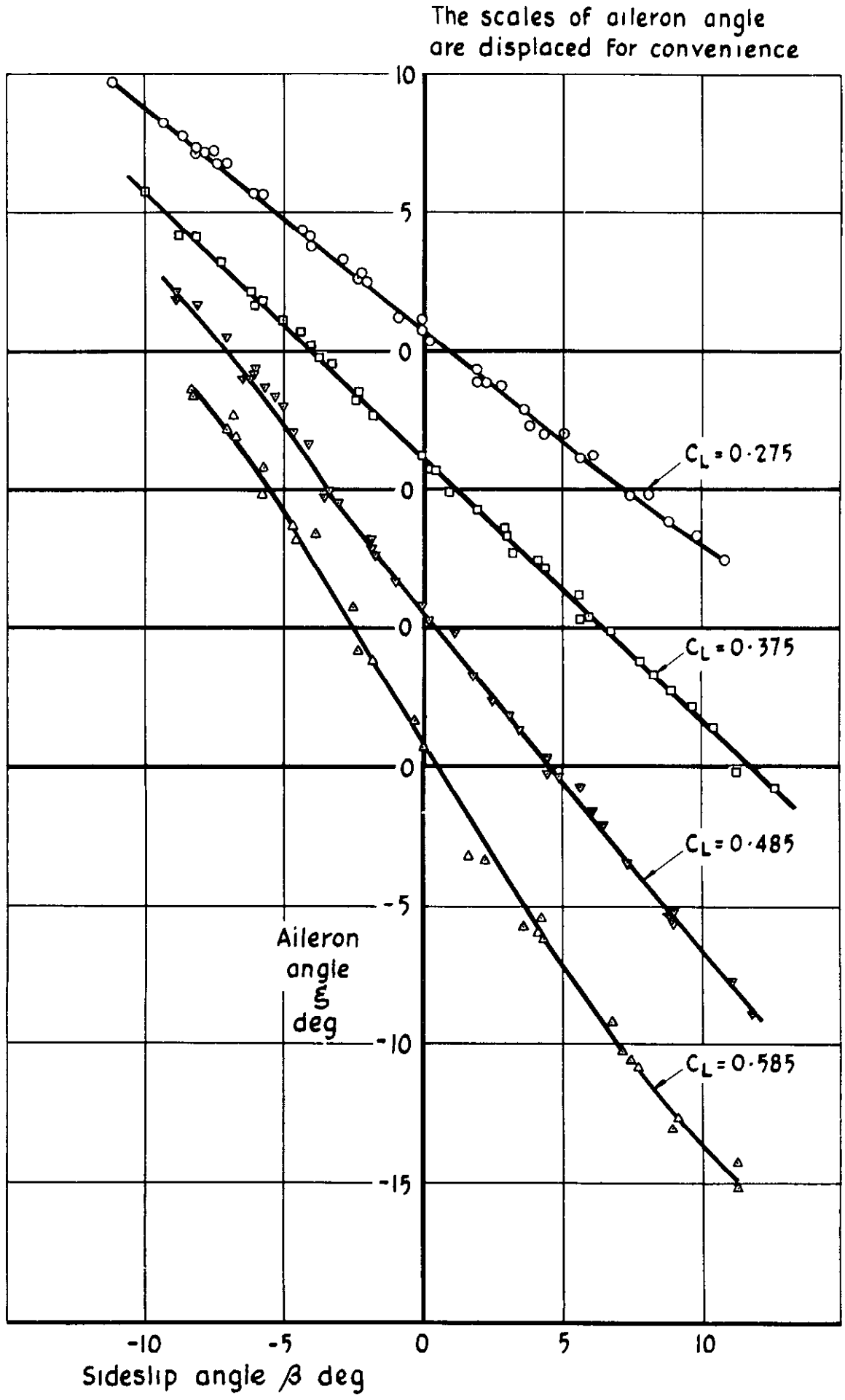

Fig. 18 Aileron angles to trim straight sideslips Landing configuration

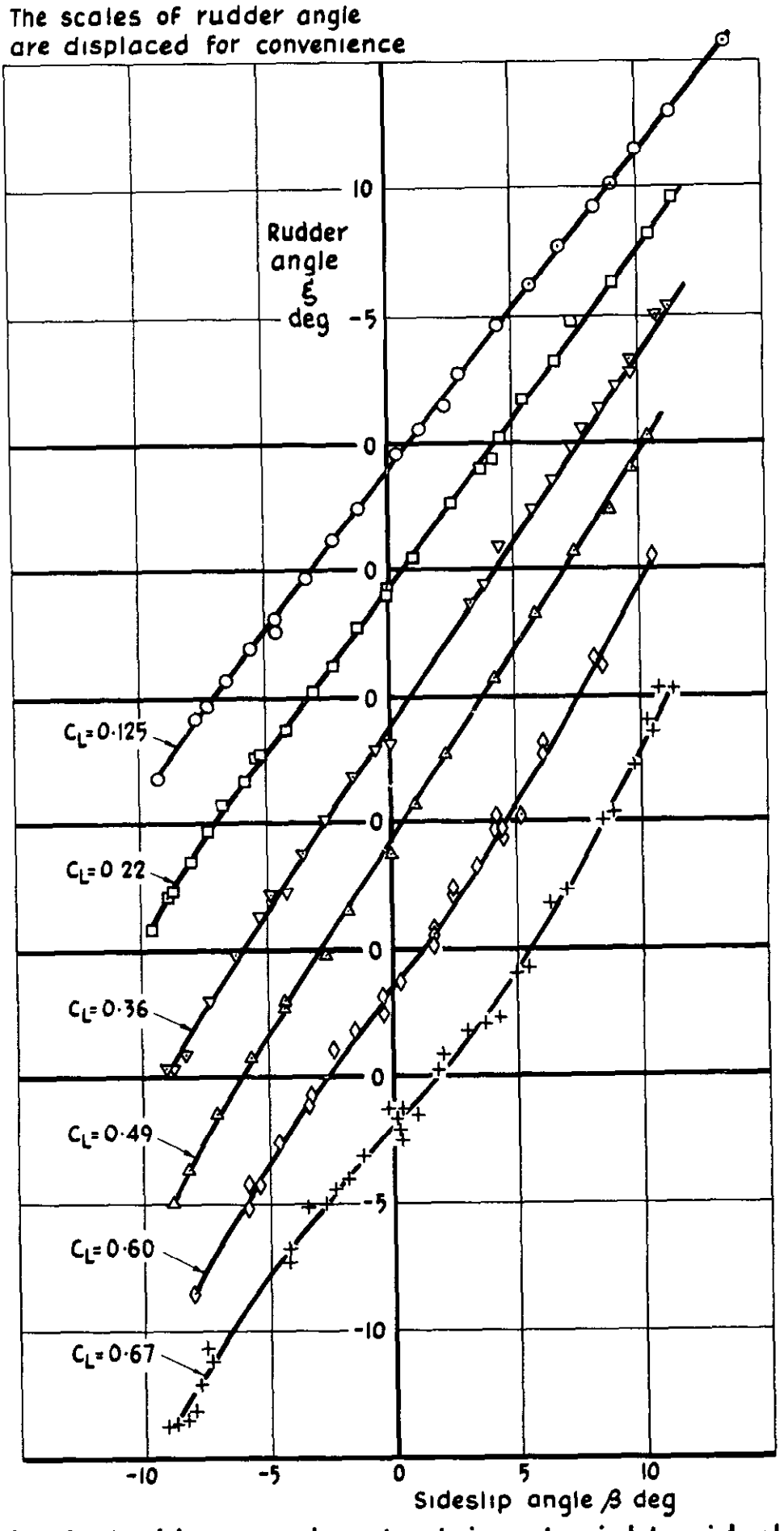

Fig.19 Rudder angles to trim straight sideslips. Cruising configuration

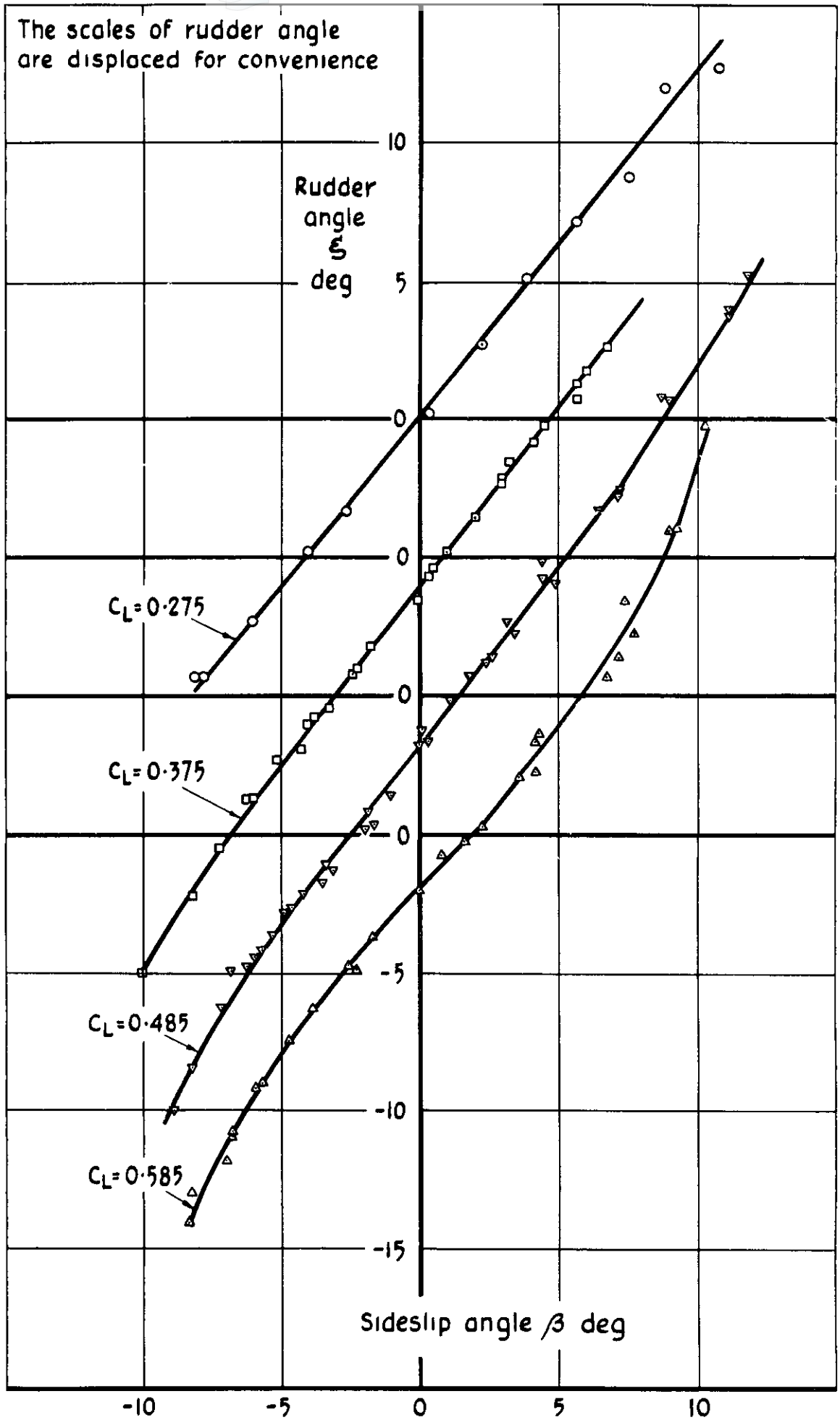

Fig 20 Rudder angles to trim straight sideslips. Landing configuration

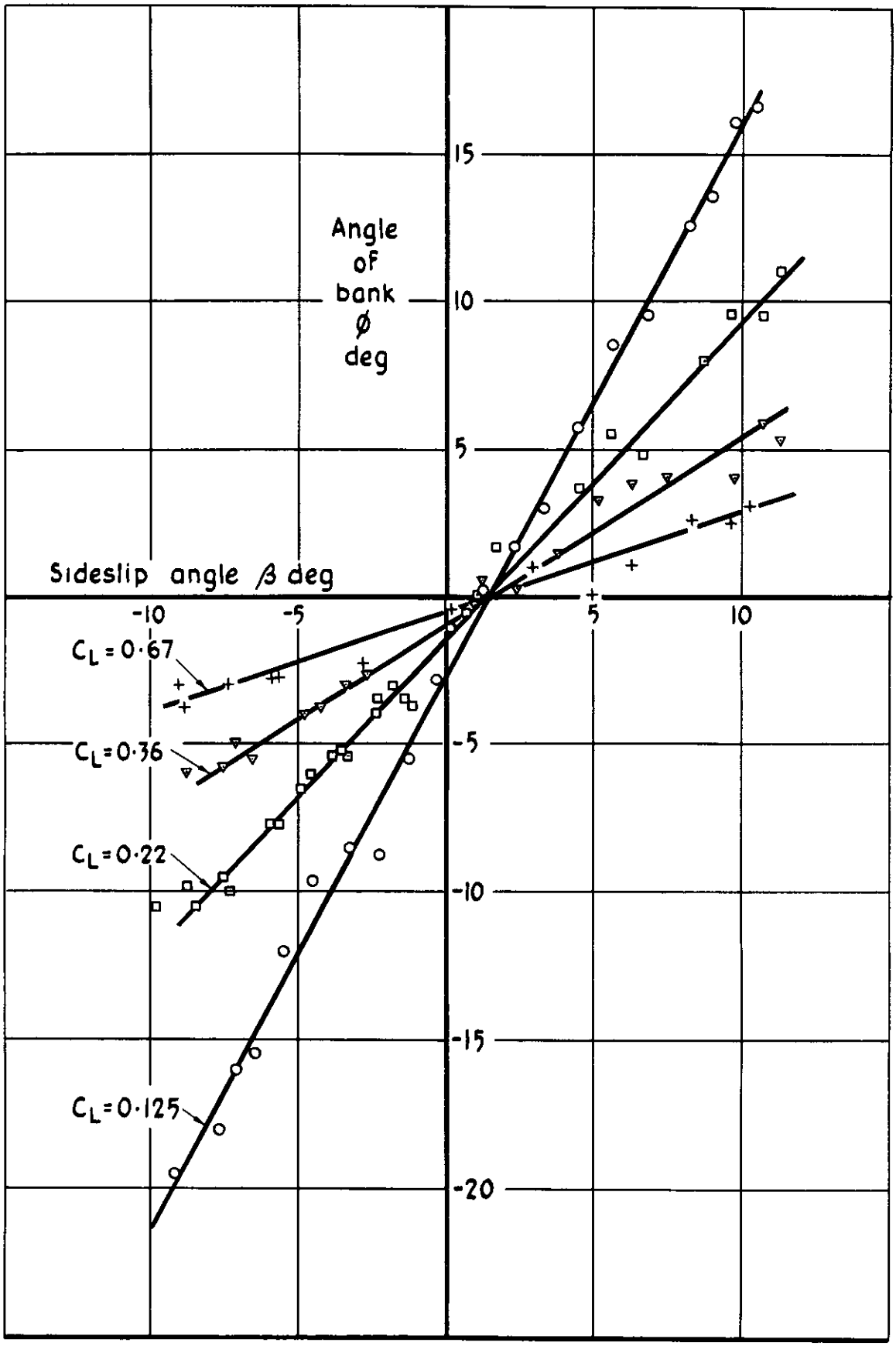

Fig 21 Angles of bank in straight sideslips. Cruising configuration

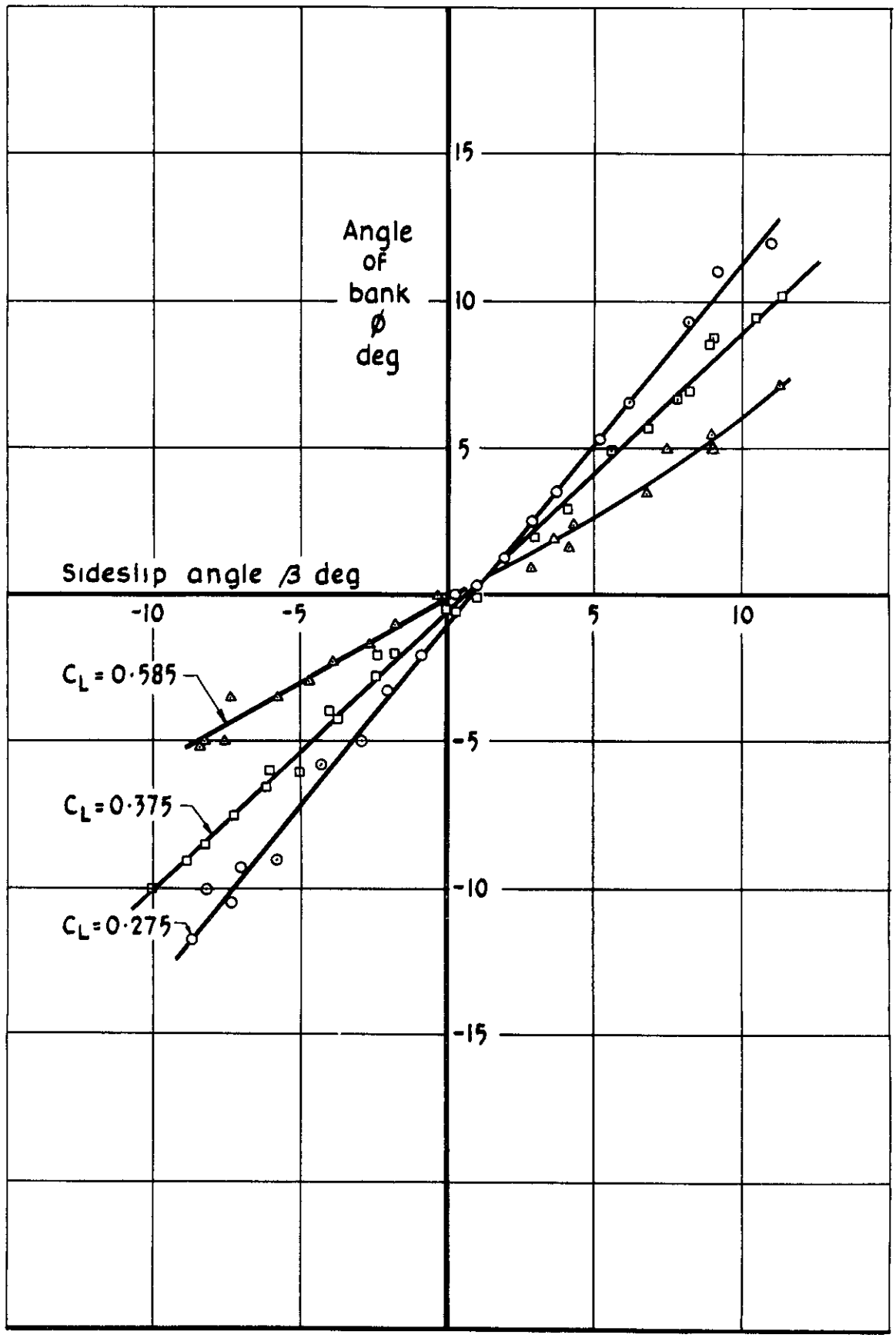

Fig 22 Angles of bank in straight sideslips. Landing configuration

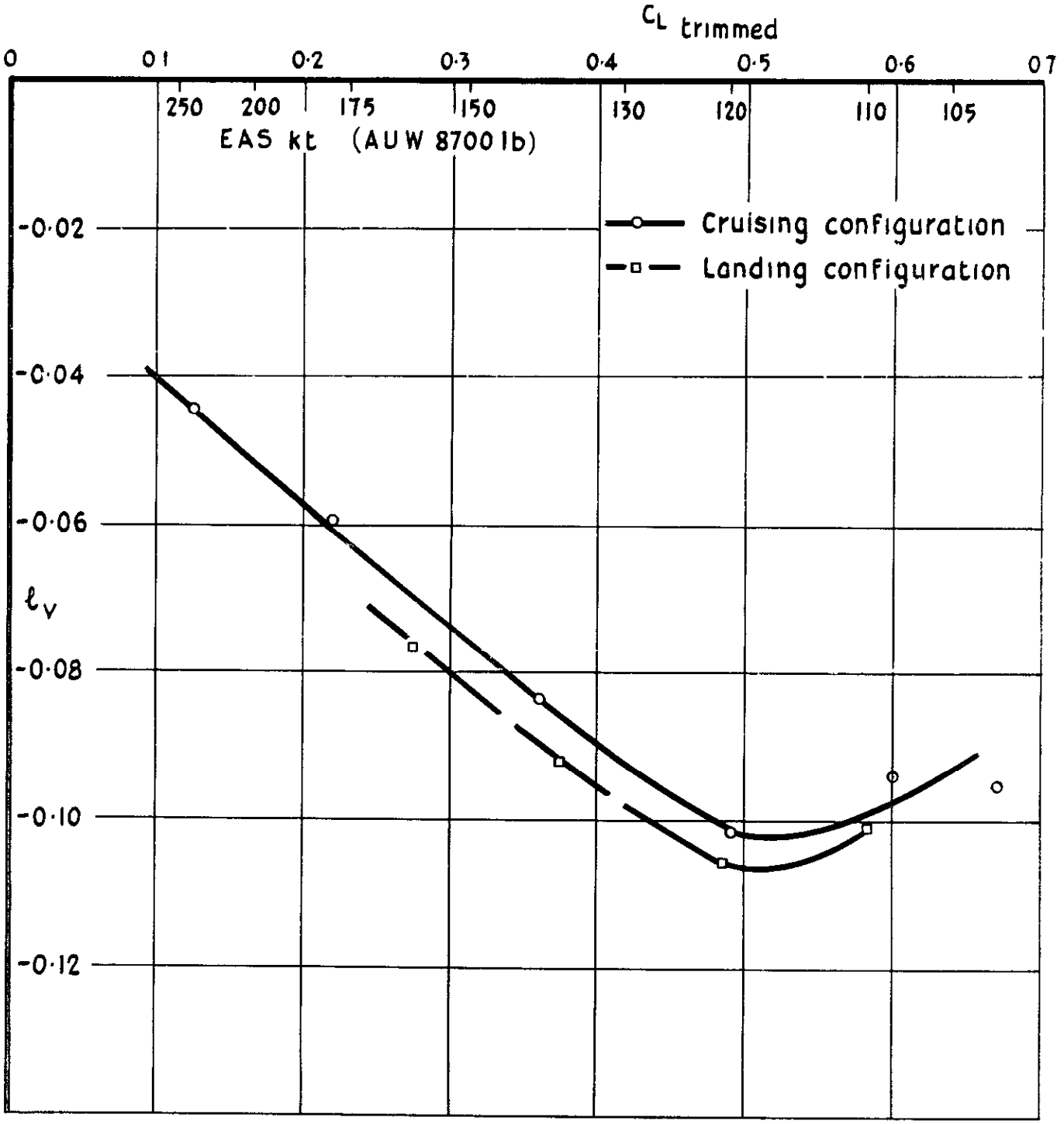

Fig 23 Variation of the derivative ℓ_v with lift coefficient

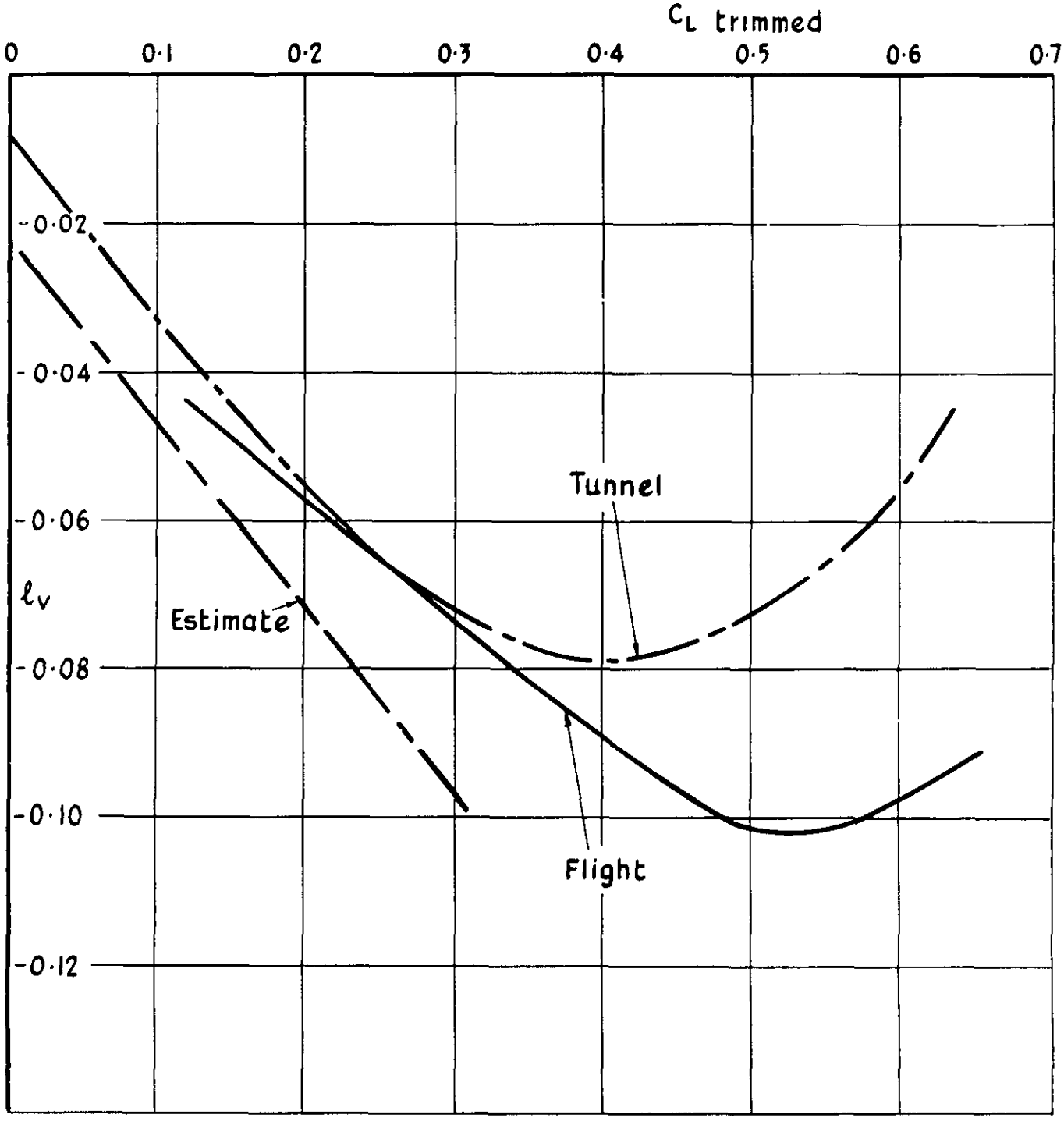

Fig 24 Comparison of flight, tunnel and estimated values of ℓ_v

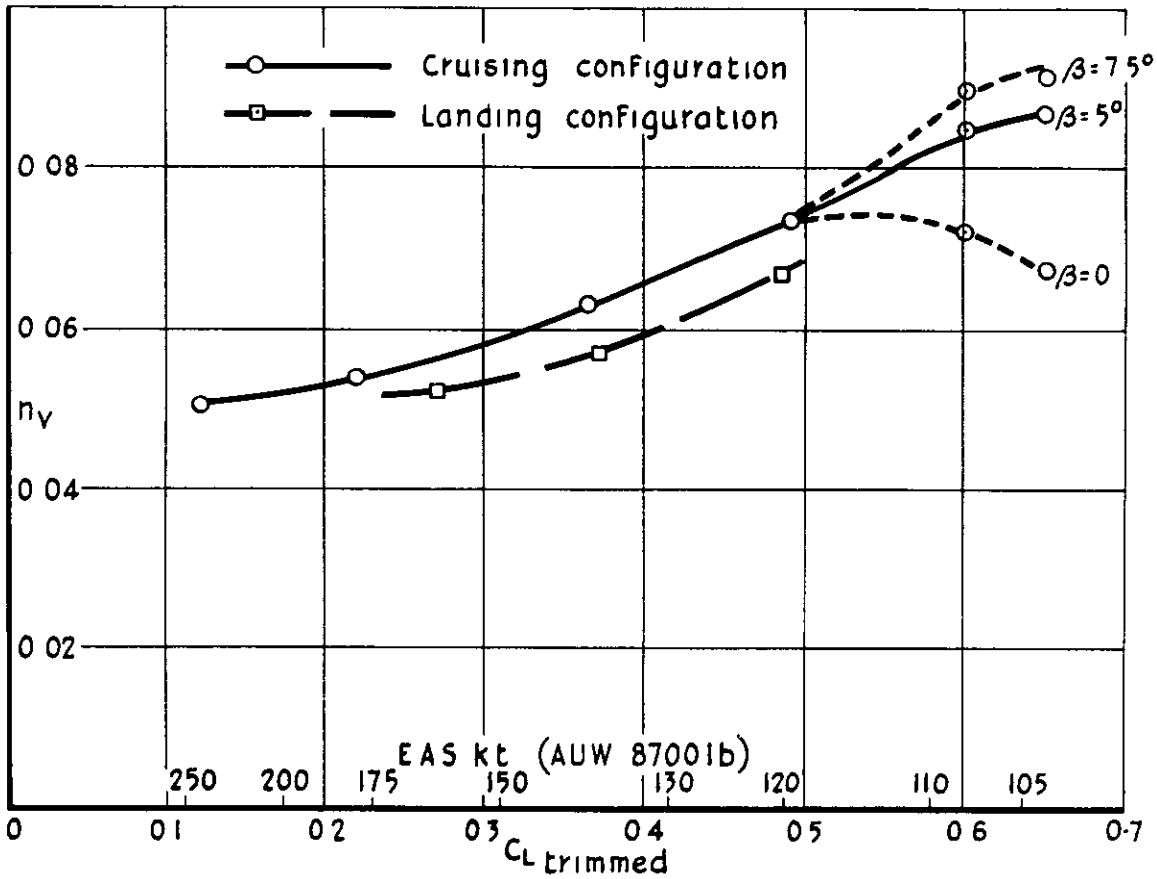

Fig.25 Variation of the derivative n_v with lift coefficient

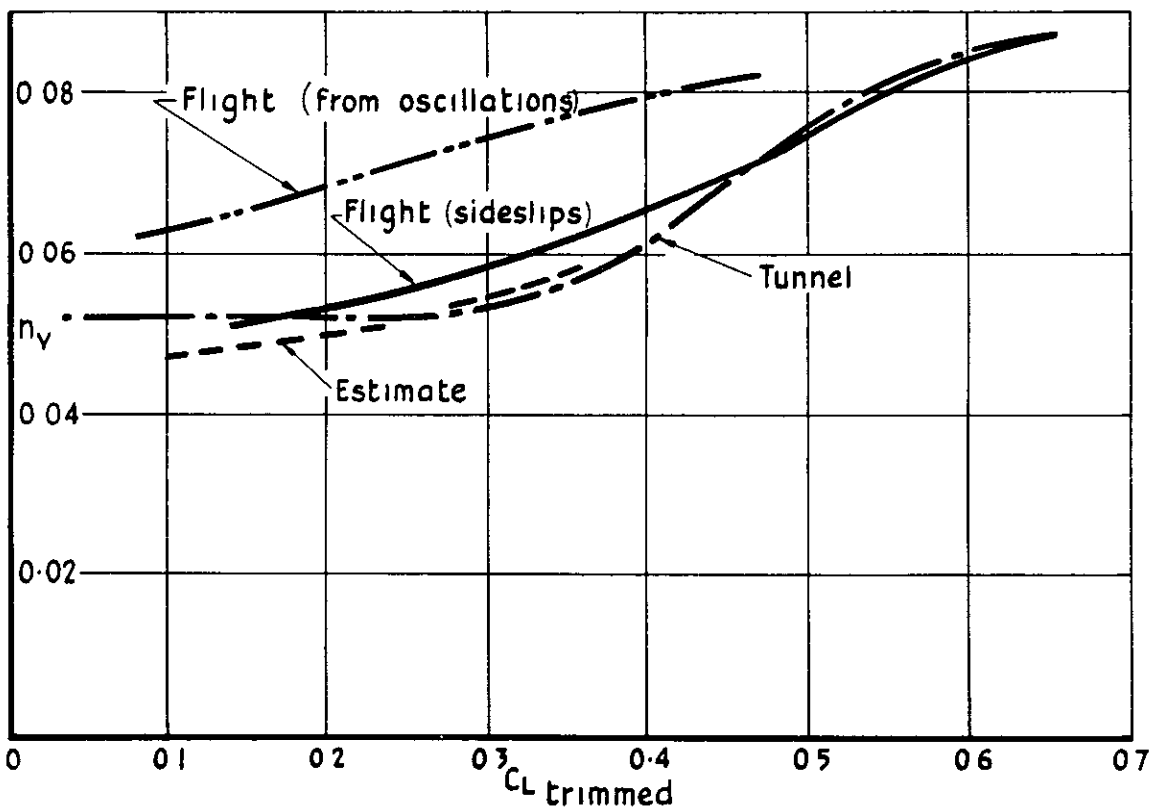

Fig.26 Comparison of flight, tunnel and estimated values of n_v

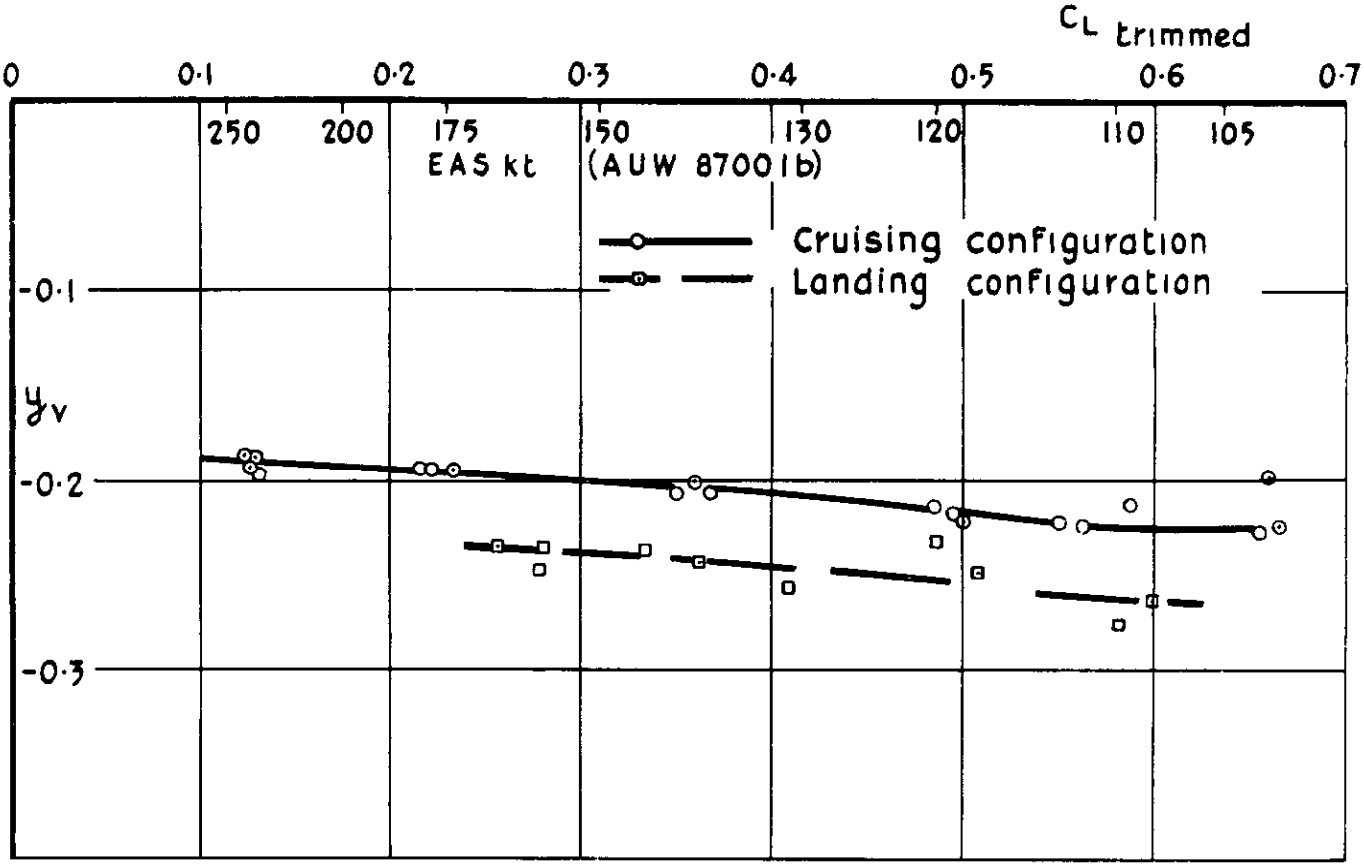

Fig 27 Variation of the derivative y_v with lift coefficient

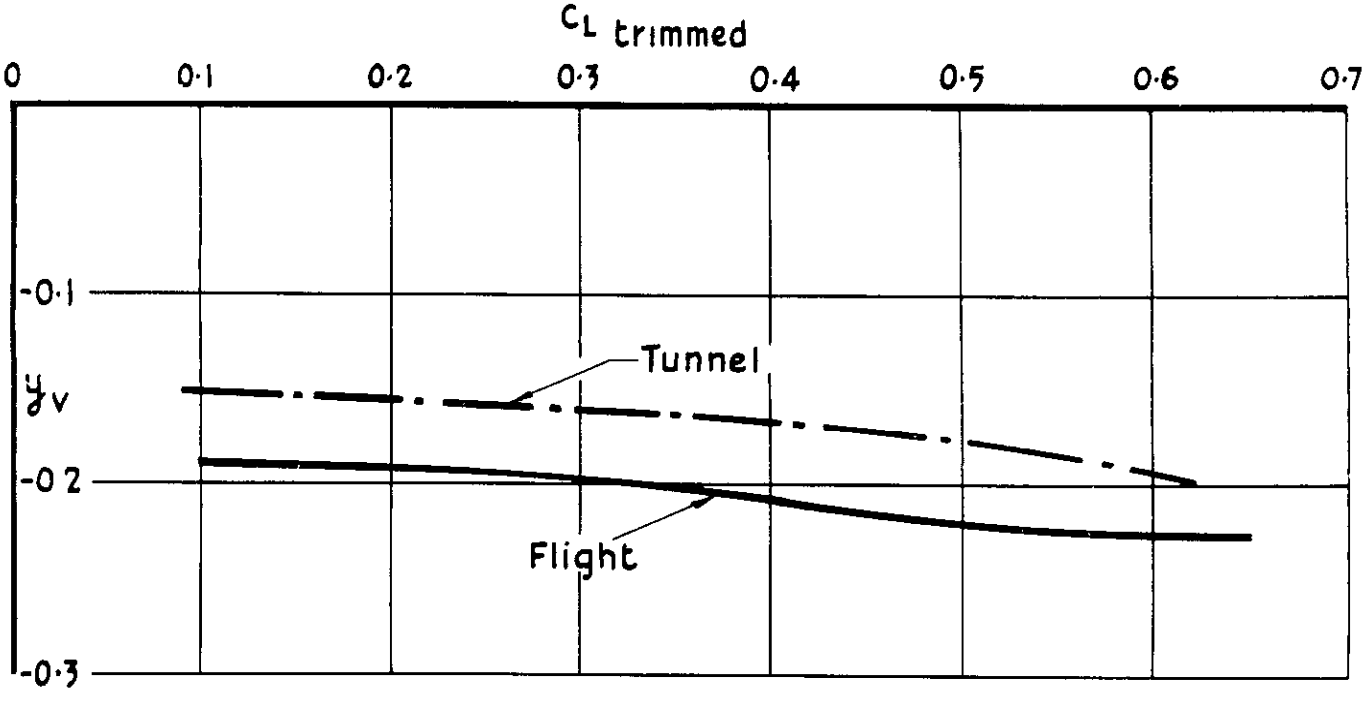

Fig 28 Comparison of flight and tunnel values of y_v

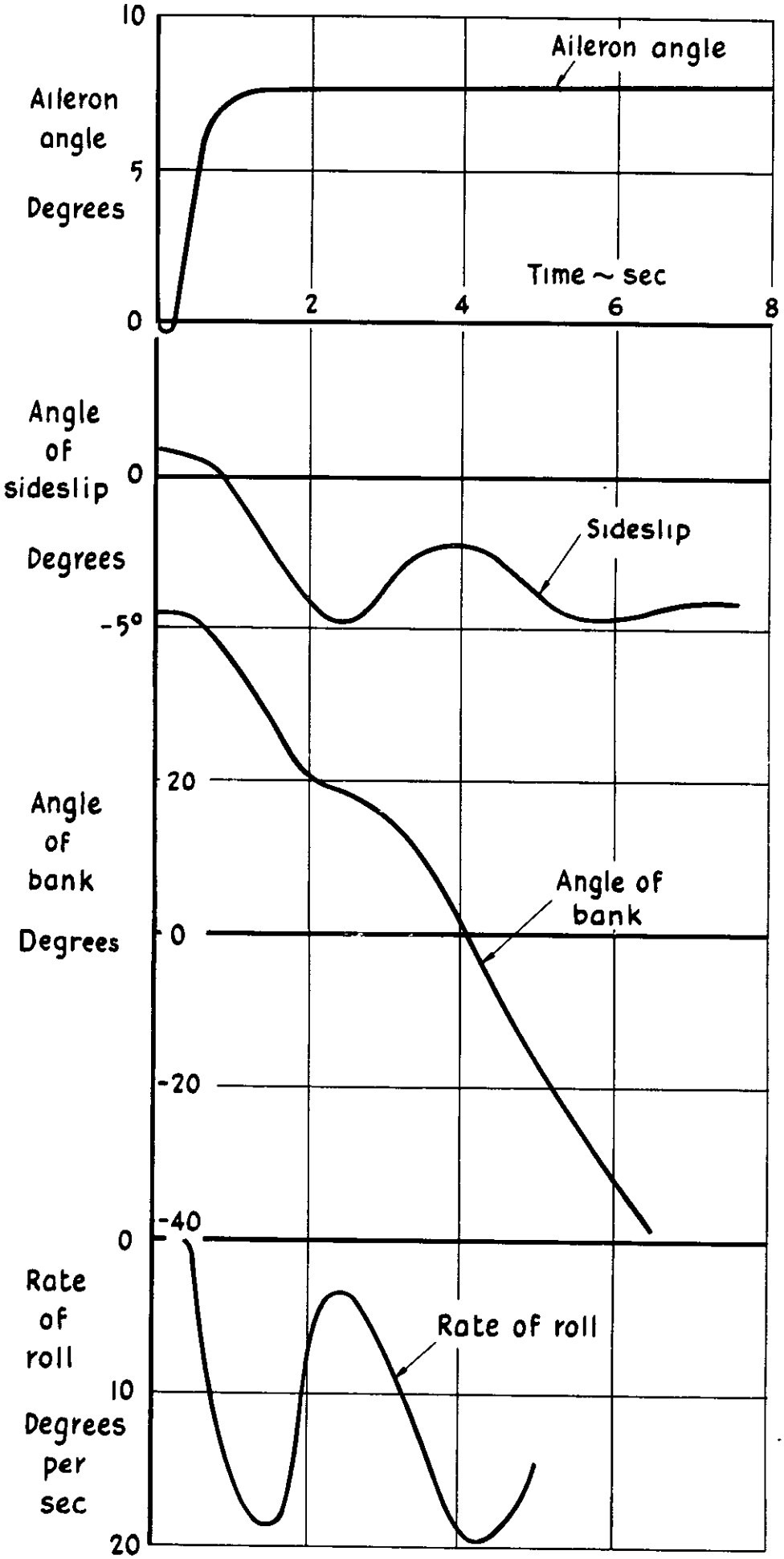

Fig 29 Time history of an aileron roll at 120 knots. Landing configuration

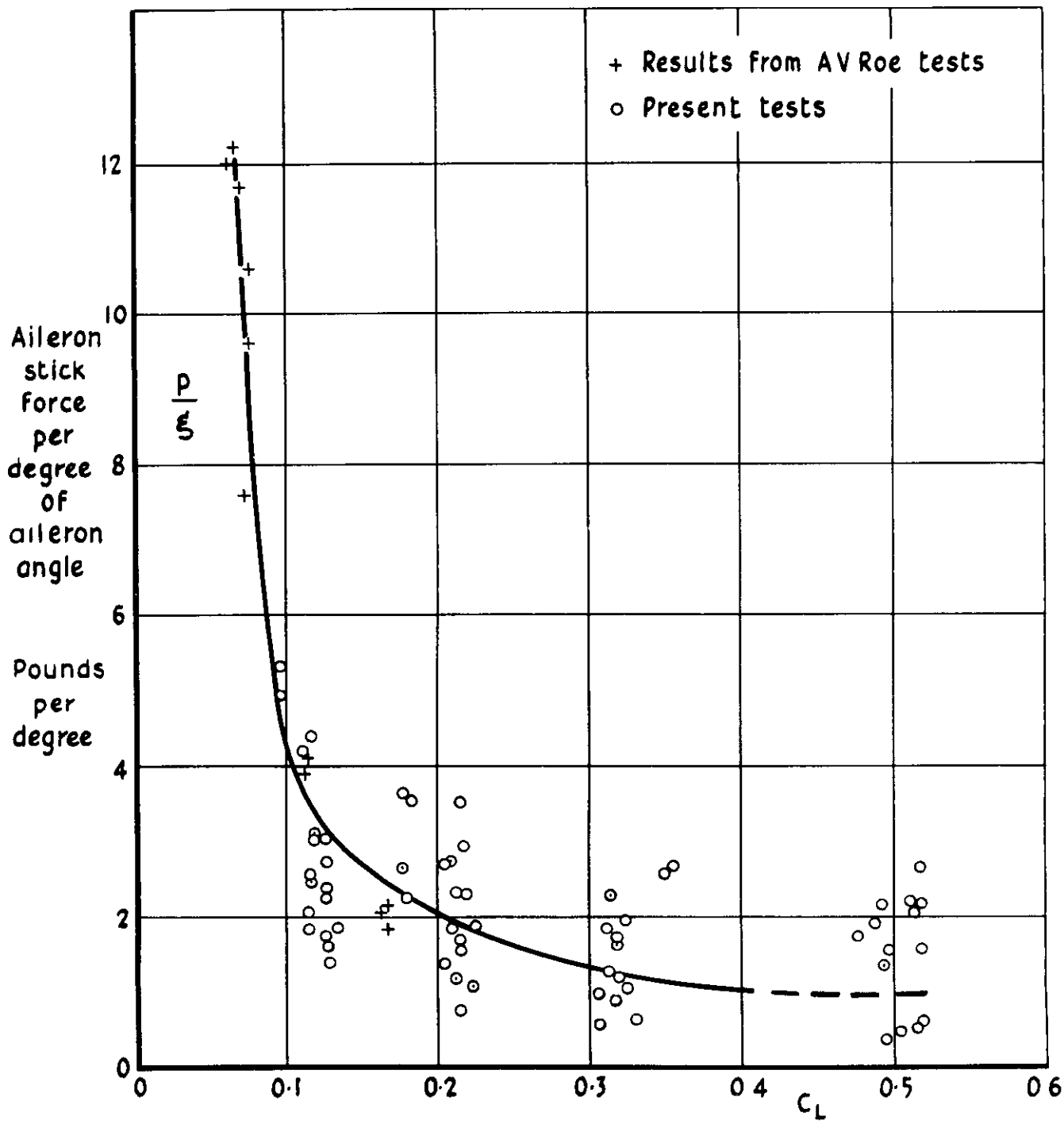

Fig 30 Variation of aileron stick force with trimmed lift coefficient

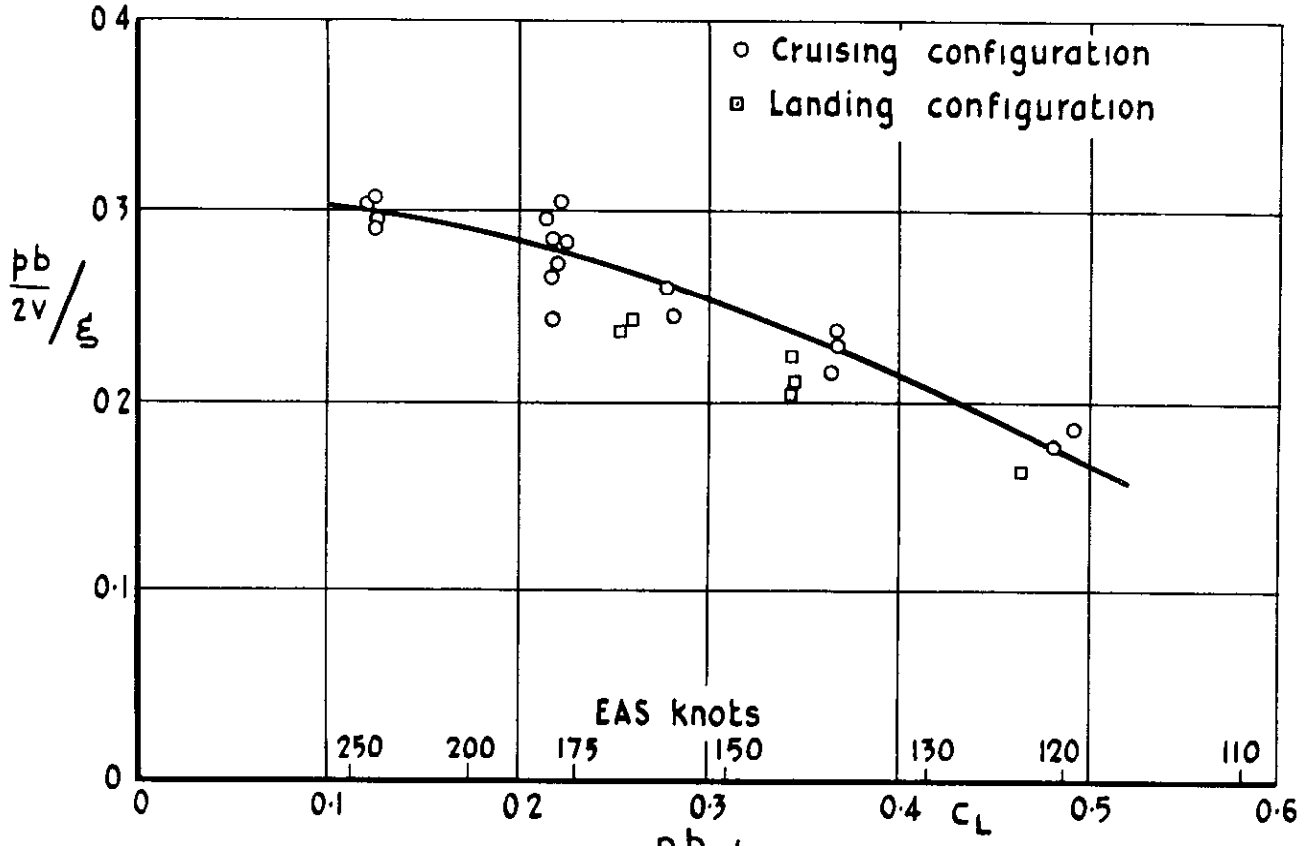

Fig 31 Variation of $\frac{pb}{2V}/\xi$ with lift coefficient.
Rudder fixed. Normal inertia

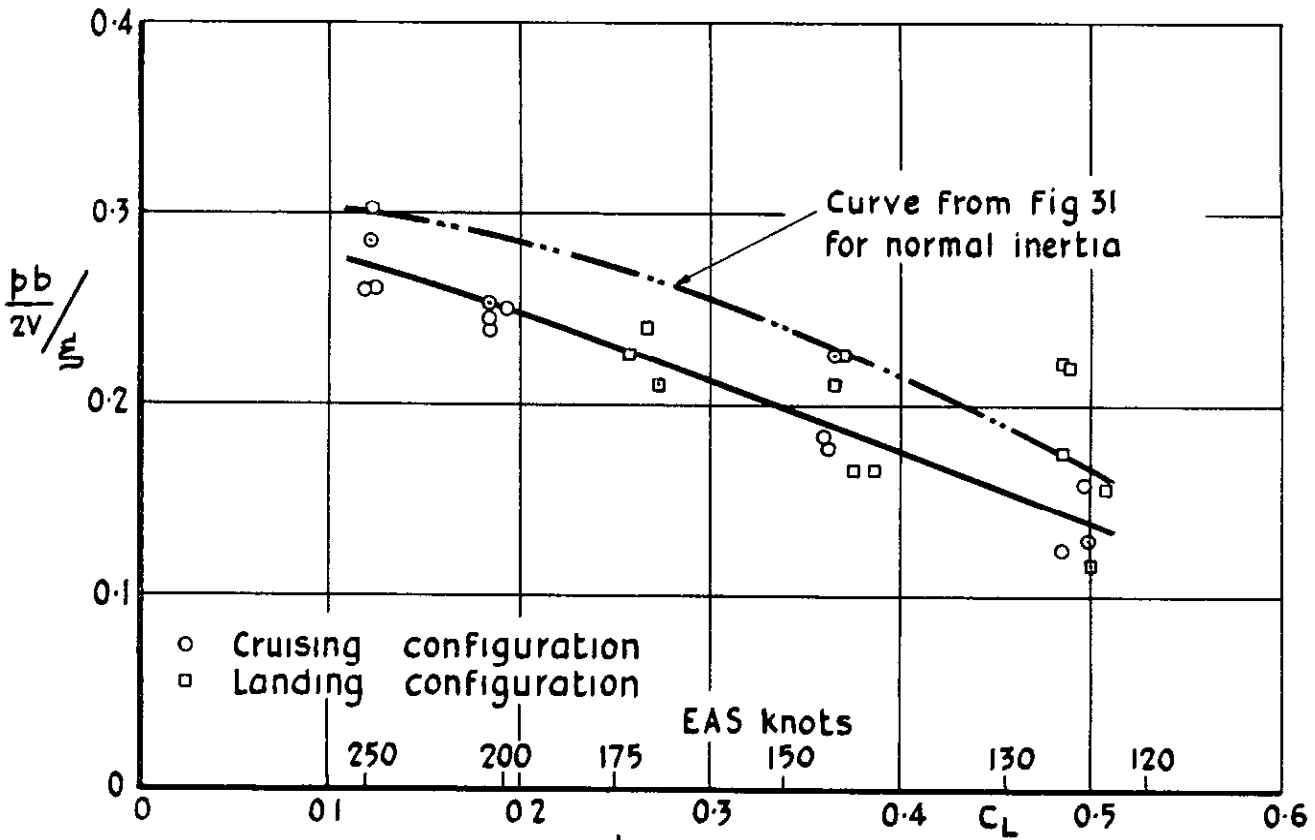

Fig. 32 Variation of $\frac{pb}{2V}/\xi$ with lift coefficient.
Rudder fixed. Increased inertia

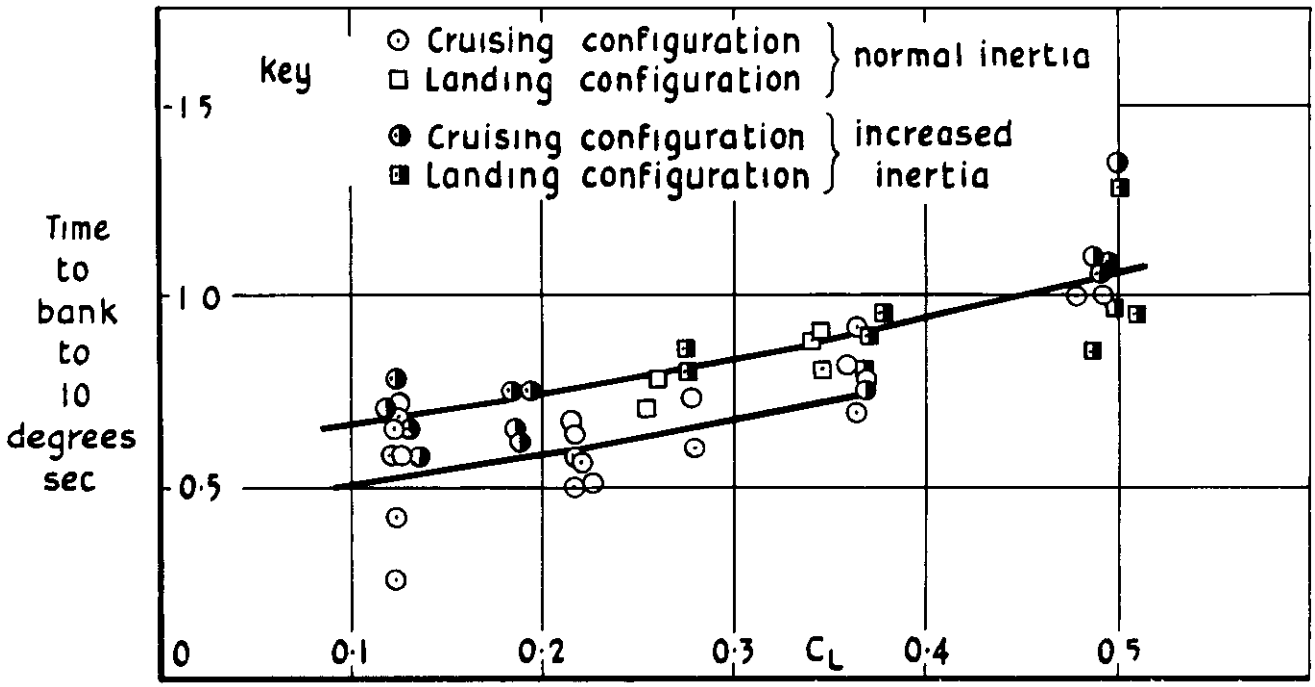

Fig 33 Time to bank to 10° using half aileron travel 10 000 ft

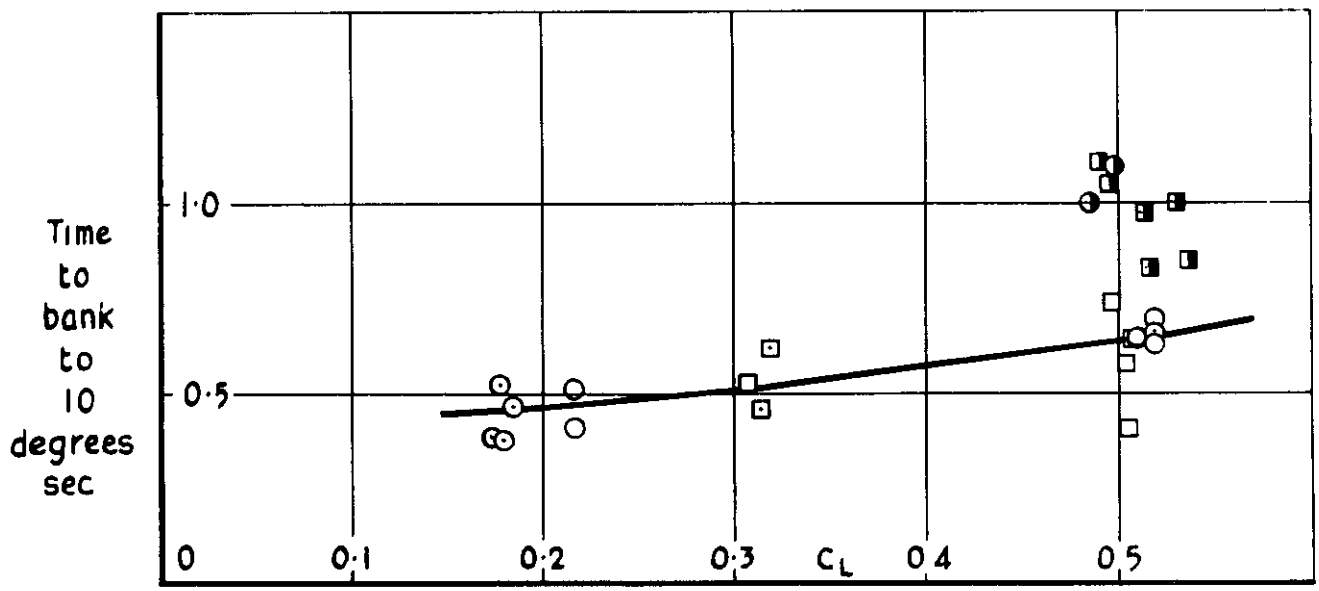

Fig 34 Time to bank to 10° using full aileron travel 10 000 ft

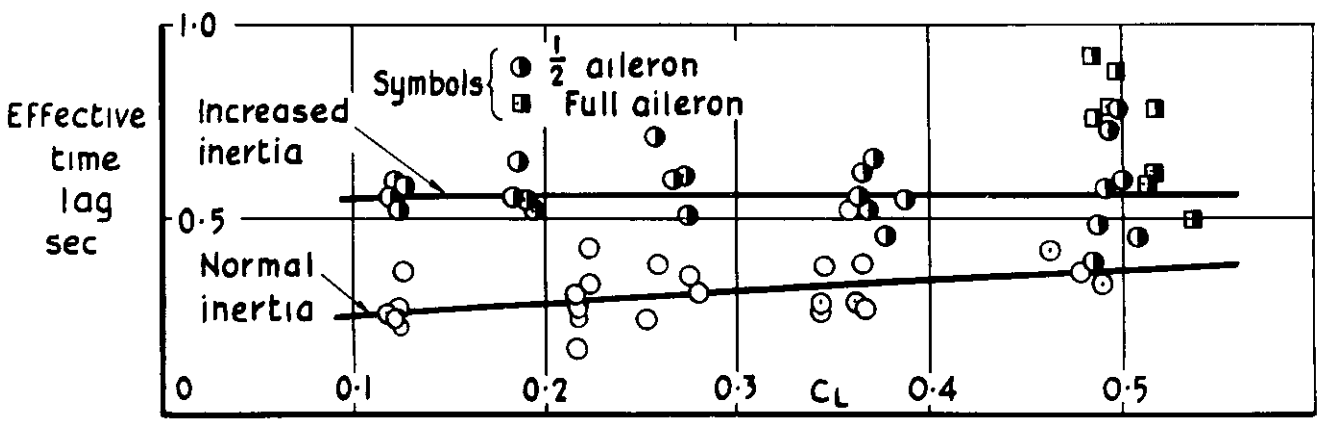

Fig 35 Effective time lag of rate of roll due to ailerons 10000 ft

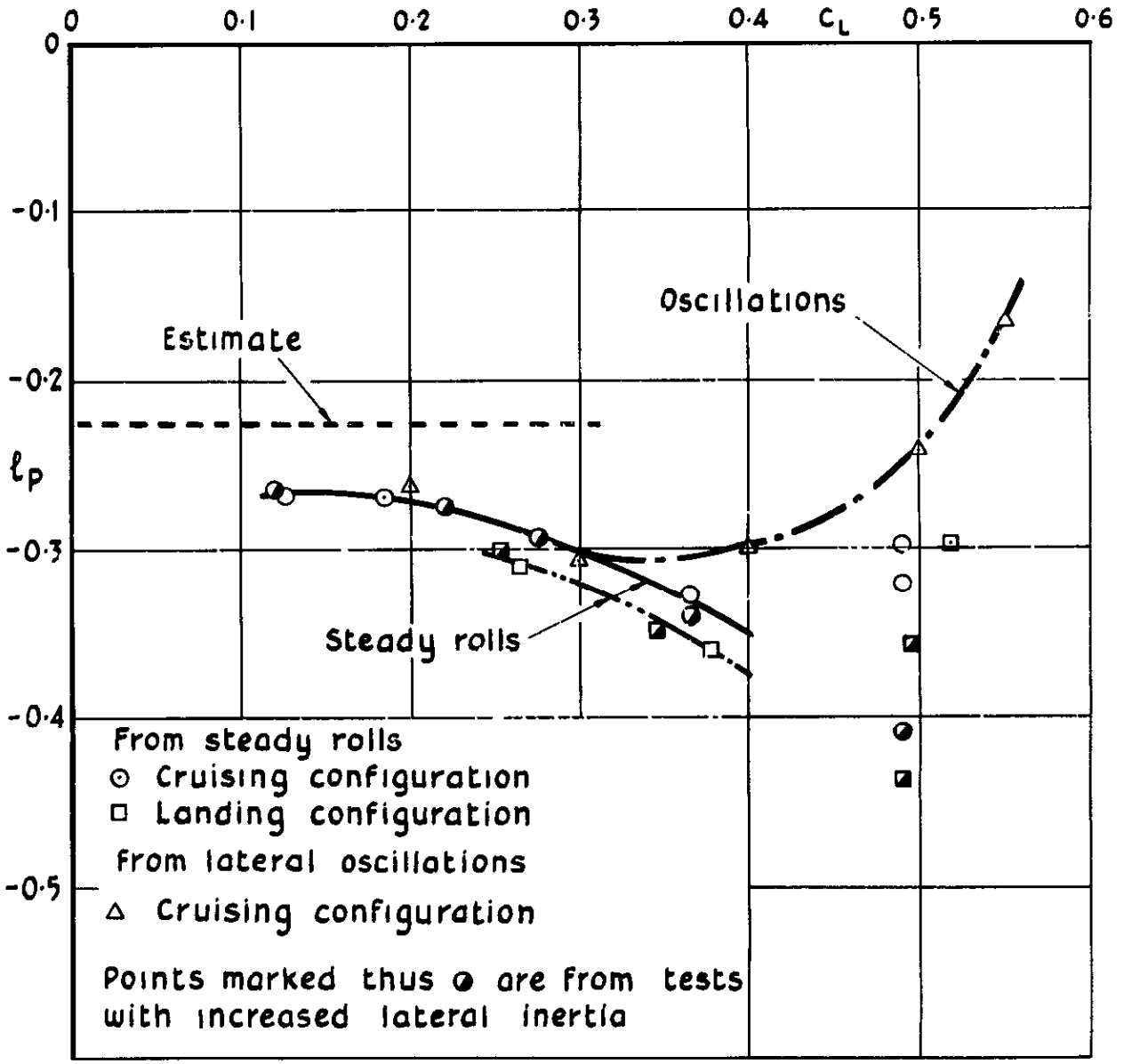

Fig 36 Comparison of the damping derivative in roll (l_p) measured in steady rolls and in lateral oscillations

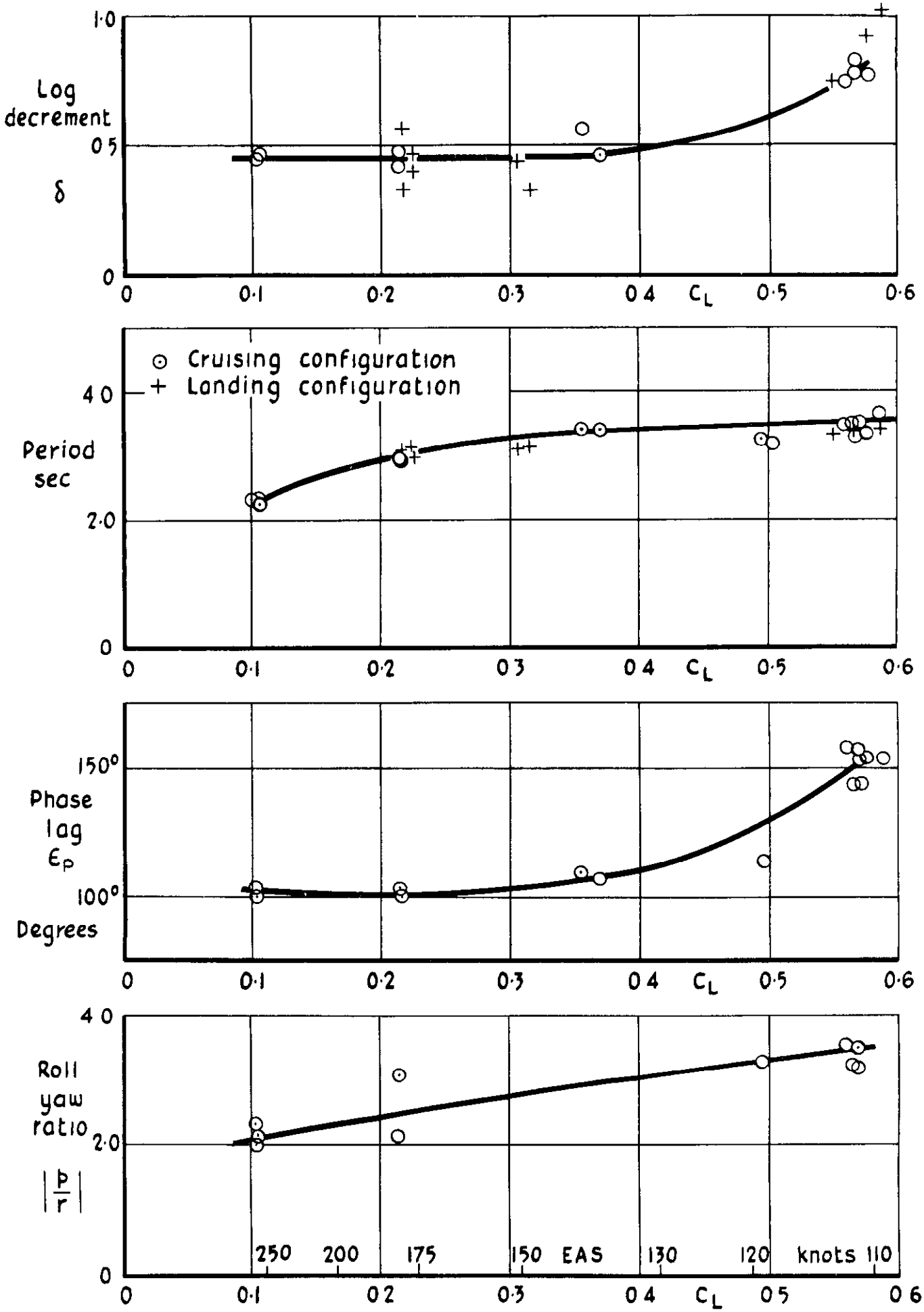

Fig 37 Damping, period, phase lag and roll yaw ratio of the lateral oscillation. Normal inertia. 10 000 ft

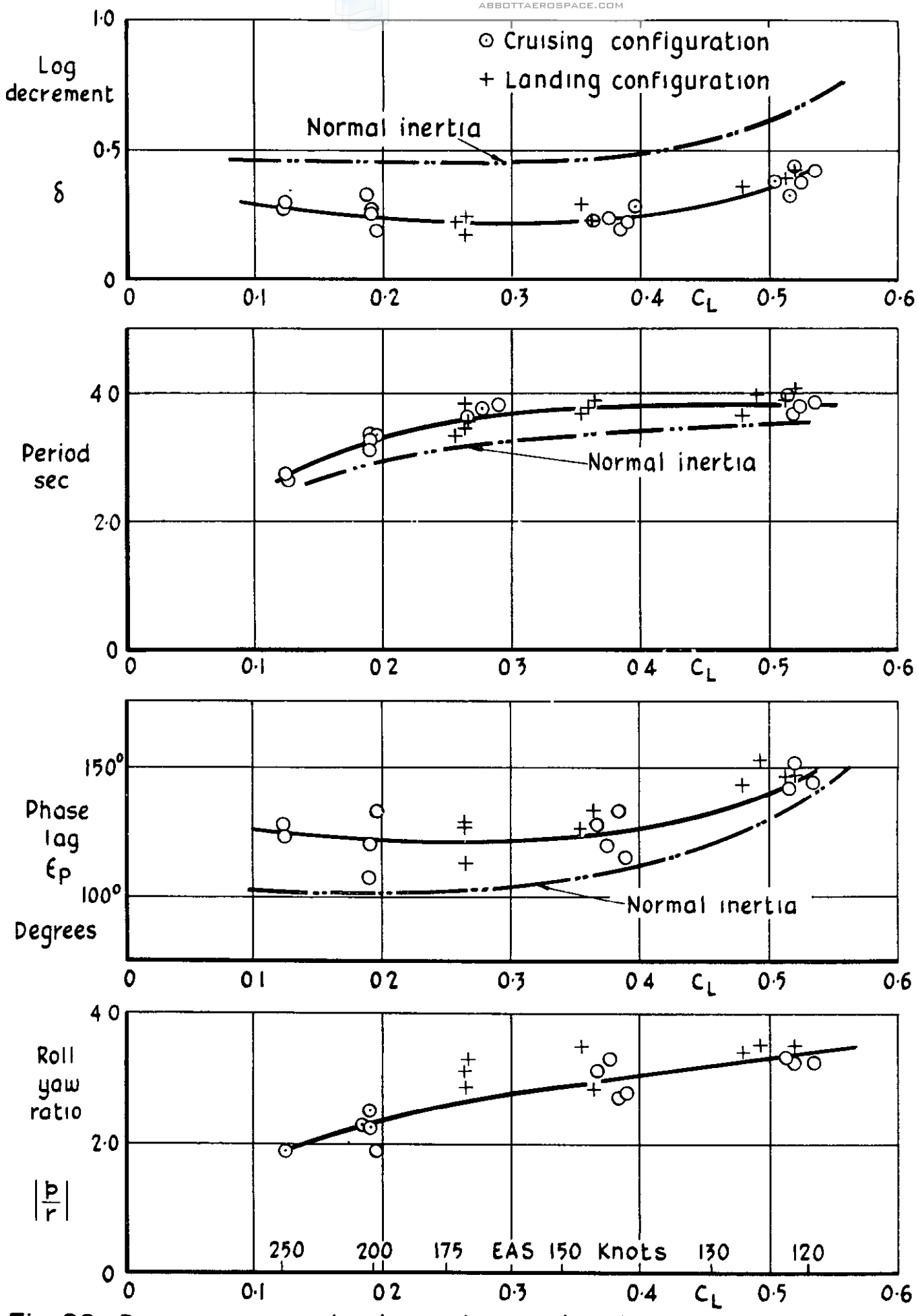

Fig 38 Damping, period, phase lag and roll yaw ratio of the lateral oscillation. Increased inertia. 10000 ft

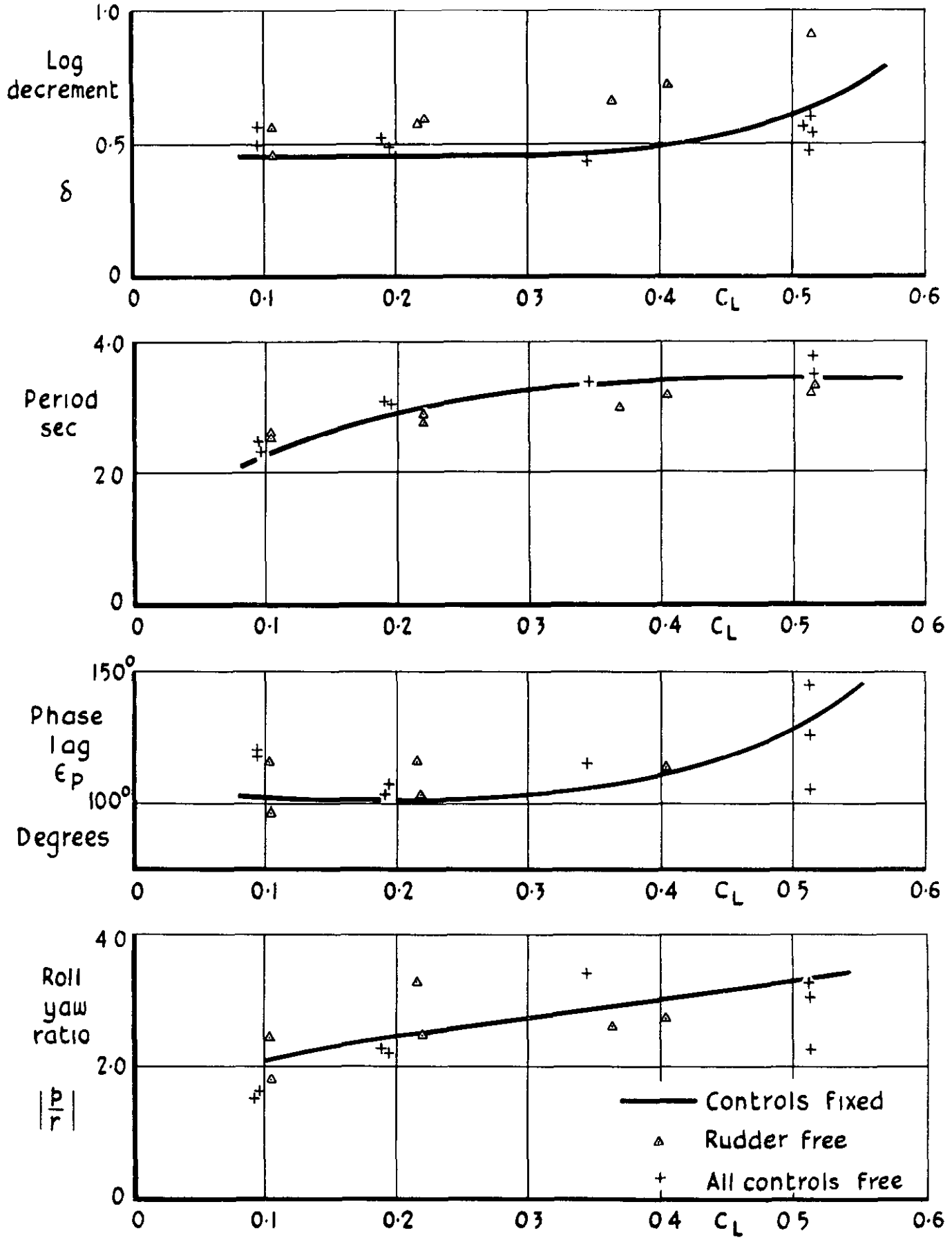

Fig 39 The effect of freeing the controls on the characteristics of the lateral oscillation

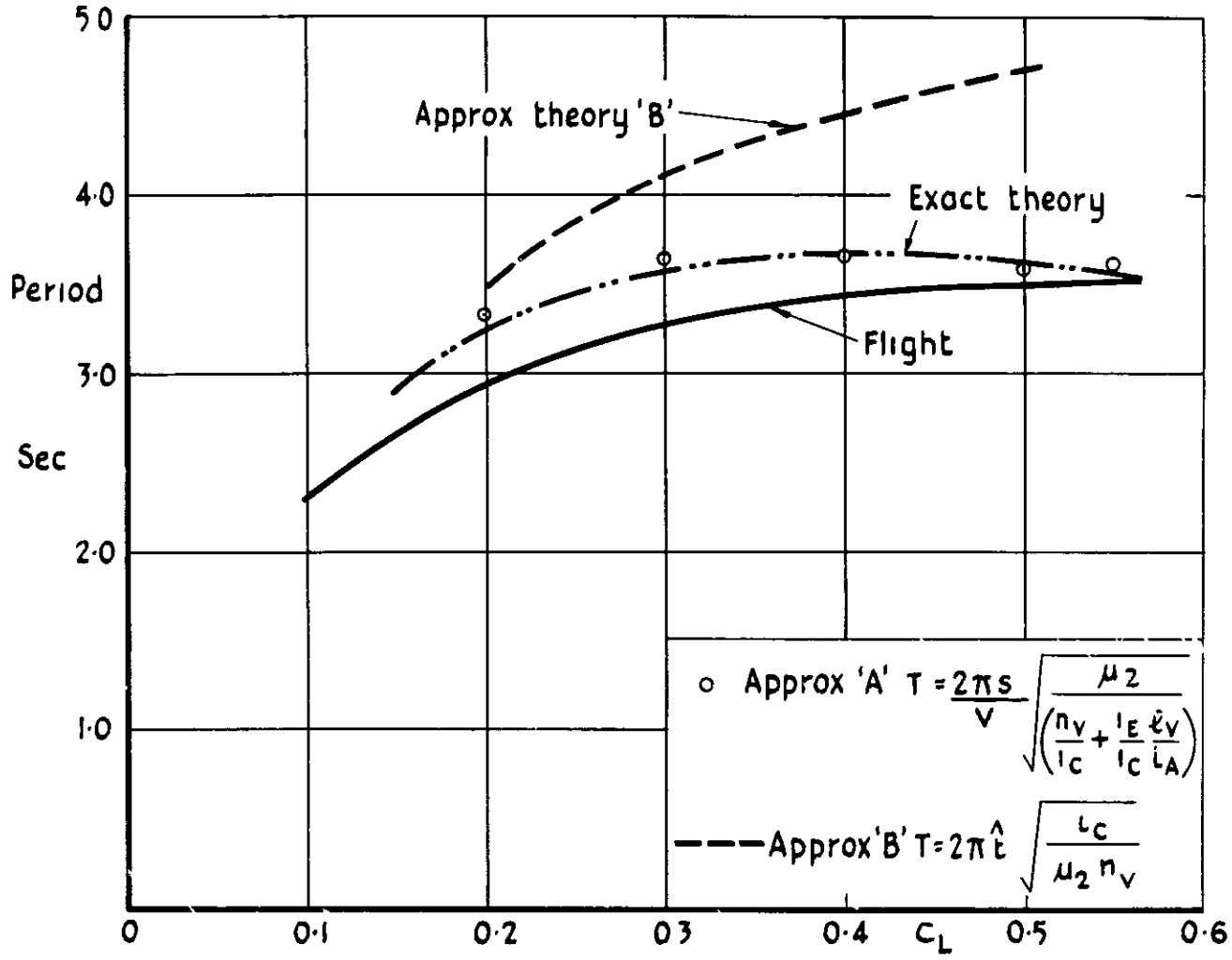

Fig.40 Comparison of flight and estimated periods of the lateral oscillation

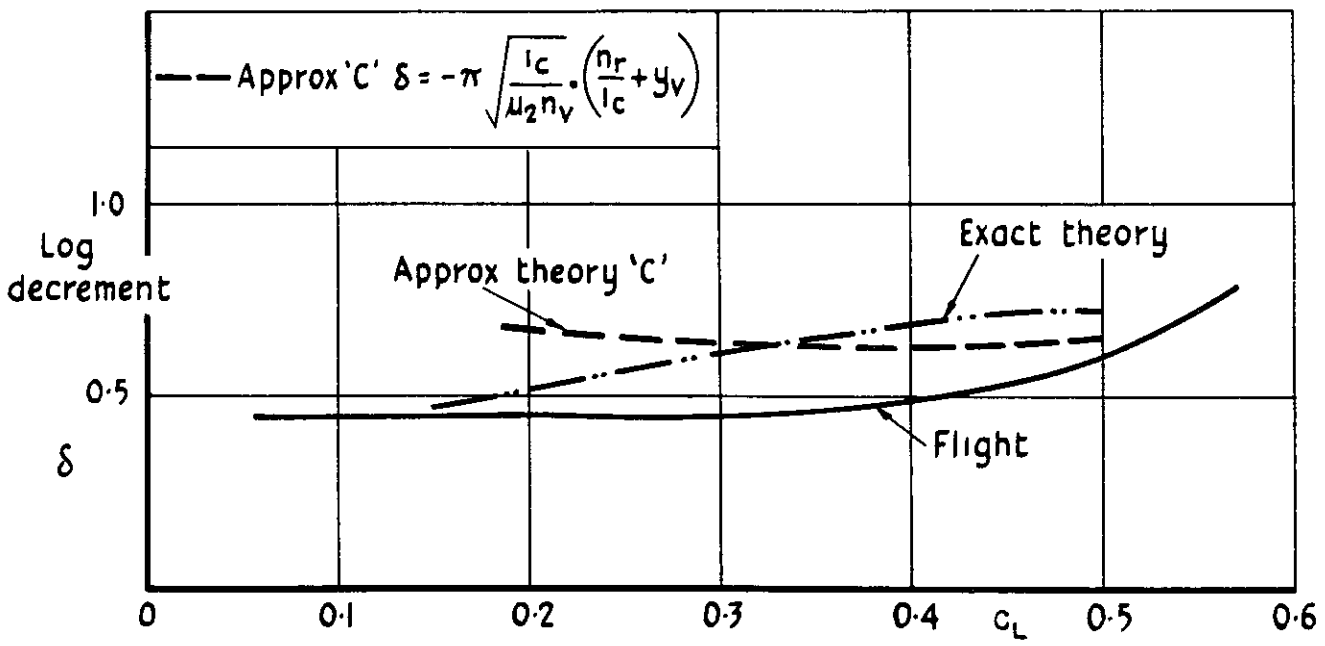

Fig.41 Comparison of flight and estimated dampings of the lateral oscillation

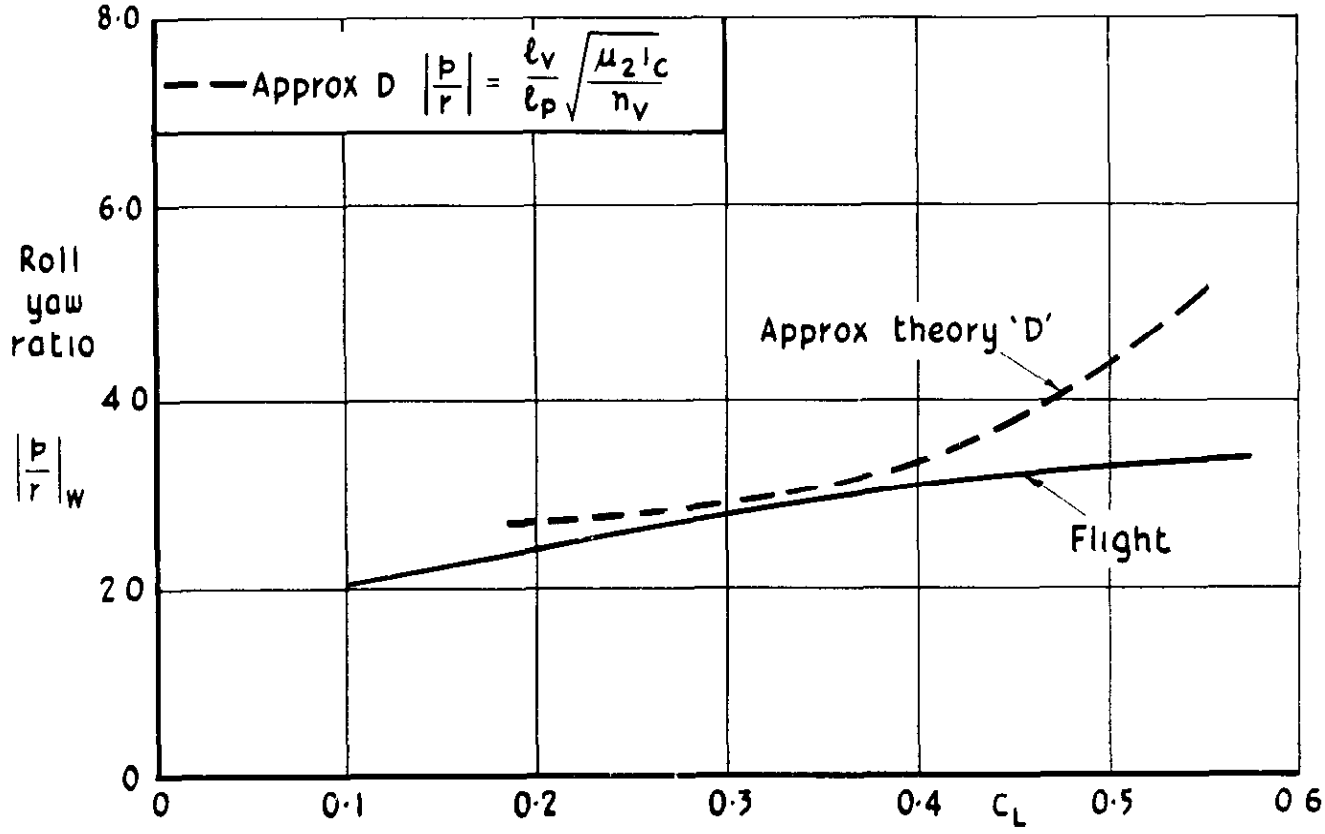

Fig 42 Comparison of flight and estimated roll–yaw ratios for the lateral oscillation

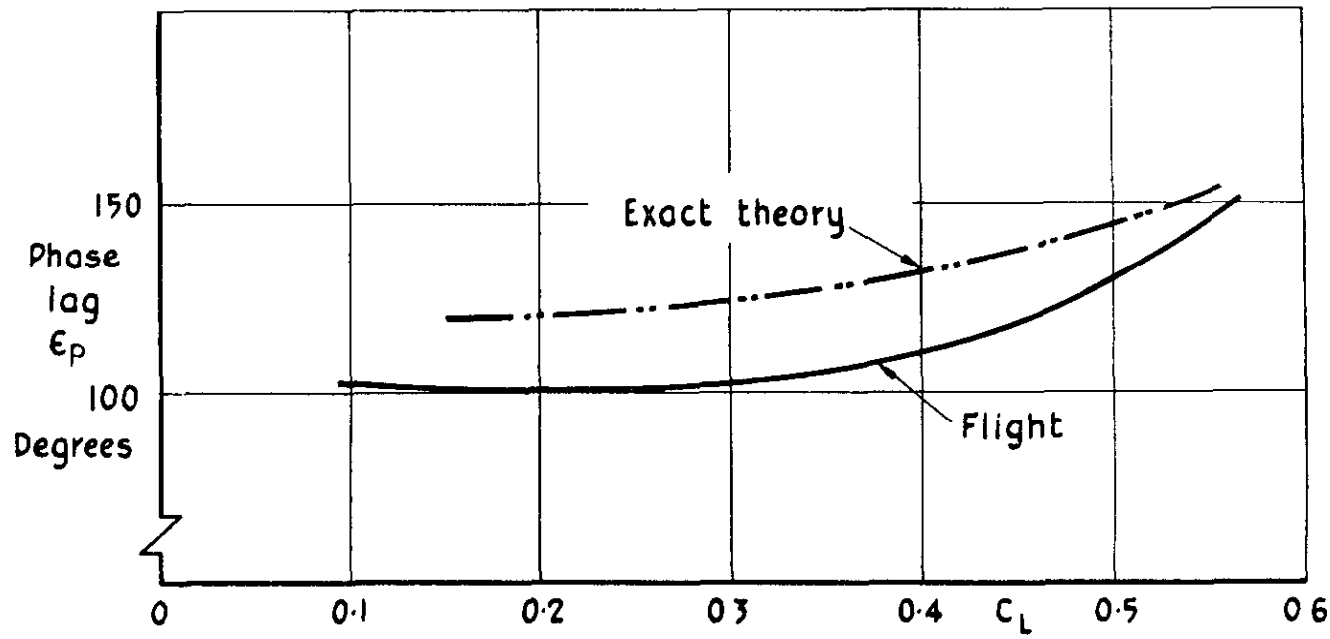

Fig 43 Comparison of flight and estimated phase lags of the lateral oscillation

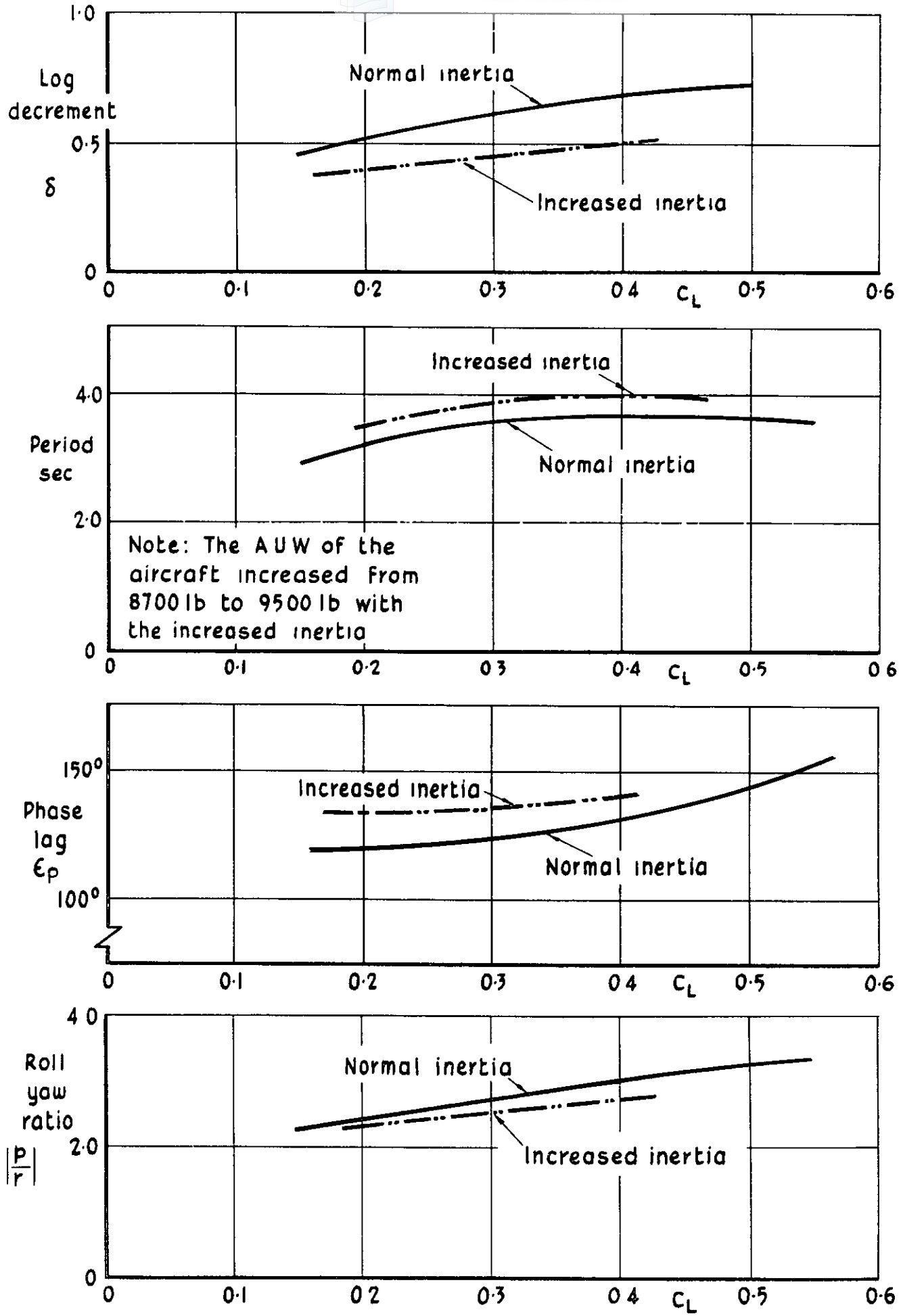

Fig 44 Theoretical changes in the characteristics of the lateral oscillation with increased inertia

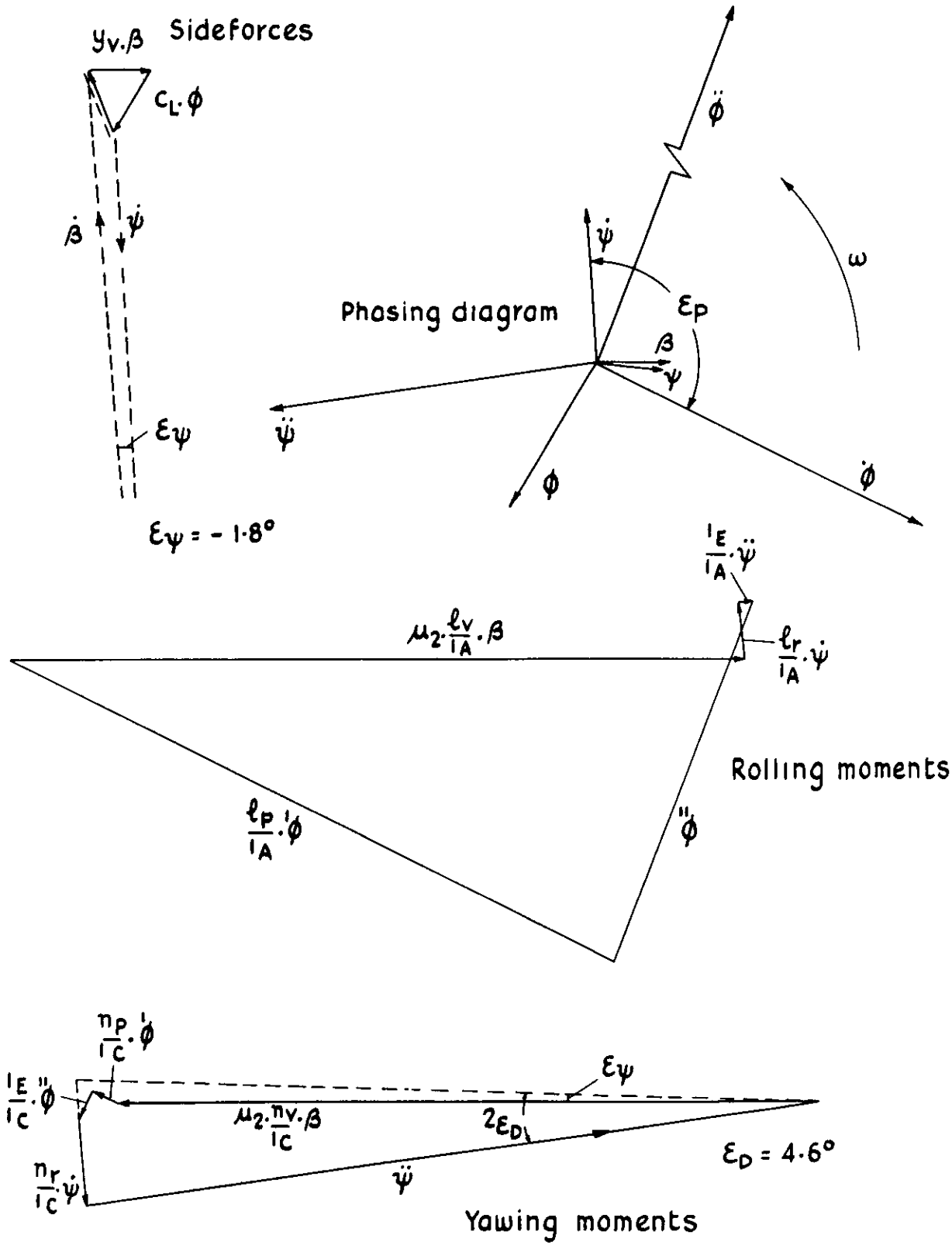

Fig 45 Vector diagrams of the lateral oscillation.
Normal inertia $C_L = 0.20$. 10 000 ft

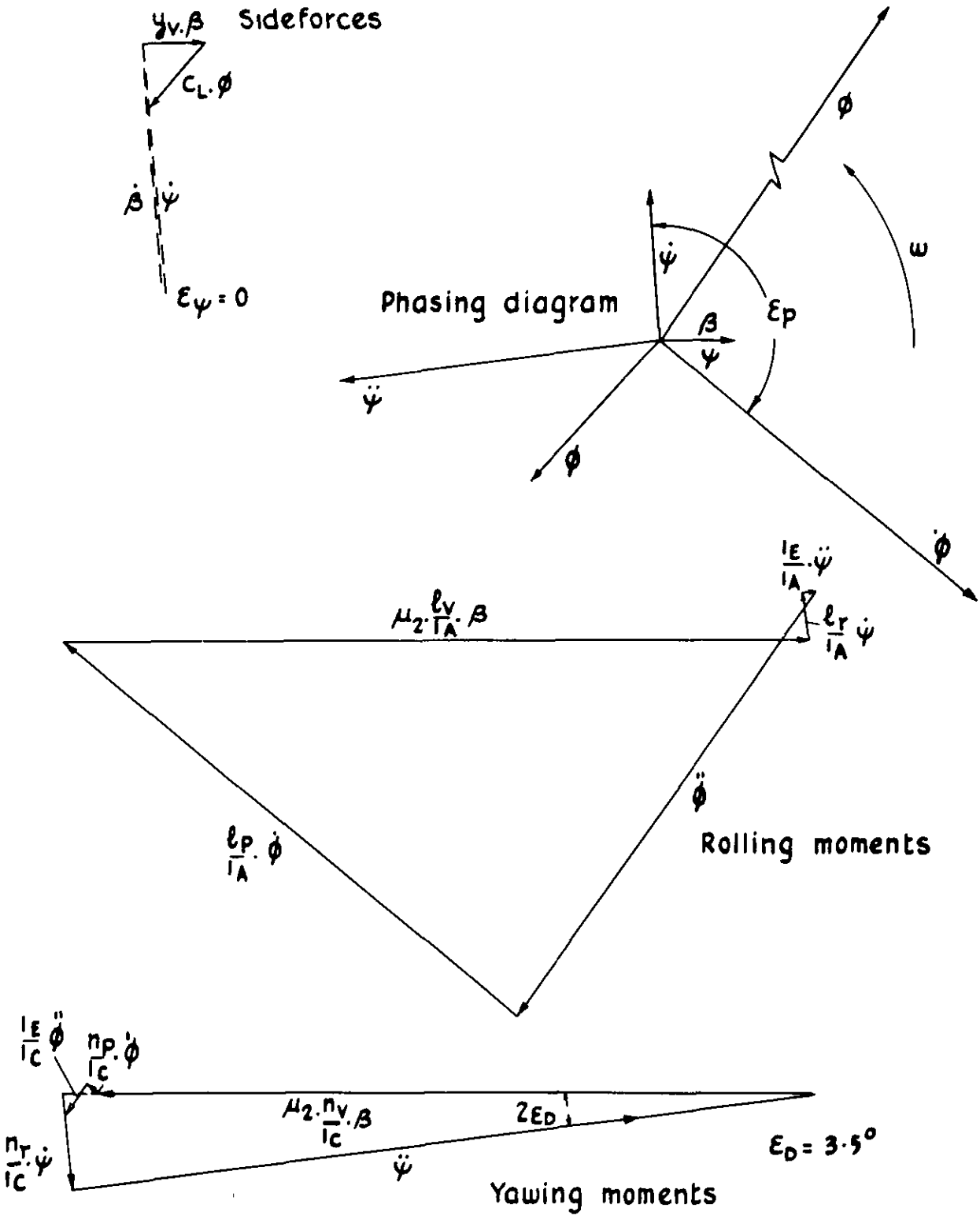

Fig 46 Vector diagram of the lateral oscillation.
Increased inertia. $C_L = 0{\cdot}20$. 10 000 ft

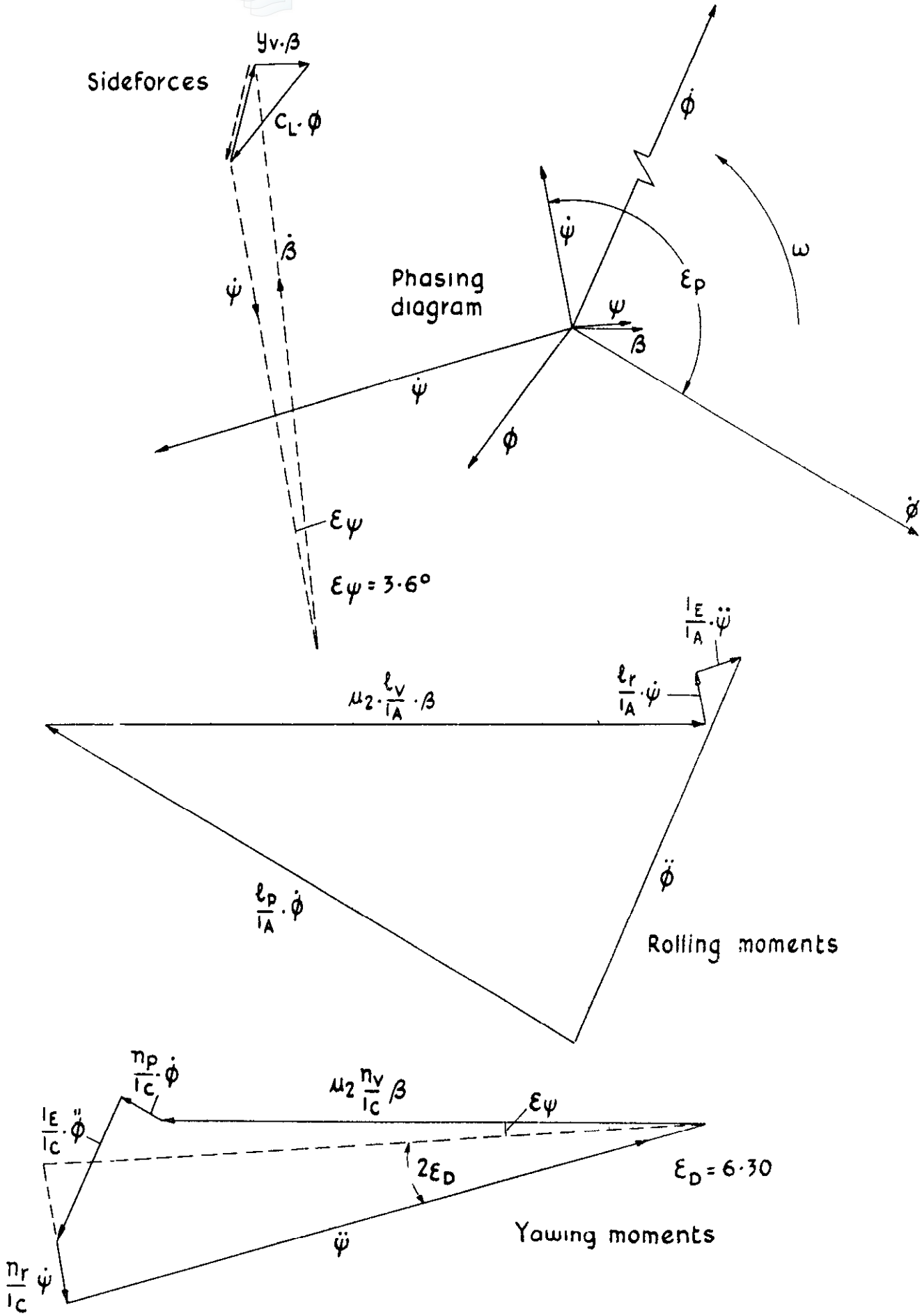

Fig. 47 Vector diagram of the lateral oscillation.
Normal inertia. $C_L = 0{\cdot}40$. 10 000 ft

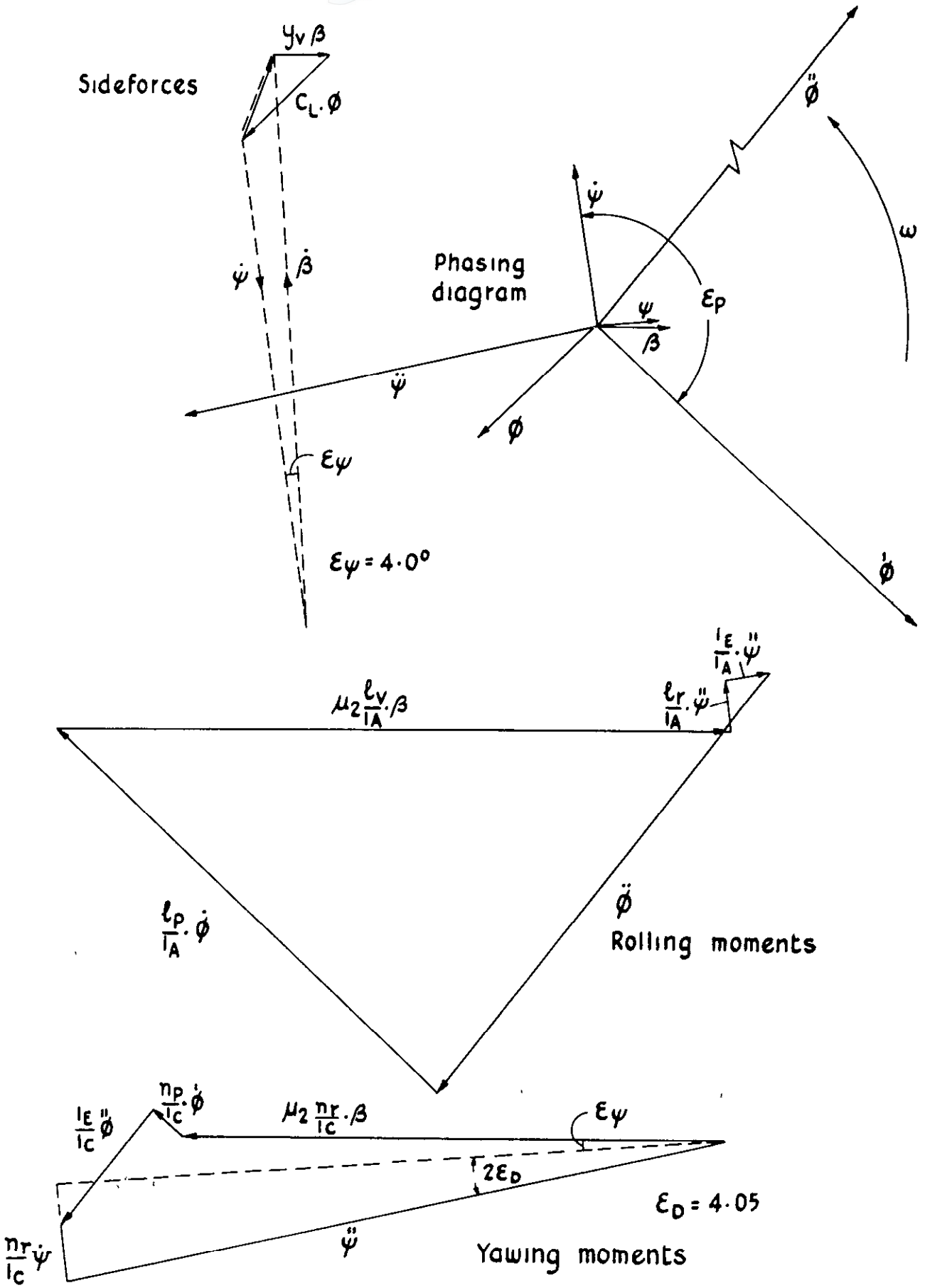

Fig. 48 Vector diagram of the lateral oscillation—increased inertia. $C_L = 0{\cdot}40$. 10 000 ft

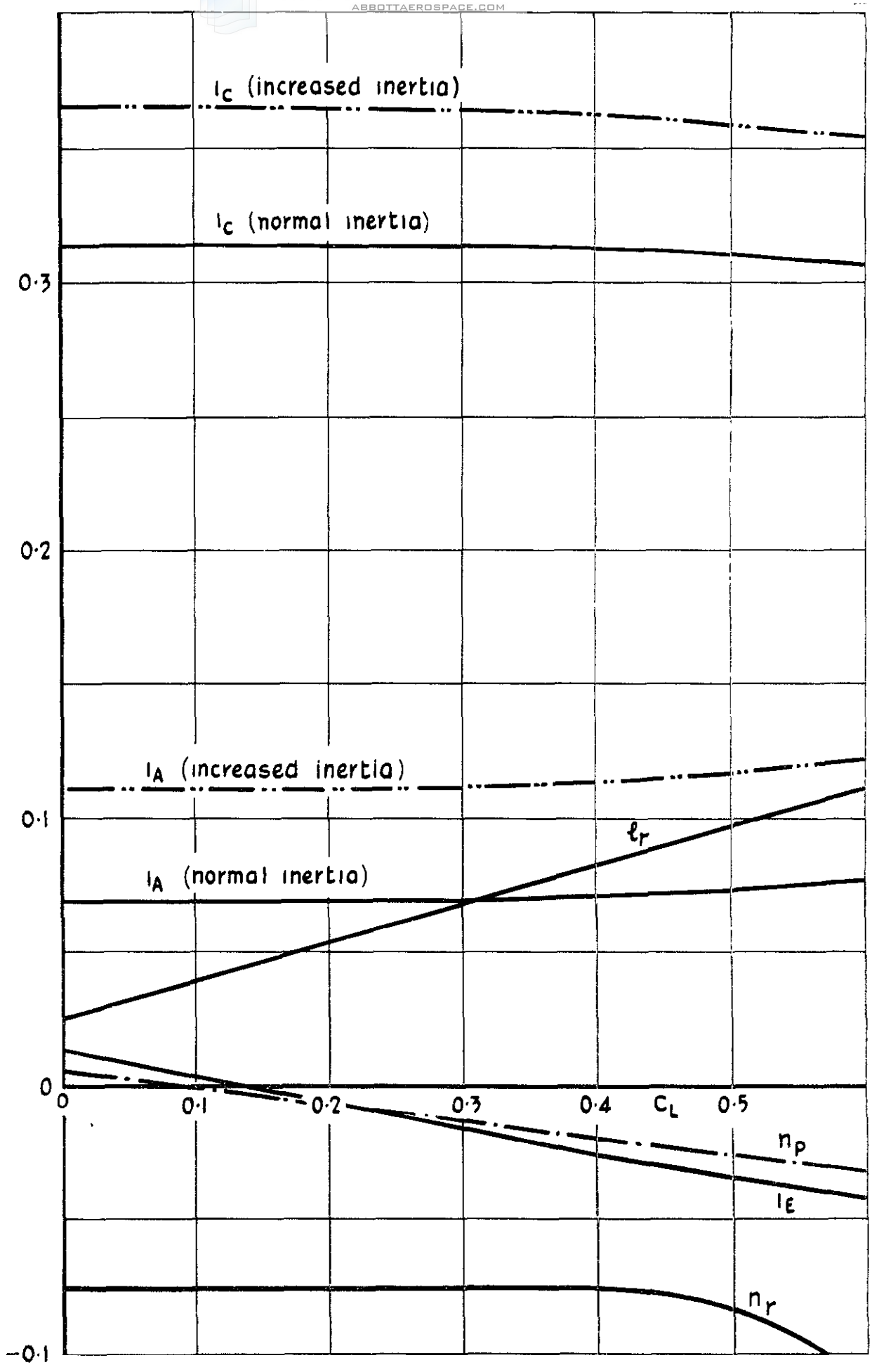

Fig 49 Estimates of the lateral derivatives and inertia coefficients used in the stability calculations

Printed in England for Her Majesty's Stationery Office by the Royal Aircraft Establishment, Farnborough. Dd.146915. K.4.

DETACHABLE ABSTRACT CARD

A.R.C. C.P.1106
April 1960

Perry, D.H. : 533.65
Morrall, J.C. : 533.693.3
Port, W.G.A. 533.6.013.413

LOW SPEED FLIGHT TESTS ON A TAILLESS DELTA WING AIRCRAFT (AVRO 707B) PART 3 - LATERAL STABILITY AND CONTROL 1.7.1.2 1.2.2.2.3.1 1.8.1.1.2 1.8.1.2.2

Royal Aircraft Establishment Technical Report Aero 2638 1.8.2.2

This report describes some measurements of lateral stability and control which were made as part of a series of low speed flight tests on the Avro 707B.

Measurements of the aileron and rudder powers, by flying the aircraft with asymmetric wing weights and with a small parachute attached to one wing tip, enabled the sideslip derivatives ℓ_v, n_v, y_v and the damping derivative

(Over)

A.R.C. C.P.1106
April 1960

Perry, D.H. : 533.65
Morrall, J.C. : 533.693.3
Port, W.G.A. 533.6.013.413

LOW SPEED FLIGHT TESTS ON A TAILLESS DELTA WING AIRCRAFT (AVRO 707B) PART 3 - LATERAL STABILITY AND CONTROL 1.7.1.2 1.2.2.2.3.1 1.8.1.1.2 1.8.1.2.2

Royal Aircraft Establishment Technical Report Aero 2638 1.8.2.2

This report describes some measurements of lateral stability and control which were made as part of a series of low speed flight tests on the Avro 707B.

Measurements of the aileron and rudder powers, by flying the aircraft with asymmetric wing weights and with a small parachute attached to one wing tip, enabled the sideslip derivatives ℓ_v, n_v, y_v and the damping derivative

(Over)

ℓ_p to be measured. These derivatives were used to estimate the period, damping and roll-yaw ratio of the lateral oscillation for comparison with actual flight measurements.

The measurements of the control powers and sideslip derivatives were in reasonable agreement with the wind tunnel measurements, and the changes which occurred at high lift coefficient were consistent with the changes in wing flow shown by smoke and tuft studies, reported in Part 4 of this series of reports. The derived period and roll-yaw ratio of the lateral oscillation were in fair agreement with the flight measurements but analysis of the damping of the motion emphasised the need for more accurate methods of estimating the rotary derivatives, n_r and n_p, and the lateral inertia of the aircraft.

Pilot opinion of the lateral handling of the aircraft at low speed is also reported.

ℓ_p to be measured. These derivatives were used to estimate the period, damping and roll-yaw ratio of the lateral oscillation for comparison with actual flight measurements.

The measurements of the control powers and sideslip derivatives were in reasonable agreement with the wind tunnel measurements, and the changes which occurred at high lift coefficient were consistent with the changes in wing flow shown by smoke and tuft studies, reported in Part 4 of this series of reports. The derived period and roll-yaw ratio of the lateral oscillation were in fair agreement with the flight measurements but analysis of the damping of the motion emphasised the need for more accurate methods of estimating the rotary derivatives, n_r and n_p, and the lateral inertia of the aircraft.

Pilot opinion of the lateral handling of the aircraft at low speed is also reported.

C.P. No. 1106

Published by
HER MAJESTY'S STATIONERY OFFICE

To be purchased from
49 High Holborn, London W C 1
13a Castle Street, Edinburgh EH 2 3AR
109 St. Mary Street, Cardiff CF1 1JW
Brazennose Street, Manchester 2
50 Fairfax Street, Bristol BS1 3DE
258 Broad Street, Birmingham 1
7 Linenhall Street, Belfast BT2 8AY
or through any bookseller

C.P. No. 1106

SBN 11 470346 9